

## ABSTRACT

Title of Document: EXAMINATION OF DYNAMIC PROCESSES IN LIVING ZIEGLER-NATTA POLYMERIZATION AND NEW POLYPROPYLENE ARCHITECTURES THROUGH BIMOLECULAR CONTROL

Matthew Brian Harney, Doctor of Philosophy, 2006

Directed By: Professor Lawrence R. Sita, Department of Chemistry and Biochemistry

The cationic cyclopentadienyl zirconium acetamidinate (CPZA) complex  $\{\text{Cp}^*\text{ZrMe}[\text{N}(\text{Et})\text{C}(\text{Me})\text{N}(\text{tBu})]\}[\text{B}(\text{C}_6\text{F}_5)_4]$ , ( $\text{Cp}^* = \eta^5\text{-C}_5\text{Me}_5$ ) generated through activation of  $\text{Cp}^*\text{ZrMe}_2[\text{N}(\text{Et})\text{C}(\text{Me})\text{N}(\text{tBu})]$  via protonolysis of a methyl group with one equivalent of  $[\text{PhNMe}_2\text{H}][\text{B}(\text{C}_6\text{F}_5)_4]$ , has been shown to be a highly active initiator for living  $\alpha$ -olefin polymerization. Discrete cationic CPZA alkyl complexes of the general structure  $\{\text{Cp}^*\text{ZrR}[\text{N}(\text{Et})\text{C}(\text{Me})\text{N}(\text{tBu})]\}[\text{B}(\text{C}_6\text{F}_5)_4]$  were studied as model complexes for living polymers derived from this system. Detailed analysis of models in which  $\text{R} = {}^n\text{Pr}$ ,  ${}^i\text{Pr}$ ,  ${}^i\text{Bu}$ , and 2-Et-Bu, as well as living isotactic poly(1-butene) and living isotactic poly( $1\text{-}^{13}\text{C}$ -decene) revealed significant differences with respect to isomerization and decomposition. Studies carried out with various isotopically labeled *iso*-butyl derivatives revealed isomerization concurrent with decomposition, while the only case which *did not* provide evidence for isomerization was an isotopically labeled *n*-propyl derivative. Products of decomposition in cases of  $\text{R} = {}^i\text{Bu}$  and 2-Et-Bu included not only the

expected alkenes from isomerization/ $\beta$ -hydride elimination, but significant quantities of alkane. This is proposed to arise from competitive intramolecular abstraction of a hydrogen from the Cp\* ligand. During decomposition, all species mentioned above disappeared in a first order manner, and all products of decomposition/isomerization appeared in a zero order manner. This is consistent with slow  $\beta$ -hydride elimination followed by rapid isomerization, decomposition or reinsertion. Possible mechanisms of isomerization are discussed.

The  $\{\text{Cp}^*\text{ZrMe}[\text{N}(\text{Et})\text{C}(\text{Me})\text{N}(\text{tBu})]\}\text{[B}(\text{C}_6\text{F}_5)_4]$  initiator was found to be an active initiator for the living isotactic polymerization of propylene ( $[mmmm] = 0.71$ ). When substoichiometrically activated with only 0.5 equivalents of  $[\text{PhNMe}_2\text{H}][\text{B}(\text{C}_6\text{F}_5)_4]$ , atactic polypropylene was produced due to the rapid degenerative transfer of methyl groups between active and dormant centers, which results in the racemization of active sites by virtue of the configurational instability of the dormant state. Successive additions of  $[\text{PhNMe}_2\text{H}][\text{B}(\text{C}_6\text{F}_5)_4]$  and a methylating agent were used to modulate the conditions of the polymerization system between degenerative transfer (at 50% activation) and fully activated conditions to produce the first discrete, homogeneous isotactic-atactic stereoblock polypropylene (*sb*-PP) materials. Preliminary tensile testing of three unique *sb*-PP materials displayed elastomeric properties that were heavily dependant on the stereoblock architecture. The synthesis of a wide range of polypropylene stereochemical microstructures between isotactic and atactic through bimolecular control by substoichiometric activation was also demonstrated, leading to the development of a fundamentally new architecture: stereogradient polypropylene.

EXAMINATION OF DYNAMIC PROCESSES IN LIVING ZIEGLER-NATTA  
POLYMERIZATION AND NEW POLYPROPYLENE ARCHITECTURES  
THROUGH BIMOLECULAR CONTROL

By

Matthew Brian Harney

Dissertation submitted to the Faculty of the Graduate School of the  
University of Maryland, College Park, in partial fulfillment  
of the requirements for the degree of  
Doctor of Philosophy  
2006

Advisory Committee:  
Professor Lawrence R. Sita, Chair  
Professor Jeffery T. Davis  
Professor Bryan W. Eichhorn  
Professor Andrei N. Vedernikov  
Professor Peter Kofinas

© Copyright by  
Matthew Brian Harney  
2006

## Dedication

I would like to dedicate this work to my wife, Christine J. Harney, without whom I would not be where I am today.

## Acknowledgements

I would like to thank my advisor, Prof. Lawrence R Sita, for his guidance and support. His passion for chemistry and commitment to excellence has made my time at the University of Maryland a truly remarkable experience.

I would also like to thank the members of the Sita group both past and present. In particular, the friendship and enthusiasm of Dr. Richard J. Keaton and Dr. Yonghui Zhang ensured that each day was not only productive, but enjoyable.

A great deal of this work is based on NMR spectroscopic analysis. Without the expertise of Dr. Yiu-fai Lam and Dr. Yinde Wang, none of this would have been possible.

Finally, special thanks to my parents, Dr. Brian Harney and Carol Harney, my brother, Jonathan Harney, and my wife, Christine Harney. My accomplishments have only been possible with their support, and this dissertation stands as a testament to their dedication.

# Table of Contents

Dedication .....	ii
Acknowledgements .....	iii
Table of Contents .....	iv
List of Figures .....	vi
List of Schemes .....	viii
List of Tables .....	x
List of Abbreviations .....	xi
Chapter 1: Dynamic Processes in Ziegler-Natta Polymerization .....	1
1.1 Introduction .....	1
1.1.1 Ziegler-Natta Polymerization .....	2
1.1.2 Symmetry-Microstructure Relationships .....	6
1.1.3 Termination Events .....	8
1.1.4 Microstructural Analysis .....	9
1.2 Site Isomerization .....	13
1.2.1 C <sub>1</sub> -symmetric Metallocenes: Hemiisotactic and Isotactic Polypropylene .....	13
1.2.2 C <sub>1</sub> -symmetric Metallocenes: Elastomeric Polypropylene .....	16
1.3 Chain-End Epimerization .....	19
1.4 Ligand Isomerization .....	22
1.4.1 Oscillating Metallocenes .....	22
1.4.2 Post-Metallocene .....	24
1.5 Reversible Chain Transfer .....	27
1.5.2 Direct Site Transfer .....	31
1.6 Degenerative Group Transfer .....	32
1.7 Living Polymerization .....	34
Chapter 2: Discrete Cationic CPZA Alkyl Complexes as Models for Living Polymers ..	36
2.1 Mechanistic Studies in Living Ziegler-Natta Polymerization .....	36
2.2 Chain Walking and Cationic CPZA Model Complexes .....	41
2.3 Synthesis and Structure .....	46
2.3.1 CPZA Alkyl, Chloro Complexes .....	46
2.3.2 CPZA Alkyl, Methyl Complexes .....	49
2.3.3 Cationic CPZA Alkyl Complexes .....	51
2.3.4 Isotopically Labeled Derivatives .....	56
2.3.5 Hafnium Derivatives .....	60
2.4 Results .....	65
2.4.1 Stability of CPZA Alkyl Cations .....	65
2.4.2 Stability of CPHA Alkyl Cations .....	73
2.5 Discussion .....	74
2.5.1 Decomposition of CPZA Alkyl Cations .....	74
2.5.2 Isomerization of CPZA Alkyl Cations – Busico’s Mechanism .....	77

2.5.3 Isomerization of CPZA Alkyl Cations – Alternate Mechanism .....	80
2.5.4 Hafnium Derivatives .....	84
2.6 Conclusions .....	85
Chapter 3: Application of Living Degenerative Transfer Polymerizations .....	86
3.1 Living Propylene Polymerization .....	86
3.1.1 Propylene Polymerization by CPZA Initiators .....	87
3.2 Stereoblock Polypropylene .....	91
3.2.1 Stereoblock Polymers .....	91
3.2.2 Synthesis and Microstructural Analysis .....	93
3.2.3 Materials Properties .....	97
3.3 Conclusions .....	99
Chapter 4: Bimolecular Control of Polypropylene Microstructure .....	101
4.1 Control of Microstructure Through Substoichiometric Activation .....	101
4.2 Stereogradient Polypropylene .....	106
4.3 Conclusions .....	110
Appendix .....	111
Experimentals .....	111
References .....	127

## List of Figures

Figure 1: The structures of linear PE, or HDPE, and branched PE, or LDPE.....	3
Figure 2: <i>Isotactic</i> and <i>atactic</i> polypropylene. ....	3
Figure 3: The <i>meso</i> ( <i>m</i> ) and <i>racemic</i> ( <i>r</i> ) dyads.....	10
Figure 4: The ten possible stereochemical pentads of PP.....	11
Figure 5: Stereoerrors in isotactic and syndiotactic PP under enantiomeric-site control. .....	12
Figure 6: Stereoerrors in isotactic and syndiotactic PP under chain-end control. ....	12
Figure 7: Complex <b>6</b> produces <i>iso</i> -PP with $[mmmm] > 99\%$ . ....	16
Figure 8: Atactic-isotactic stereoblock polypropylene ( <i>sb</i> -PP) .....	17
Figure 9: $C_1$ -symmetric metallocenes capable of producing elastomeric polypropylene. ....	17
Figure 10: Deuterium label scrambling observed in the polymerization of 1- <i>d</i> <sub>1</sub> -propylene. .....	20
Figure 11: Sita's acetamidinate and formamidinate preinitiators.....	25
Figure 12: Gibson's catalyst for PE growth on zinc. ....	30
Figure 13: Precatalyst used in combination with <b>17</b> by Dow Chemical to synthesize polyethylene elastomers via chain exchange using ZnEt <sub>2</sub> as a chain-shuttling agent.....	31
Figure 14: The configurational instability of alkyl, methyl CPZA complexes, coupled with the degenerative methyl group transfer process, results in atactic polymers from substoichiometrically activated <b>12</b> . ....	34
Figure 15: Schrock's initiators for living $\alpha$ -olefin polymerization. ....	37
Figure 16: Fujita's preinitiator for living propylene and ethylene polymerization and the activated ethylene insertion product modeled by DFT calculations, and Chan's model complex displaying a weak F...H interaction.....	38
Figure 17: <sup>1</sup> H NMR spectra of the alkene region of oligomeric poly(1-butene) quenched immediately and after 72 h at -10 °C.....	43
Figure 18: Low molecular weight alkyl groups as models for living polymers .....	44
Figure 19: Retrosynthetic strategy for <b>33</b> . ....	46
Figure 20: Molecular structure of <b>36'</b> -( <b>2-Et-Bu</b> ). ....	48
Figure 21: <sup>1</sup> H NMR of <b>33</b> - <sup>i</sup> <b>Bu</b> . ....	53
Figure 22: <sup>1</sup> H NMR of <b>33</b> -( <b>2-Et-Bu</b> ).....	54
Figure 23: Molecular structure of <b>33</b> - <sup>i</sup> <b>Bu</b> . ....	55
Figure 24: <sup>1</sup> H NMR of <b>33</b> -( <b>2-d</b> )- <sup>i</sup> <b>Bu</b> . ....	58
Figure 25: <sup>1</sup> H NMR of <b>33</b> -( <b>1-<sup>13</sup>C</b> )- <sup>i</sup> <b>Bu</b> . ....	59
Figure 26: <sup>1</sup> H NMR of <b>33</b> -( <b>1-<sup>13</sup>C-2-d</b> )- <sup>i</sup> <b>Bu</b> . ....	60
Figure 27: <sup>1</sup> H NMR of <b>43</b> . ....	62
Figure 28: Molecular structure of <b>46</b> and <b>36</b> - <sup>t</sup> <b>Bu</b> . ....	63
Figure 29: <sup>1</sup> H NMR of <b>44</b> . ....	65
Figure 30: Subset of CPZA cations chosen for detailed low-temperature studies. ....	66
Figure 31: Decomposition of <b>33</b> - <sup>i</sup> <b>Bu</b> , <b>33</b> -( <b>2-Et-Bu</b> ) and <b>16-PD</b> at 0 °C in chlorobenzene- <i>d</i> <sub>5</sub> , as observed by <sup>1</sup> H or <sup>13</sup> C NMR. ....	67

Figure 32: Graph of the intensity of the $\beta$ -agostic peak (relative to amidinate ethyl CH <sub>2</sub> peaks) vs. time, and the $\beta$ -agostic region of the <sup>1</sup> H NMR of <b>33-(2-<i>d</i>)-<sup>1</sup>Bu</b> .....	68
Figure 33: <sup>13</sup> C{ <sup>1</sup> H} NMR of <b>33-(1-<sup>13</sup>C-2-<i>d</i>)-<sup>1</sup>Bu</b> after 15 hours at 0 °C.....	69
Figure 34: <sup>1</sup> H NMR of <b>33-(2-<i>d</i>)-<sup>n</sup>Pr</b> as a 1:1 mixture of diastereomers. ....	72
Figure 35: Eyring plots for the decomposition/isomerization of <b>33-<sup>n</sup>Pr</b> and <b>33-<sup>i</sup>Pr</b> .....	73
Figure 36: <sup>13</sup> C{ <sup>1</sup> H} NMR methyl region of atactic PP prepared under DT conditions and isotactic PP prepared under non-DT conditions .....	88
Figure 37: Kinetic profile of living DT propylene polymerization by <b>16</b> . ....	89
Figure 38: Kinetic profile of non-DT living propylene polymerization by <b>16</b> . ....	90
Figure 39: <sup>13</sup> C{ <sup>1</sup> H} NMR of the methyl region of aliquots taken during the synthesis of an <i>a-iso-a</i> -PP triblock prepared with a <sup>13</sup> C-labeled methyl end group.....	97
Figure 40: Schematic representation of the isotactic-atactic <i>sb</i> -PP architectures targeted for tensile testing.....	98
Figure 41: Stress-strain curves showing ultimate elongation to break for the 30-40-30 <i>a-iso-a</i> -PP triblock, the 60-40 <i>a-iso</i> -PP diblock, and the 30-20-30-20 <i>a-iso-a-iso</i> -PP tetrablock. ....	100
Figure 42: <sup>13</sup> C{ <sup>1</sup> H} NMR of polypropylene samples synthesized at varying levels of activation. ....	102
Figure 43: % <i>mm</i> of the spectra of Figure 42 and other polypropylene materials obtained as a function of % activation under the same polymerization conditions.....	103
Figure 44: Comparison of the pentad distribution at 100%, 95%, 92.5%, and 90% activation.....	105
Figure 45: <sup>13</sup> C{ <sup>1</sup> H} NMR of polypropylene samples synthesized at 100%, 95% and 90% activation, showing heptad and higher levels of stereoerror assignments....	106
Figure 46: <sup>13</sup> C{ <sup>1</sup> H} NMR spectra of aliquots taken as a function of time and their difference spectra using the resonances of the <sup>13</sup> C-labeled methyl end group as an internal reference.....	108
Figure 47: Ramp profile for addition of 0.4 equivalents of <b>13</b> to change the level of activation from 60% to 100% and <i>mmmm</i> content as a function of time as determined by <sup>13</sup> C NMR. ....	109

## List of Schemes

Scheme 1: Activation of $\text{Cp}_2\text{TiCl}_2$ by $\text{AlEt}_3$ .....	4
Scheme 2: Formation of the active cationic center.....	4
Scheme 3: The Arlman-Cossee mechanism.....	5
Scheme 4: Mechanism of MAO activation.....	6
Scheme 5: Mechanism of stereocontrol in $\text{C}_2$ -symmetric metallocenes.....	7
Scheme 6: Mechanism of stereocontrol in $\text{C}_s$ -symmetric metallocenes.....	7
Scheme 7: $\beta$ -hydride transfer reactions.....	8
Scheme 8: Hemiisotactic PP from $\text{C}_1$ -symmetric metallocenes.....	14
Scheme 9: Isotactic PP from $\text{C}_1$ -symmetric metallocenes.....	15
Scheme 10: Mechanism of stereoblock-PP formation from $\text{C}_1$ -symmetric metallocenes.....	18
Scheme 11: Chain-end epimerization.....	20
Scheme 12: Proposed mechanisms of chain-end epimerization.....	21
Scheme 13: Pendant vinylidene units in PP as resulting from displacement of the coordinated $\text{H}_2$ by propylene monomer.....	22
Scheme 14: Mechanism of stereoblock-PP formation by oscillating metallocenes.....	23
Scheme 15: Counterion association mechanism proposed by Busico.....	24
Scheme 16: Coates' initiator for living propene polymerization. Syndiotactic PP is formed from the MAO-activated <b>17</b> , despite the $\text{C}_2$ -symmetry of the complex.....	26
Scheme 17: Mechanism of <i>syn</i> -PP production from derivatives of <b>17</b> .....	26
Scheme 18: Eisen's dynamic polymerization system.....	27
Scheme 19: Stereoblock-PP via reversible chain transfer to aluminum.....	29
Scheme 20: Polymer, methyl exchange in CPZA initiators.....	32
Scheme 21: Degenerative methyl group transfer.....	33
Scheme 22: Chain-end epimerization products observed by Landis.....	39
Scheme 23: Isomerization of cyclopentene insertion product.....	41
Scheme 24: Mechanism of formation of end groups <b>I-III</b> .....	43
Scheme 25: Comparison of the $\beta$ -hydride elimination of a low molecular weight alkyl group to that of a living polymer.....	45
Scheme 26: Formation of 1,3-insertions through the isomerization of 2,1-insertions.....	46
Scheme 27: Synthesis of CPZA alkyl, chloro and alkyl, methyl derivatives.....	47
Scheme 28: Treating <b>36-Me</b> with <i>tert</i> -butyl lithium produced the TMM derivative in low yield.....	50
Scheme 29: Activation of <b>37-R</b> via methyl group protonolysis.....	52
Scheme 30: Synthesis of isotopically labeled compounds via hydrozirconation.....	57
Scheme 31: Synthesis of isotopically labeled hafnium derivatives.....	61
Scheme 32: Synthesis of the hafnium <i>tert</i> -butyl cation.....	64
Scheme 33: Isotopic scrambling observed in <b>33-(1-<math>^{13}\text{C}</math>-2-<math>d</math>)-<math>^i\text{Bu}</math></b> .....	69
Scheme 34: Proposed mechanism of isobutane formation via the 'tuck-in' decomposition pathway.....	76

Scheme 35: The transition state of $\beta$ -hydride elimination of <b>33-<sup>i</sup>Bu</b> .....	77
Scheme 36: Isotopic label scrambling in <b>33-(1-<sup>13</sup>C-2-<sup>d</sup>)-<sup>i</sup>Bu</b> according to the Busico mechanism. ....	78
Scheme 37: Formation of a <i>tert</i> -butyl intermediate through coordinated alkene rotation.	79
Scheme 38: Possible transformations of <b>33-<sup>n</sup>Pr</b> and <b>33-<sup>i</sup>Pr</b> . ....	80
Scheme 39: Possible isomerization of an isobutylene, hydride complex. ....	81
Scheme 40: Formation of a <i>tert</i> -butyl intermediate through metal-assisted 1,2-hydride shift. ....	82
Scheme 41: Isotopic label scrambling in <b>33-(1-<sup>13</sup>C-2-<sup>d</sup>)-<sup>i</sup>Bu</b> according to the metal-assisted 1,2-hydride shift mechanism ....	83
Scheme 42: Synthesis of <i>a-syn</i> -PP diblock polymers via <b>53</b> . ....	92
Scheme 43: Irreversible methyl group transfer from <b>56</b> to living polymers from <b>16</b> . ....	95
Scheme 44: Synthesis of 1-( <sup>13</sup> C)- <i>a-iso-a</i> -PP. ....	96
Scheme 45: Synthesis of stereogradient-PP.....	108

## List of Tables

Table 1: Bond angles of the $\alpha$ - and $\beta$ -carbons of <b>36'-(2-Et-Bu)</b> .....	49
Table 2: Comparison of Zr-N bond lengths of <b>36-R</b> and <b>37-R</b> for R = <sup>i</sup> Pr and <sup>i</sup> Bu. ....	51
Table 3: <sup>1</sup> J( <sup>13</sup> C- <sup>1</sup> H) coupling constants for <b>33-R</b> .....	52
Table 4: Bond angles of the $\alpha$ - and $\beta$ -carbons of <b>33-<sup>i</sup>Bu</b> .....	56
Table 5: Comparison in selected bond lengths of <b>46</b> and <b>36-<sup>i</sup>Bu</b> .....	63
Table 6: Kinetic parameters of isomerization/decomposition of <b>33-R</b> .....	72
Table 7: Kinetic parameters of decomposition of <b>44</b> .....	74
Table 8: Pentad distributions of PP produced at 100% activation and 50% activation....	88
Table 9: Pentad distributions of PP stereoblocks and quenched samples.....	98
Table 10: Pentad distributions of PP synthesized at varying levels of activation. ....	103
Table 11: Pentad distributions of samples taken during stereogradient-PP synthesis....	109
Table 12: Pentad distributions of individual stereogradient-PP segments.....	109

## List of Abbreviations

acac – acetyl acetone  
<sup>n</sup>Bu – *n*-butyl  
<sup>i</sup>Bu – *iso*-butyl  
<sup>t</sup>Bu – *tert*-butyl  
Cp –  $\eta^5$ -C<sub>5</sub>H<sub>5</sub>  
Cp\* –  $\eta^5$ -C<sub>5</sub>(CH<sub>3</sub>)<sub>5</sub>  
CPHA – cyclopentadienyl hafnium acetamidinate  
CPZA – cyclopentadienyl zirconium acetamidinate  
DP – degree of polymerization  
DT – degenerative transfer  
EBI – ethylene bis-indenyl  
EBTHI – ethylene bis-tetrahydroindenyl  
Et – ethyl  
Flu –  $\eta^5$ -fluorine  
GPC – gel permeation chromatography  
Ind –  $\eta^5$ -indenyl  
MAO – methylaluminoxane  
Me – methyl  
MesNpy - H<sub>3</sub>CC(2-C<sub>5</sub>H<sub>4</sub>N)(CH<sub>2</sub>Nmesityl)<sub>2</sub>  
MMAO – modified methylaluminoxane  
MW – molecular weight  
*M<sub>n</sub>* – number average molecular weight  
*M<sub>w</sub>* – weight average molecular weight  
Naph – naphthalene  
NON – (<sup>t</sup>Bu-*d*<sub>6</sub>-*N-o*-C<sub>6</sub>H<sub>4</sub>)<sub>2</sub>O  
PDI – polydispersity (*M<sub>n</sub>*/*M<sub>w</sub>*)  
PD – poly(1-decene)  
PE – polyethylene  
PH – poly(1-hexene)  
Ph – phenyl  
PMCP – poly(methylenecyclopentane)  
PO – poly(1-octene)  
PP – polypropylene  
*a*-PP – atactic polypropylene  
*el*-PP – elastomeric polypropylene  
*iso*-PP – isotactic polypropylene  
*sb*-PP – stereoblock polypropylene  
*syn*-PP – syndiotactic polypropylene  
<sup>n</sup>Pr – *n*-propyl  
<sup>i</sup>Pr – *iso*-propyl  
py – pyridine

$R_a$  – rate of activation  
 $R_p$  – rate of propagation  
TMM – trimethylenemethane

# Chapter 1: Dynamic Processes in Ziegler-Natta Polymerization

## 1.1 Introduction

The polymerization of inexpensive, readily available monomers into high molecular weight (MW) materials with technologically relevant properties is one of the most significant accomplishments of modern chemistry. The production of high value commodity polyolefins, such as polyethylene (PE) and polypropylene (PP), reached 110 million tons in 2005.<sup>1</sup> Indeed, it is no surprise that a tremendous amount of research has focused on efforts to tailor the properties of PE and PP-based polymers in hopes of widening the scope of their applications.

Transition metal catalysts have played an important role in the development of modern polymer science ever since the seminal discoveries of Ziegler<sup>2,3</sup> and Natta<sup>4,5</sup> in the early 1950's (vide infra). Since Natta first attributed the differences in physical properties of various polypropylene materials to the relative configuration of stereocenters along the polymer backbone, one of the primary focuses of polyolefin research has been controlling the stereochemical arrangement, or *microstructure*. With the extensive library of Ziegler-Natta catalysts currently reported,<sup>6-8</sup> a wide range of polyolefins with microstructures of varying degrees of regio- and stereoregularity are currently available. However, most systems rely on the structure of the catalytic species to direct stereocontrol during polymerization, such that a particular catalyst provides a single, and hopefully unique, microstructure. The drawback to this method is that if one should require a different microstructure than what is produced by a given catalyst, the

only option is to alter the catalyst. As such, the field of Ziegler-Natta polymerization catalyst development has been fairly combinatorial in nature.

A more attractive approach would be to access a variety of microstructures from a single catalytic system, achievable by varying the reaction conditions. One way to accomplish this is to take advantage of reversible, competitive reactions (*dynamic processes*) that affect the microstructure by occurring competitively with propagation.

### 1.1.1 Ziegler-Natta Polymerization

In 1952, Ziegler<sup>2</sup> reported that insertion of ethylene into the aluminum-carbon bonds of triethyl aluminum was observed at high ethylene pressure (50-300 bar), providing long-chain trialkyl aluminum compounds. Subsequently, in an attempt to probe the effect of transition metals on this reaction, Ziegler demonstrated the *linear* polymerization of ethylene, providing high-density polyethylene (HDPE) using a supported  $\text{TiCl}_4$  catalyst activated by an alkyl aluminum cocatalyst.<sup>3</sup> Previous polymerizations of ethylene using radical initiators produced only branched PE, or low-density polyethylene (LDPE),<sup>9</sup> as shown in Figure 1. Independently, Natta<sup>4,5</sup> was able to use  $\text{TiCl}_3$ , similarly activated by alkyl aluminum cocatalysts, to produce PP which could be solvent-separated into fractions containing varying amounts of crystalline and amorphous materials. He proposed that the crystalline material contained long segments along the polymer backbone in which the chiral carbons were of the same relative stereochemistry (*isotactic*), while the amorphous material contained chiral carbons of random stereochemistry (*atactic*) (Figure 2). Today, a Ziegler-Natta catalyst has come to describe any transition metal based catalyst in combination with a main group

organometallic cocatalyst.<sup>10</sup> Having paved the way for the production of polyolefins as commodity plastics, Ziegler and Natta were jointly awarded the Nobel Prize in Chemistry in 1963.

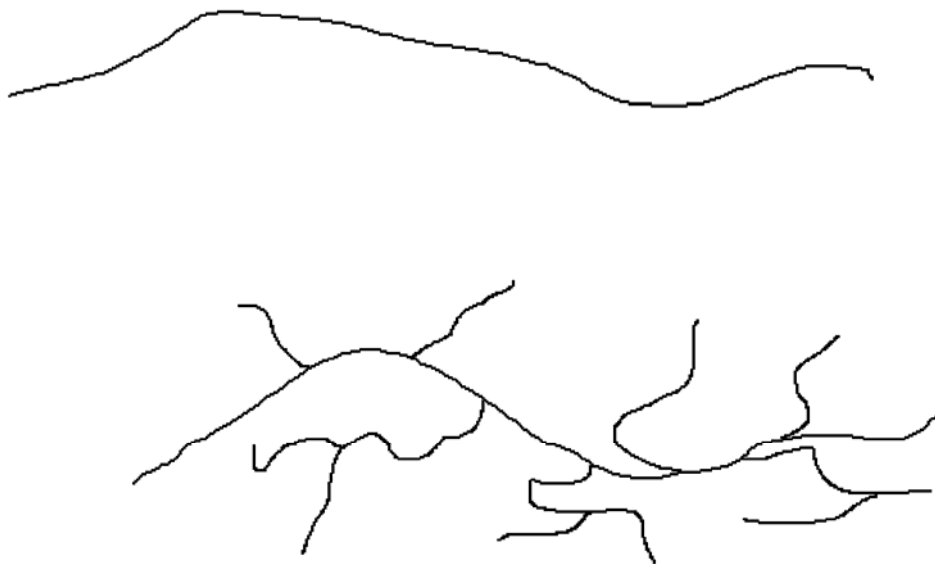


**Figure 1:** The structures of linear PE, or HDPE (top), and branched PE, or LDPE (bottom)

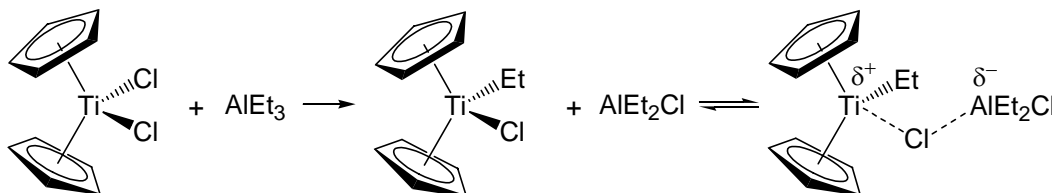


**Figure 2:** *Isotactic* and *atactic* polypropylene.

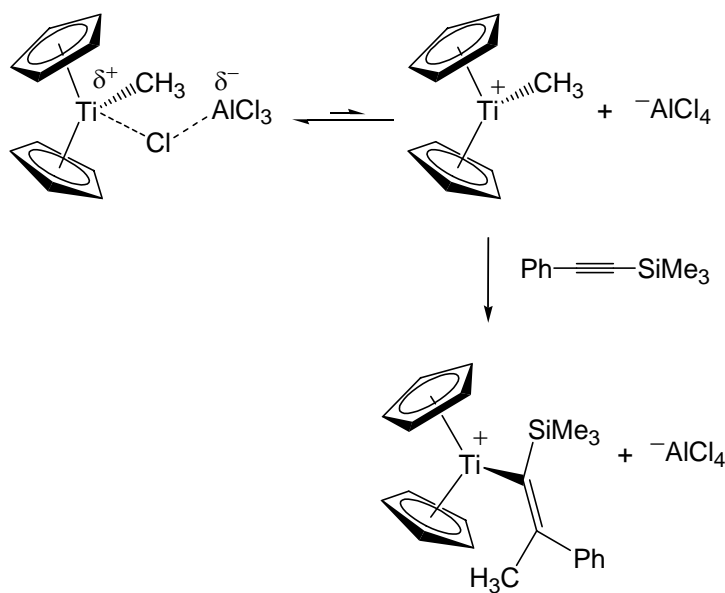
The heterogeneous nature of Ziegler-Natta catalysts made it difficult to study the mechanisms of activation and propagation. Natta<sup>11</sup> and Breslow<sup>12-14</sup> found that titanocene dichloride ( $\text{Cp}_2\text{TiCl}_2$ ,  $\text{Cp} = \eta^5\text{-C}_5\text{H}_5$ ) could be homogeneously activated with

aluminum alkyls to provide systems capable of ethylene polymerization. Breslow proposed that activation begins with alkylation of the titanium center, followed by coordination of the remaining chloride to the aluminum (Scheme 1). Eisch and co-workers<sup>15</sup> later confirmed that the active species was a cationic Ti(IV) species, generated through full abstraction of the chloride by aluminum. This was accomplished by combining  $\text{Cp}_2\text{TiCl}_2/\text{AlMeCl}_3$  with trimethyl(phenylethynyl)silane to trap the cationic species and provide the isolatable  $\{\text{Cp}_2[(\text{E})\text{-2-Me-2-Ph-1-(TMS)ethenyl}]\text{Ti}\}^+ \text{AlCl}_4^-$ , as shown in Scheme 2. While these systems provided an avenue for mechanistic studies, they unfortunately suffered from extremely low activity and rapid termination.

**Scheme 1:** Activation of  $\text{Cp}_2\text{TiCl}_2$  by  $\text{AlEt}_3$ .

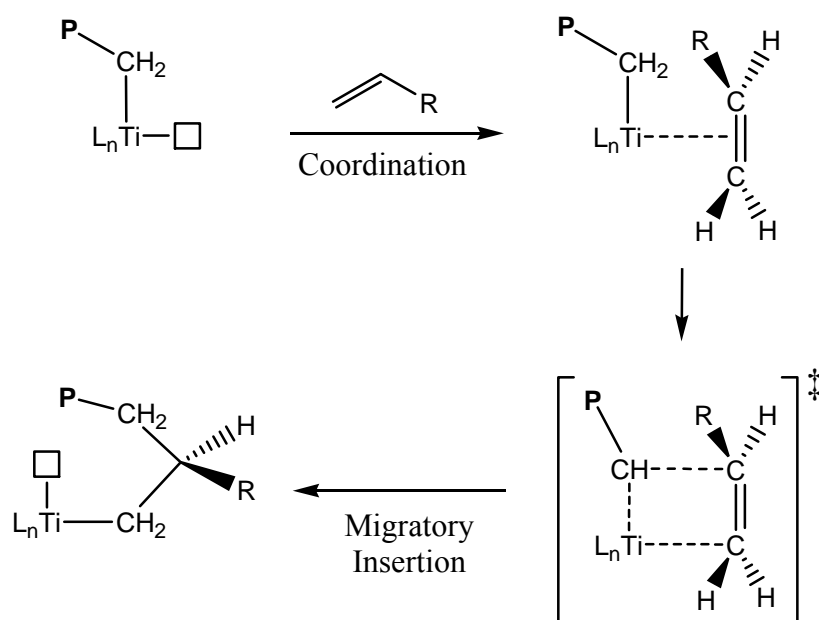


**Scheme 2:** Formation of the active cationic center



In 1964, a mechanism for propagation was proposed by Arlman<sup>16,17</sup> and Cossee<sup>18</sup>, and has since gained general acceptance (Scheme 3). It begins with an olefin coordinating to the metal center at an open coordination site, which then undergoes migratory insertion into the metal-polymer bond through a cyclic four-membered transition state. This then opens a new coordination site for olefin complexation, and the process is repeated.

**Scheme 3:** The Arlman-Cossee mechanism.

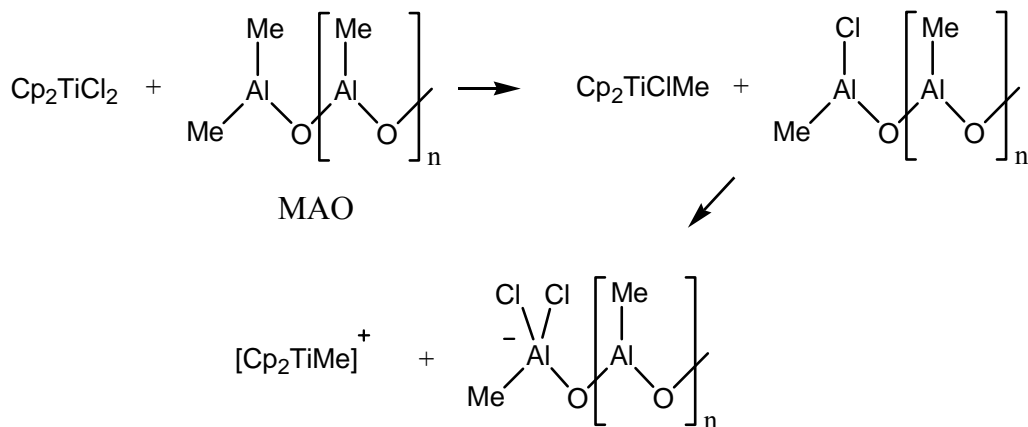


In 1980, Kaminsky<sup>19,20</sup> reported the serendipitous discovery that upon adding a trace amount of water to a  $\text{Cp}_2\text{MCl}_2/\text{AlMe}_3$  system, ethylene polymerization activities were dramatically increased. It was later determined that the water would react with trimethyl aluminum *in situ* to produce methylaluminumoxane (MAO), and polymerizations utilizing pre-prepared MAO as the cocatalyst confirmed that this was indeed the cause of the increased activity. MAO is believed to be oligomeric in nature, although the exact structure is unclear. The mechanism of activation proceeds in a similar manner as the aluminum alkyls through a methyl/chloro exchange, followed by a chloride abstraction to

produce a cationic metal center (Scheme 4).<sup>21</sup> Since the activation with MAO is a reversible process, an extremely large excess is commonly used.<sup>22</sup> Despite the success with ethylene polymerization, these systems produced only low molecular weight *a*-PP.<sup>19</sup>

20

**Scheme 4:** Mechanism of MAO activation.

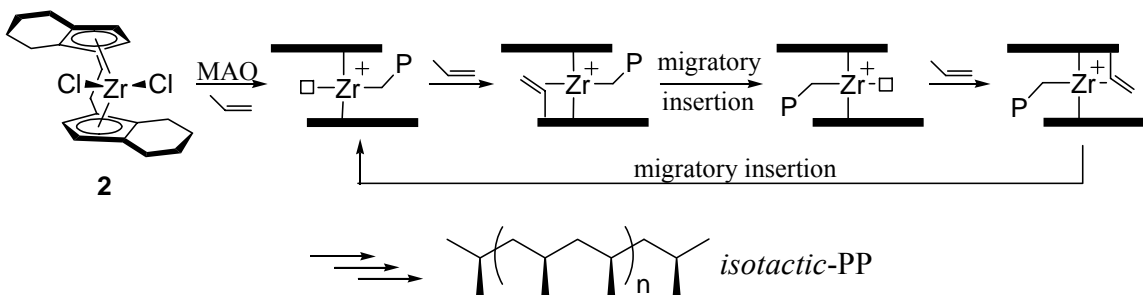


### 1.1.2 Symmetry-Microstructure Relationships

A significant advance in propylene polymerization was accomplished by the development of *ansa*-bridged metallocenes. Ewen<sup>23</sup> was first able to show the relationship between catalyst symmetry and microstructural control in 1984, when he used Brintzinger's<sup>24</sup> *ansa*-bridged titanocene (EBI)TiCl<sub>2</sub> (**1**, EBI = ethylene bis-indenyl) to initiate propylene polymerization when activated with MAO. The material consisted of a mixture of atactic PP (*a*-PP) and isotactic PP (*iso*-PP), leading Ewen to propose that the *racemic* (*rac*) isomer of **1** was highly enantioselective (producing *iso*-PP) while the *meso* isomer had no enantiofacial selectivity (producing *a*-PP). His theory was later confirmed when Kaminsky and Brintzinger<sup>25</sup> initiated the polymerization of propylene using MAO activated (EBTHI)ZrCl<sub>2</sub> (**2**, EBTHI = ethylene bis-tetrahydroindenyl) as the

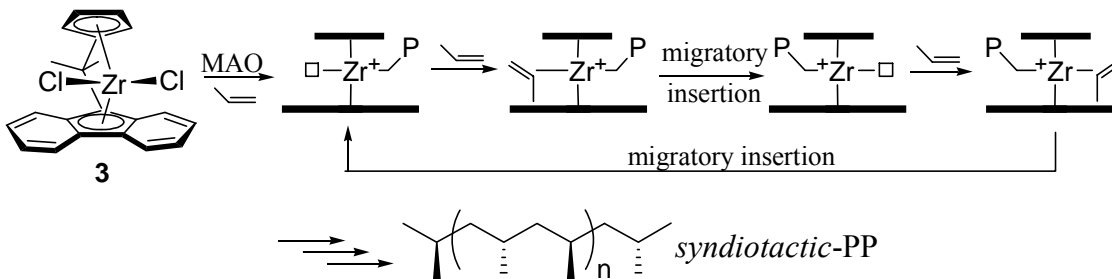
pure *racemic* isomer to produce only *iso*-PP. Steric interactions direct the polymer chain away from the indenyl ligands, and methyl group of the coordinating propylene is directed *anti* to the polymer chain.<sup>22</sup> Since these catalysts are  $C_2$ -symmetric, the coordination sites are homotopic and incoming propylene units will coordinate to both with the same face selectivity, as shown in Scheme 5.

**Scheme 5:** Mechanism of stereocontrol in  $C_2$ -symmetric metallocenes.



Ewen,<sup>26</sup> recognizing how the relationship between the coordination sites could effect the microstructure, later developed a  $C_s$ -symmetric catalyst,  $Me_2C(Cp)(9-Flu)ZrCl_2$  (**3**, Flu = fluorenyl). The coordination sites of **3** are enantiotopic by mirror symmetry, and will coordinate propylene units with the *opposite* face selectivity (Scheme 6). This results in *syndiotactic* polypropylene (*syn*-PP), in which each chiral center is of opposite chirality. This microstructure had not been previously achieved with heterogeneous systems. The relationships between PP stereochemical microstructure and the symmetry of the catalyst are commonly referred to as “Ewen’s symmetry rules”.<sup>22</sup>

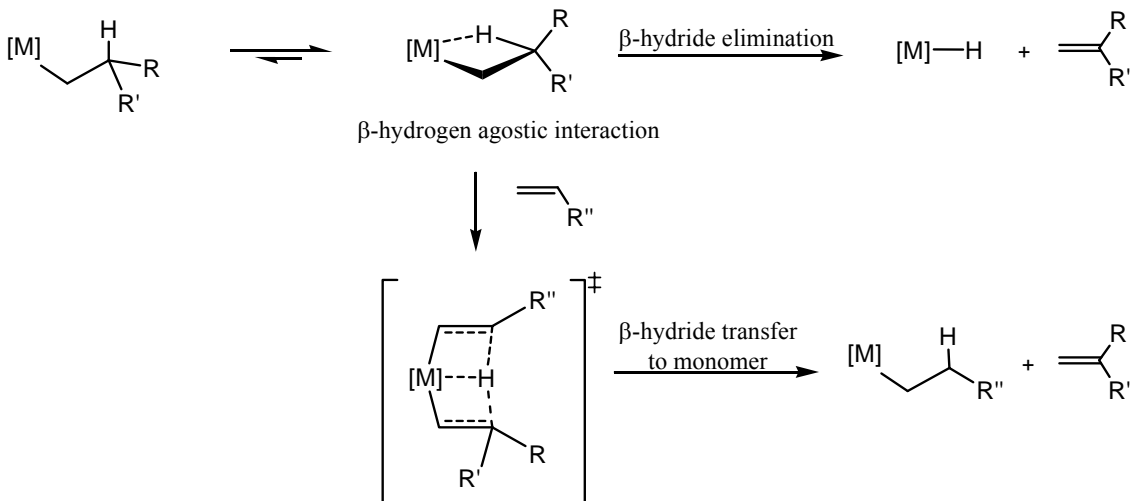
**Scheme 6:** Mechanism of stereocontrol in  $C_s$ -symmetric metallocenes.



### 1.1.3 Termination Events

Termination events are competitive, irreversible reactions that halt further growth of a polymer chain. Once such termination event, *β-hydride elimination*, is a unimolecular process in which the  $\beta$ -hydrogen of the growing polymer chain is transferred to the metal center through a four-centered transition state, resulting in a metal-hydride complex and a polymer with an alkene end group (Scheme 7).<sup>27</sup> The metal-hydride species can then insert monomer into the M-H bond and reinitiate propagation of a new polymer chain. It is widely believed that an agostic interaction between the  $\beta$ -hydrogen and the metal center precedes formation of the transition state,<sup>28</sup> and so attempts have been made at preventing the elimination through the use of bulky ligands which prevent formation of a  $\beta$ -agostic interaction.

**Scheme 7:**  $\beta$ -hydride transfer reactions.



Another termination event, *β-hydride transfer to monomer*, is a bimolecular process in which the  $\beta$ -hydrogen of the growing chain is transferred to a free monomer, producing the alkene terminated polymer and a new metal-alkyl complex (equivalent to monomer insertion into a M-H bond).<sup>27</sup> The reaction involves a cyclic 6-center transition

state in which the  $\beta$ -hydrogen is transferred to the monomer as the monomer binds to the metal center in a concerted manner. Theoretical studies suggest that the  $\beta$ -hydride transfer is metal assisted,<sup>29, 30</sup> and so the  $\beta$ -agostic interaction could be considered a precursor to this reaction as well.

A third common termination event is *chain transfer to aluminum*. Since MAO often contains unreacted trimethylaluminum,<sup>31</sup> and other trialkyl aluminum compounds are frequently used as scavengers,<sup>32-34</sup> this is a common facet of Ziegler-Natta polymerization systems. In this reaction, the polymer chain on the active metal is exchanged with an alkyl group on the aluminum center, providing an active metal-alkyl species and an aluminum terminated polymer. Recently, Dong and co-workers<sup>35</sup> have shown that the *rac*-Me<sub>2</sub>Si(2-Me-4-Naph-Ind)<sub>2</sub>ZrC<sub>2</sub>/MAO (Naph = naphthyl, Ind = indenyl) system engages in efficient chain transfer to aluminum, such that aluminum terminated *iso*-PP ( $M_n = 24,600-179,000$  PDI = 2.10-2.94) is produced with high end-group selectivity. Such Al-terminated polymers have been used as precursors to hydroxyl-terminated PP<sup>36</sup> and block copolymers.<sup>37</sup>

#### 1.1.4 Microstructural Analysis

The ability to generate unique microstructures of polypropylene and other polyolefins necessitated a reliable method to analyze these microstructures. The most common technique employed is <sup>13</sup>C NMR spectroscopy.<sup>22, 38-40</sup> The resonance of a pendant methyl group in a PP chain is affected by not only its own chirality, but the relative chirality of the surrounding methyl groups within several units. Two adjacent methyl groups along the PP back bone, called a *dyad*, have two possible relative

configurations. A pair of the same chirality is called a *meso* dyad, abbreviated *m*, while a pair of opposite chirality called a *racemic* (or *racemo*) dyad, and abbreviated *r* (Figure 3). The microstructure is commonly described in terms of groups of five stereocenters, or *pentads*, although larger groups can be resolved at higher field strengths. There are ten possible unique pentads, which are referred to in terms of the dyads of which they are comprised (Figure 4). Pentads which are mirror images of each other, such as *mmrm* and *mrmm*, are not distinguishable by NMR and are considered the same pentad.

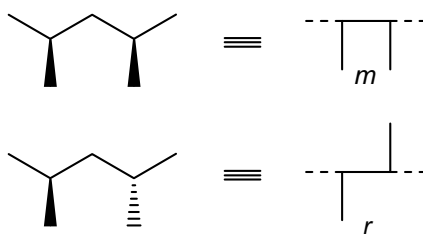


**Figure 3:** The *meso* (*m*) and *racemic* (*r*) dyads.

Using this terminology, a perfectly isotactic PP sample would have a single resonance in the  $^{13}\text{C}$  NMR in the *mmmm* region, and a perfectly syndiotactic PP sample would have a single resonance in the *rrrr* region. Perfectly atactic PP would feature all pentads, with a *mmmm:mmmr:rmmr:mmrr:(mmrm+rmrr):rmm:rrrr:rrrm:mrrm* ratio of 1:2:1:2:4:2:1:2:1. Pentad distributions are often presented in this manner because it is in this order, from high field to low field, respectively, that they appear in the  $^{13}\text{C}$  NMR, with the *mmrm* and *rmrr* regions overlapping. PP samples of low stereoregularity are commonly described in terms of the *triad* content; perfectly atactic PP would have a *mm:mr:rr* ratio of 1:2:1.

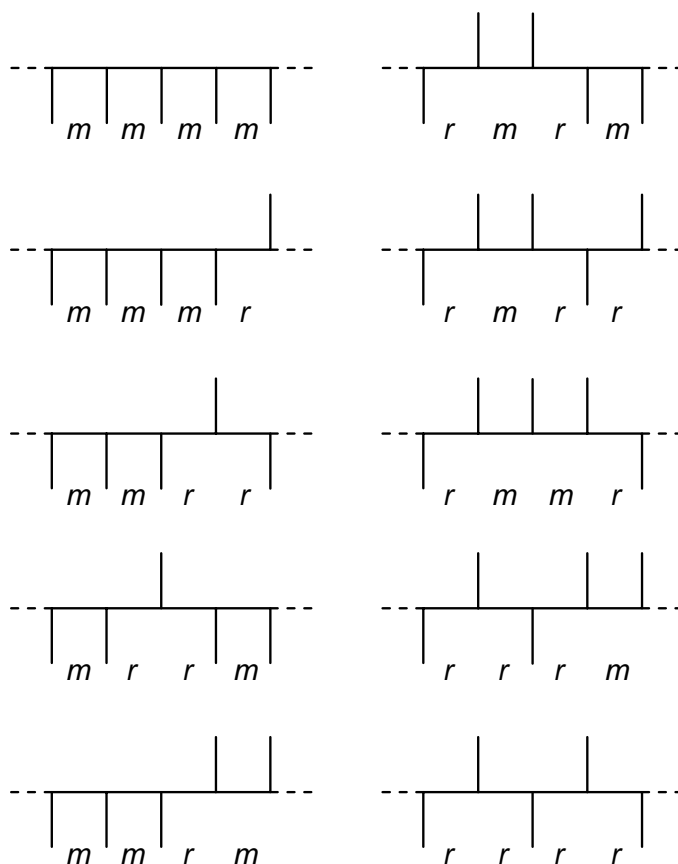


**Figure 4:** The ten possible stereochemical pentads of PP.

Of course, the vast majority of polymerization systems do not produce perfectly stereoregular polymers.<sup>7, 22</sup> The stereoerror resonances are not only useful to quantify the stereoregularity (reported as  $[mmmm]$  for *iso*-PP and  $[rrrr]$  for *syn*-PP), but the types of stereoerrors present are indicative of the mechanism of stereocontrol. If the ligands of a catalyst are directing face selectivity, the system is said to be under *enantiomorphic-site control*, which is commonly referred to simply as *site control*. For *iso*-PP from site control catalysts such as **2**, a stereoerror has no effect on the stereoselectivity of the next insertion, and isolated stereoerrors are observed (Figure 5). These appear in the <sup>13</sup>C NMR as resonances in the *mmm**r*, *mm**rr* and *mrr**m* regions in a 2:2:1 ratio, respectively. Syndiotactic PP from site control catalysts such as **3** has stereoerror resonances in the

*rrrm*, *rrmm* and *rmmr* regions, once again in a 2:2:1 ratio, respectively. Since the next insertion after a stereoerror is unaffected, site control is said to have error correction.

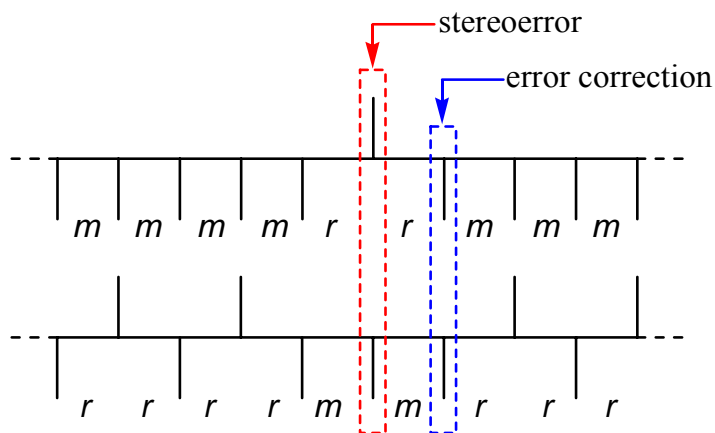


**Figure 5:** Stereoerrors in isotactic (top) and syndiotactic (bottom) PP under enantiomorphic-site control.

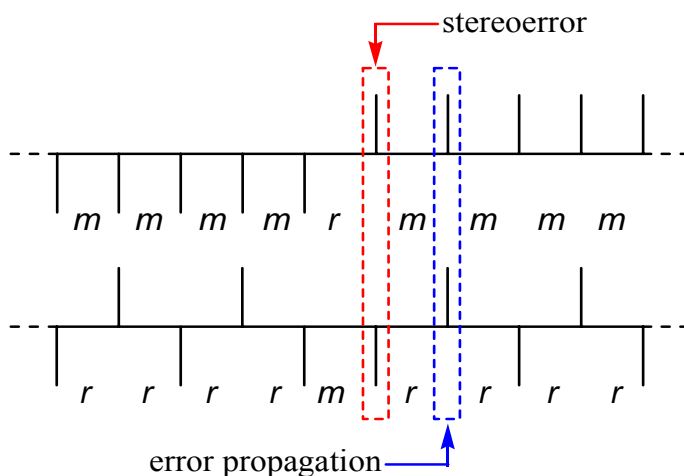


**Figure 6:** Stereoerrors in isotactic (top) and syndiotactic (bottom) PP under chain-end control.

Another mechanism of stereoselectivity is called *chain-end control*, which is much less common than site control. During isotactic propagation under chain-end control, the chirality of the last inserted monomer determines the face selectivity of the next. When a stereoerror occurs in this case, the chain-end now has the opposite chirality and the error is propagated until the next stereoerror, resulting in an isotactic-isotactic

block structure (Figure 6). This can be observed in the  $^{13}\text{C}$  NMR by the resonances in the *mmmr* and *mrrm* regions in a 1:1 ratio. Similarly, *syn*-PP from catalysts under chain-end control exhibit resonances in the *rrrm* and *rrmr* regions in a 1:1 ratio.

### 1.2 Site Isomerization

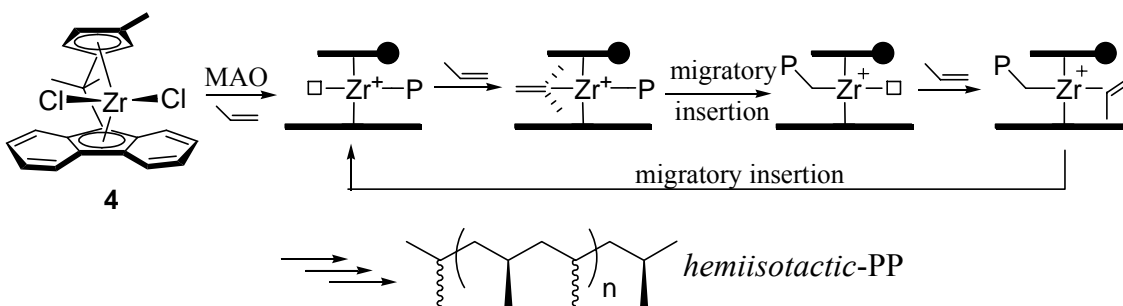
Occasionally, the polymer chain will move from one site to the other *without* a migratory insertion step. This process will be referred to as *site isomerization*, although it is also commonly referred to as *site epimerization* or *back-skipping*. In the case of the  $\text{C}_2$ -symmetric metallocenes, site isomerization has no effect on the microstructure of the material by virtue of the homotopic coordination sites. In the  $\text{C}_s$ -symmetric metallocenes, site isomerization results in two consecutive insertions of the same enantioface, and will be evident in the polymer as an isolated *m* stereoerror (i.e.: ...*rrrmrrr*...). In this case, it is clear how ability of the site isomerization process to compete with propagation can have a significant effect on the microstructure, and hence the properties, of the polymer. With this in mind, some catalysts are designed to take advantage of site isomerization.

#### 1.2.1 $\text{C}_1$ -symmetric Metallocenes: Hemiisotactic and Isotactic Polypropylene

Substituting alkyl groups onto one side of the Cp ligand of **3** removes the mirror plane of symmetry, resulting in chiral complexes. These  $\text{C}_1$ -symmetric catalysts, depending on the size of the alkyl group, can provide varying microstructures. The methyl substituted catalyst **4**<sup>41</sup> polymerizes according to the two site model in the same manner as **3**. However, the steric interaction of the methyl group removes the ability of the ligands to direct the facial selectivity of the opposite site, such that every other

insertion is without stereocontrol. This results in PP with methyl groups of alternating random and uniform chirality, called *hemiisotactic* (Scheme 8). Perfectly hemiisotactic PP has a pentad distribution of 3:2:1:4:0:0:3:2:1. Recently, Bercaw<sup>42</sup> and Ewen<sup>43</sup> have developed several  $C_1$ -symmetric metallocene derivatives that produce an isotactic-hemiisotactic-PP microstructure, meaning that every other stereocenter is of uniform configuration and the rest are aligned with its neighbors 60-75% of the time. This produces an isotactic-hemiisotactic stereoblock-like microstructure, and it was found that some of these materials had elastomeric properties.

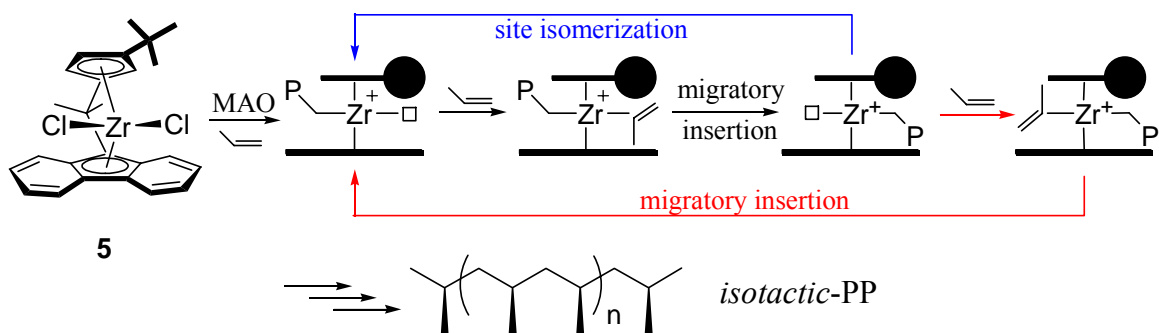
**Scheme 8:** Hemiisotactic PP from  $C_1$ -symmetric metallocenes.



Marks<sup>44</sup> and Kaminsky<sup>45</sup> demonstrated that different microstructures, some with higher levels of isotacticity, could be achieved with other  $C_1$ -symmetric metallocenes. It was proposed that increased steric crowding of one coordination site would favor site isomerization of the polymer chain to the less hindered site. Therefore, upon migratory insertion, a competition exists between site isomerization and olefin coordination to the less hindered site. The microstructure of the PP produced will be dependant upon the relative rates of olefin insertion and site isomerization at each site. If the steric repulsions at one site are strong enough, the polymer will back-skip after each insertion, and propagation will only proceed at the isoselective site. This mechanism was invoked to explain the *iso*-PP ( $M_n = 40,000-185,000$ ) obtained from **5**<sup>45</sup> (Scheme 9, blue pathway).

A wide variety of  $C_1$ -symmetric metallocenes catalysts are now available, capable of producing many microstructures with varying degrees of control.<sup>22, 46</sup>

**Scheme 9:** Isotactic PP from  $C_1$ -symmetric metallocenes.



Recently, the Bercaw<sup>47</sup> group published a study analyzing the mechanism of *iso*-PP formation from **5**. It was previously noted<sup>44, 48</sup> that the isotacticity of the polymers from  $C_1$ -metallocenes may not be a result of site isomerization, but that both sites may preferentially coordinate the same monomer face. In the case of **5**, the *tert*-butyl group may have a stronger influence on the orientation of the polymer, and hence the monomer coordination, than the fluorenyl ligand. As such, the complex would undergo insertions at both sites with the same face selectivity, acting as a pseudo- $C_2$ -symmetric metallocene (Scheme 9, red pathway). Through a variety of kinetic studies and microstructural analyses involving **5** and structurally similar derivatives, Bercaw claims that the pseudo- $C_2$ -symmetric mechanism (alternating insertion sites) is dominant over the site isomerization mechanism. Furthermore, using the information gathered from derivatives of **5** with various ligand substitutions, Bercaw designed a catalyst that was expected to produce *iso*-PP via the exclusive site-isomerization mechanism. By replacing the *tert*-butyl group with a 2-methyl-2-adamantyl group and the fluorenyl ligand with the enormous 1,1,4,4,7,7,10,10-octamethyl-1,2,3,4,7,8,9,10-octahydrodibenzo[*b,h*]fluorenyl ligand (Figure 7), the authors hoped to increase the rate of site isomerization and

simultaneously increase monomer face selectivity at the active site. The PP produced from **6** was isotactic with  $[m m m m] > 99\%$  ( $M_n = 370,000-425,000$ , PDI = 1.39-1.77), and had an extremely high melting point of 167 °C.

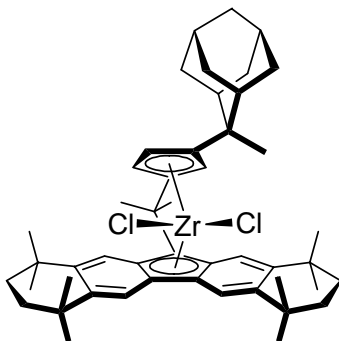


**Figure 7:** Complex **6** produces *iso*-PP with  $[m m m m] > 99\%$ .

### 1.2.2 $C_1$ -symmetric Metallocenes: Elastomeric Polypropylene

Aside from the crystalline (isotactic) and amorphous (atactic) PP materials, Natta<sup>49</sup> was able to isolate fractions exhibiting elastomeric properties. To explain this phenomenon, he proposed that the material contained alternating blocks of isotactic and atactic segments (Figure 8). The elastomeric properties were attributed to the crystallization of isotactic segments within the amorphous network, providing physical cross-links. Elastomeric PP (*el*-PP) is a thermoplastic elastomer, which means it is a soluble material that can be reversibly melted or solidified.<sup>50</sup> This provides many advantages over chemically cross-linked materials, including the abilities to be injection molded and recycled. While several groups attempted to improve upon the synthesis of *el*-PP, it wasn't until 1982 that Collette and co-workers<sup>51, 52</sup> at DuPont developed heterogeneous alumina-supported zirconium and titanium alkyls that produced significant amounts of elastomeric material. This material was found to be stereochemically

heterogeneous, with fractions containing different degrees of isotacticity and molecular weights.

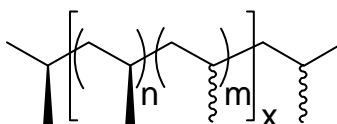


**Figure 8:** Atactic-isotactic stereoblock polypropylene (*sb*-PP)

The first homogeneous catalyst which produced *el*-PP was reported in 1990 by Chien and co-workers.<sup>53</sup> The  $C_1$ -symmetric titanium bridged-metallocene **7** (Figure 9), upon activation with MAO, provided elastomeric *el*-PP of reasonably high molecular weights and fairly narrow polydispersities ( $M_n = 98,400$ , PDI = 1.7). Chien also attributed the elasticity to an isotactic-atactic block structure, resulting from the interconversion of propagating species with the polymer chain either *syn* or *anti* to the *ansa*-methyl group during polymerization (Scheme 10). Sequential olefin insertions occur at one site before a site isomerization takes place, after which sequential insertions then take place at the opposite site. This mechanism is somewhat counterintuitive; in order to have sequential insertions at two different sites, it would require either insertion *without* migration (competitive with site isomerization) or a single back-skip after each insertion *regardless* of which site is favored.

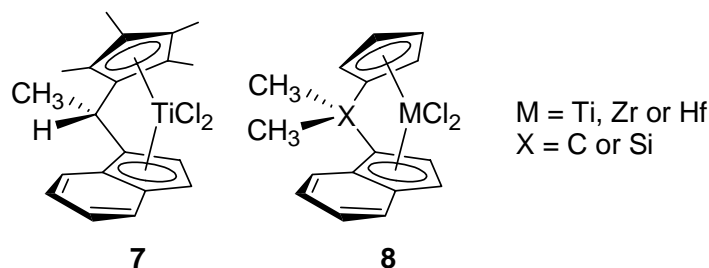
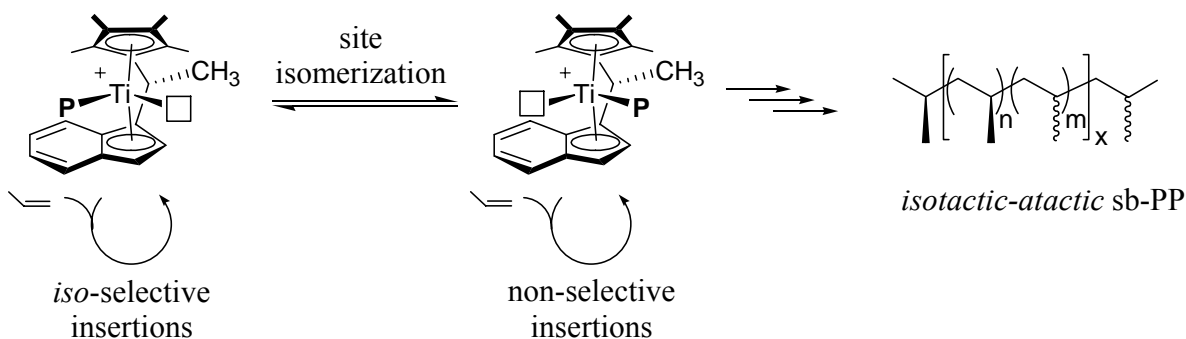


**Figure 9:**  $C_1$ -symmetric metallocenes capable of producing elastomeric polypropylene.

**Scheme 10:** Mechanism of stereoblock-PP formation from  $C_1$ -symmetric metallocenes.



Collins and co-workers<sup>54, 55</sup> used similar catalysts (**8**, Figure 9) to examine the microstructure of the *el*-PP produced with  $C_1$ -symmetric catalysts. Collins used computer modeling studies in an attempt to match three possible mechanism of propagation with the microstructures observed by <sup>13</sup>C NMR. One of the models was that invoked by Chien to account for the *el*-PP produced from **7**, in which sequential insertions occur at an isoselective site until a site isomerization, and then sequential insertions occur at a non-selective site. The second model was a random insertion model, in which monomer will insert competitively at either the isoselective or the non-selective site, which does not necessarily produce a stereoblock architecture. The final model involved strictly alternating insertions at both sites, which will produce a hemiisotactic microstructure if the selectivity at the isoselective site is particularly high. By varying certain parameters relating to the selectivities and reactivities of the sites for each model, Collins revealed that any of these three models of propagation are feasible to produce PP with the same pentad distribution as that observed for *el*-PP from  $C_1$ -symmetric metallocenes **7** and **8**, and that this does not necessarily indicate a stereoblock microstructure.

Recent work with  $C_1$ -symmetric metallocenes towards *el*-PP attributes the elastomeric properties to the low to moderate overall crystallinity of the material,<sup>56</sup> as opposed to a particular microstructure (stereoblock or otherwise). The level of crystallinity will be determined by the content of long isotactic segments, which in turn is determined by the competition between propagation and site isomerization between sites of differing facial selectivities. Despite the uncertainty in the exact microstructure, Rieger<sup>57</sup> has developed many catalysts which have produced low crystallinity PP materials with properties ranging from stiff plastomers to thermoplastic elastomers. Due to the competition between bimolecular propylene insertion and unimolecular site isomerization, some of these catalysts allow modest control over stereoerror content through varying monomer concentration.<sup>58</sup>

### 1.3 Chain-End Epimerization

When polymerizing propylene with isoselective metallocene catalysts at low monomer concentration, a larger number of stereoerrors than could be accounted for by random misinsertions was observed.<sup>59-62</sup> It was found that the last inserted propylene unit is able to reverse its stereochemistry, a process known as *chain-end epimerization* (Scheme 11). Chain-end epimerization is competitive with propagation at low propylene concentrations, leading to an inflated number of stereoerrors. Busico<sup>61, 62</sup> proposed a mechanism involving successive  $\beta$ -hydride elimination, olefin rotation and reinsertion steps through a tertiary alkyl center towards the opposite methyl group (Scheme 12a); a process similar to that which has been invoked to explain the isomerizations observed in the hydrozirconation of internal olefins,<sup>63</sup> as well as the chain-walking observed in late

transition-metal polymerizations<sup>64, 65</sup> and in 1-hexene polymerizations by metallocene catalysts.<sup>66</sup> While this may explain the reversal of stereochemistry, it does not account for the occurrence of deuterium labels on methyl groups of *correct* stereochemistry in polymerizations of 1-*d*<sub>1</sub>-propylene<sup>67, 68</sup> (Figure 10) or 2-*d*-propylene.<sup>68, 69</sup> In order to be consistent with Busico's mechanism, the system must also be able to switch coordination to the opposite enantioface (Scheme 12b).

**Scheme 11:** Chain-end epimerization.

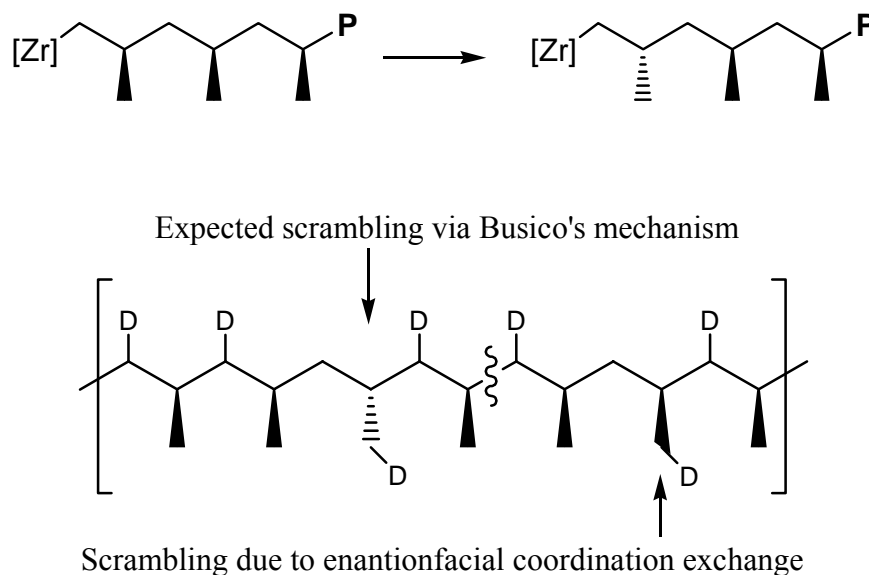


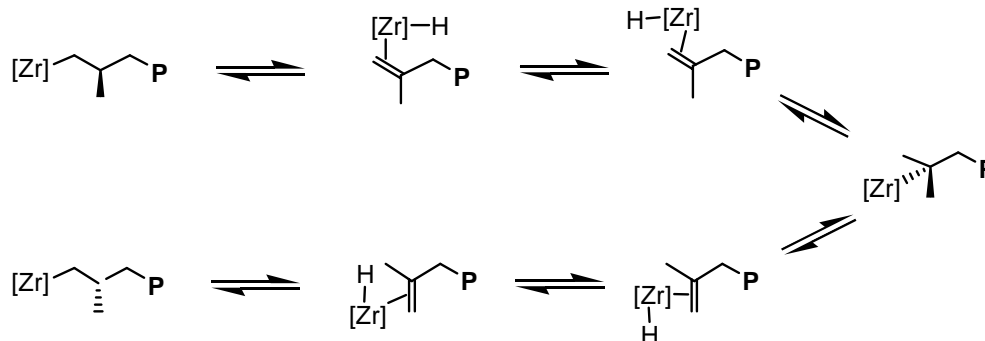
**Figure 10:** Deuterium label scrambling observed in the polymerization of 1-*d*<sub>1</sub>-propylene.

Another other mechanism, proposed by Resconi,<sup>70</sup> involves a dihydrogen/ $\eta^3$ -allyl intermediate. The advantage of this mechanism is that it allows scrambling of a deuterium label to occur independently of the chain-end epimerization process, as depicted in Scheme 12c with poly(2-*d*-propylene), eliminating the need for a

coordination-face exchange to take place. In addition, the  $\eta^3 \rightleftharpoons \eta^1$  interconversion, allowing rotation around the C-C single bond, is a well-known process.<sup>71</sup>

**Scheme 12:** Proposed mechanisms of chain-end epimerization.

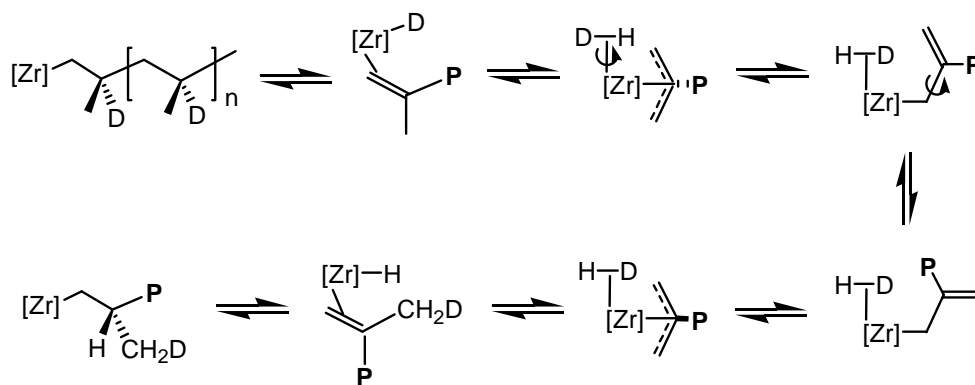
**a:** Busico's mechanism



**b:** Coordination switching



**c:** Resconi's mechanism

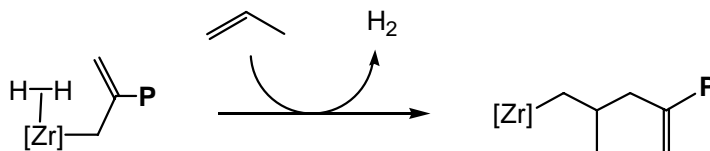


[Zr] = Zirconocene catalyst    **P** = isotactic polypropylene

In 2002, Bercaw<sup>72</sup> published the results of an experiment designed to distinguish between the two mechanisms. Using the MAO-activated zirconocene catalysts **2** and *rac*-(EBI)ZrCl<sub>2</sub> (**9**), polymerizations were carried out using a doubly labeled propylene,

$^{13}\text{CH}_3\text{-CD}=\text{CH}_2$ . Examining the polymer by  $^{13}\text{C}$  NMR DEPT experiments determined that there were no doubly labeled methyl groups ( $^{13}\text{CH}_2\text{D}$ ) present in the polymer, consistent *only* with Busico's mechanism. While the observation of pendant vinylidene units along the main chain and the generation of dihydrogen during propylene polymerizations suggests that the  $\eta^3 \rightleftharpoons \eta^1$  interconversion does occur (Scheme 13), this experiment demonstrated that the Resconi mechanism is not a cause for chain-end epimerization.

**Scheme 13:** Pendant vinylidene units in PP as resulting from displacement of the coordinated  $\text{H}_2$  by propylene monomer.



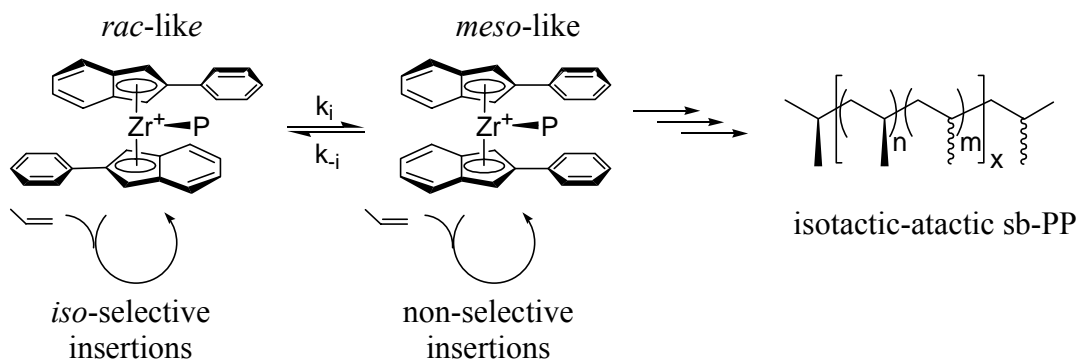
## 1.4 Ligand Isomerization

### 1.4.1 Oscillating Metallocenes

A new type of catalyst for the production of *el*-PP was reported by Coates and Waymouth<sup>73</sup> in 1995. The unbridged metallocene catalyst (2-PhInd)<sub>2</sub>ZrCl<sub>2</sub> (**11**), upon activation with MAO, produced PP with elastomeric properties ( $M_n = 8,570\text{-}423,300$ , PDI = 1.7-2.8), once again attributed to a stereoblock microstructure. The mechanism of stereoblock formation in this case was said to result from the interconversion of the active species between “*rac*-like” and “*meso*-like” rotational conformations during propagation (Scheme 14). The  $C_2$ -symmetric *rac*-like conformation produces isotactic polymer according to the two-site model of propagation, while the  $C_{2v}$ -symmetric *meso*-like conformation produces atactic polymer. Indeed, ethylene bridged analogs of **11** in both

*racemic* and *meso* isomers appeared to confirm this hypothesis. The dynamic nature of unbridged **11** enables oscillation between isotactic and atactic modes of propagation, resulting in an isotactic-atactic block structure. A variety of (2-ArInd)<sub>2</sub>ZrCl<sub>2</sub>-type catalysts with alkyl groups substituted at various positions have also been thoroughly investigated.<sup>74</sup>

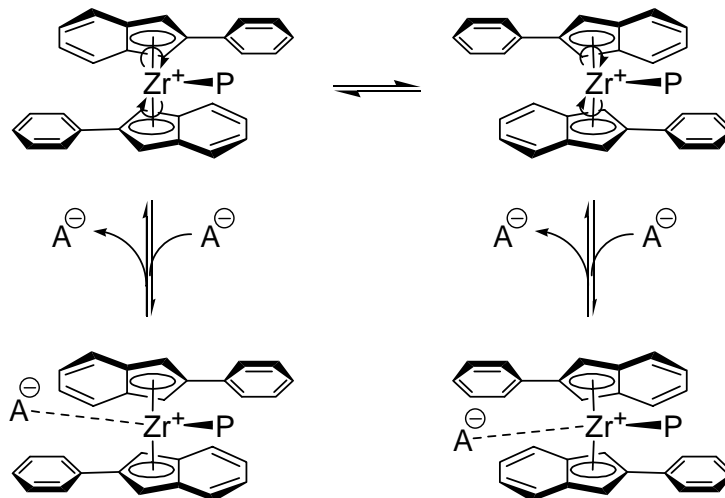
**Scheme 14:** Mechanism of stereoblock-PP formation by oscillating metallocenes.



While the mechanism depicted in Scheme 14 appears reasonable on paper, it has come under dispute due to recent theoretical and experimental findings.<sup>75-77</sup> Solution NMR investigations of the catalytic species did not provide evidence for a slow *meso/rac*-like conformation exchange, and the barrier for interconversion was calculated to be quite low at 2 – 5 kcal mol<sup>-1</sup> (*cf.* 5 – 15 kcal mol<sup>-1</sup> for monomer insertion). Also, the PP materials produced are quite heterogeneous and can be solvent-separated into fractions with properties ranging from completely amorphous to highly crystalline, suggesting the presence of more than one catalytic species. Based on the surprisingly high dependence of the microstructure on the cocatalyst and solvents employed, and detailed high-field <sup>13</sup>C-NMR analysis of the materials, Busico<sup>77</sup> has proposed a mechanism that involves the catalyst rapidly oscillating between enantiomeric *rac*-like conformations, which can be reversibly “locked” by close counteranion association

(Scheme 15). In the “unlocked” mode, the rapidly interconverting active centers produce atactic polymer, while the “locked” centers are frozen in a *rac*-like conformation and propagate in an isotactic fashion. In support of this mechanism, polymerizations run in polar solvents, favoring ion dissociation, provided almost pure *a*-PP.

**Scheme 15:** Counterion association mechanism proposed by Busico.



#### 1.4.2 Post-Metallocene

In 2000, Sita<sup>78</sup> reported the cyclopentadienyl zirconium acetamidinate (CPZA) preinitiator,  $\text{Cp}^*\text{ZrMe}_2[\text{N}(\text{Et})\text{C}(\text{Me})\text{N}(\text{tBu})]$  (**12**,  $\text{Cp}^* = \eta^5\text{-C}_5\text{Me}_5$ ). When activated by a stoichiometric amount of  $[\text{PhNMe}_2\text{H}][\text{B}(\text{C}_6\text{F}_5)_4]$  (**13**), this system is capable of *living* isoselective polymerization of 1-hexene at  $-10^\circ\text{C}$  (for more on *living* polymerization, see section 1.7). Subsequently, a report was published<sup>79</sup> detailing a modified system in which the distal methyl group was replaced by a hydrogen (Figure 11). This formamidinate derivative,  $\text{Cp}^*\text{ZrMe}_2[\text{N}(\text{Et})\text{C}(\text{H})\text{N}(\text{tBu})]$  (**14**), when activated by **13**, produces *atactic* poly(1-hexene) (*a*-PH), despite having the same  $\text{C}_1$ -symmetry as **12**. The reason for this is the inherent configurational instability of the formamidinate ligand

in the activated cationic form,  $\{\text{Cp}^*\text{ZrMe}[\text{N}(\text{Et})\text{C}(\text{H})\text{N}(\text{tBu})]\}\text{[B}(\text{C}_6\text{F}_5)_4\text{]}$  (**15**), as opposed to the cationic form of **12**,  $\{\text{Cp}^*\text{ZrMe}[\text{N}(\text{Et})\text{C}(\text{Me})\text{N}(\text{tBu})]\}\text{[B}(\text{C}_6\text{F}_5)_4\text{]}$  (**16**), which is configurationally stable. Since the racemization of **15** occurs at a higher rate than 1-hexene propagation, the isoselectivity exhibited by **16** is lost.

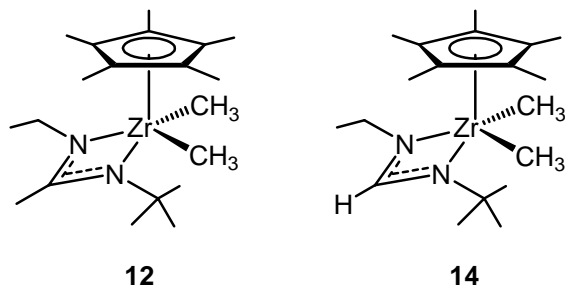
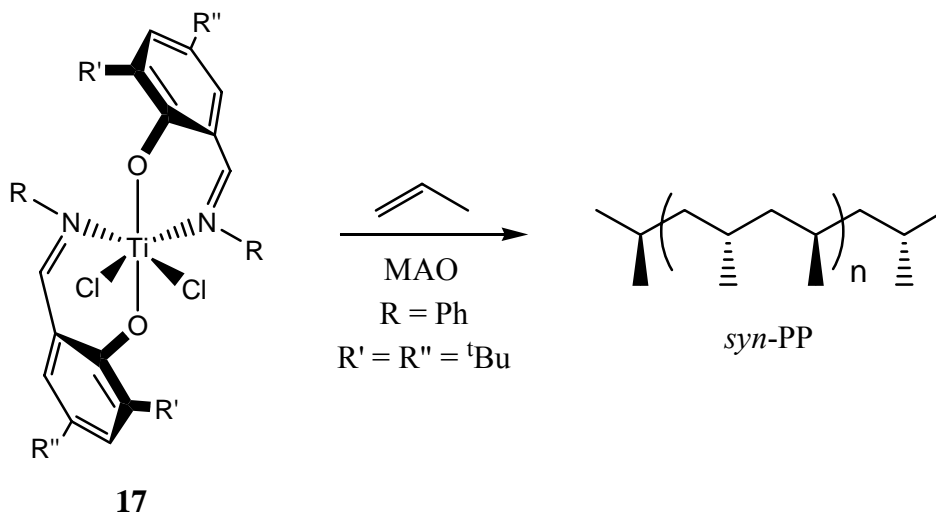


**Figure 11:** Sita's acetamidinate and formamidinate preinitiators.

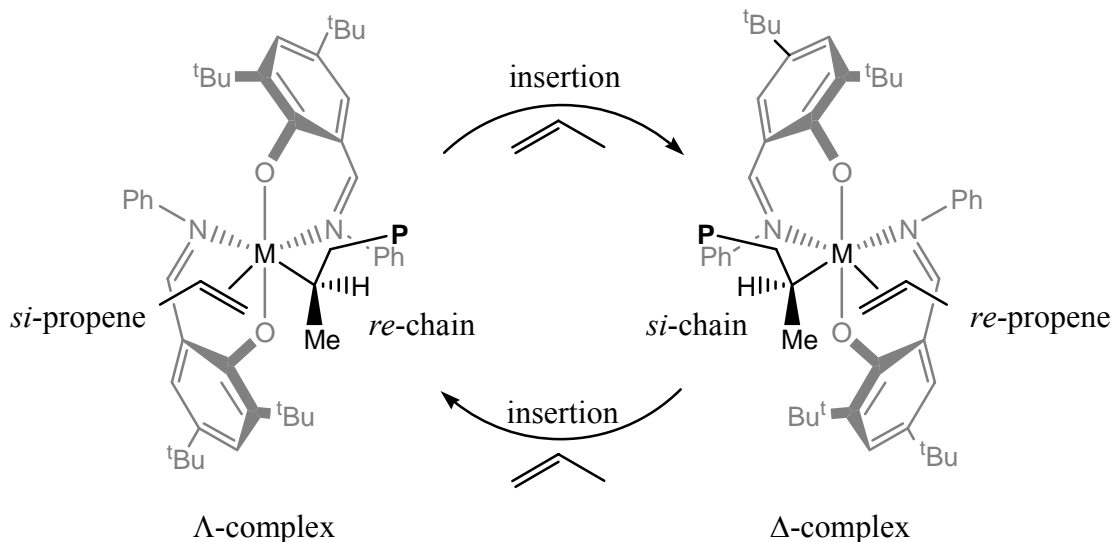
Another class of compounds capable of living polymerization are group 4 metal bis(phenoxyimine) compounds (**17**, Scheme 16). Initial investigations by Fujita<sup>80</sup> at Mitsui Chemicals discovered that upon activated by MAO, these species were active for ethylene polymerization. Subsequent investigations by Coates and co-workers,<sup>81</sup> using high-throughput screening techniques to test a wide variety of Mitsui-type ligands, led to the discovery of a derivative that produced *syn*-PP via 2,1-insertion under chain-end control in a living fashion. Given that the complexes are  $C_2$ -symmetric, the formation of *syndiotactic* polymer was quite unexpected. Theoretical studies by Cavallo and co-workers<sup>82</sup> supported Coates' original proposal that the ligands are fluxional; the chirality of the chain-end influences the chirality of the ligands, which in turn dictates face selectivity of the coordinating monomer (Scheme 17). Reports from both Fujita<sup>83, 84</sup> and the Coates group<sup>85, 86</sup> have since detailed many derivatives active for living propylene polymerization, some capable of incorporation of comonomers such as ethylene,

norbornene and 1,5-hexdiene. Recently, Coates<sup>87</sup> reported a derivative which is active for the living isotactic polymerization of propylene.

**Scheme 16:** Coates' initiator for living propene polymerization. Syndiotactic PP is formed from the MAO-activated **17** when R = Ph, R' = R'' = <sup>t</sup>Bu, despite the C<sub>2</sub>-symmetry of the complex.



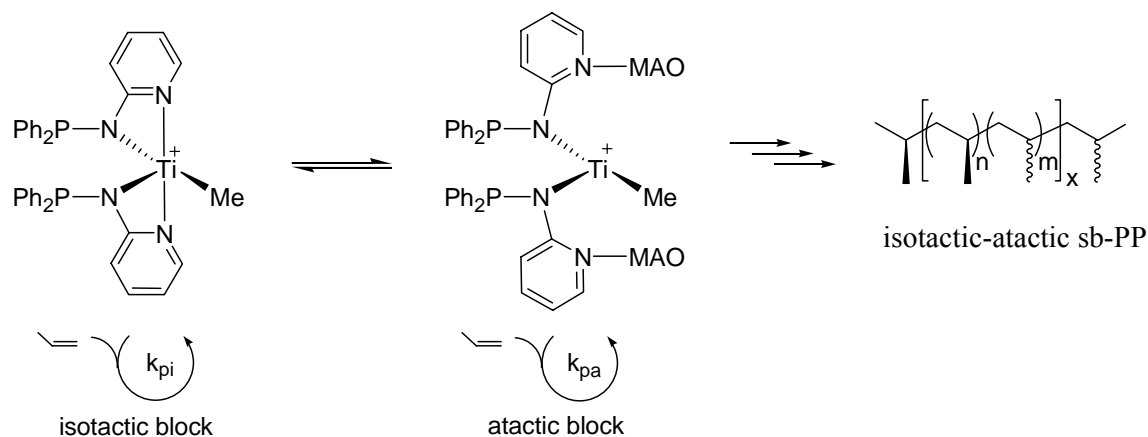
**Scheme 17:** Mechanism of *syn*-PP production from derivatives of **17**.



Recent work by Eisen<sup>88</sup> and co-workers has led to the development of a dynamic titanium complex capable of producing *el*-PP. When the Ti(Ph<sub>2</sub>PNpy)<sub>2</sub>-(NEt<sub>2</sub>)<sub>2</sub> (**18**, py = pyridine) precursor is activated by MAO, the pyridine ligands of the active cationic

species  $[\text{Ti}(\text{Ph}_2\text{PNpy})_2(\text{Me})]^+$  (**19**) are labile enough to reversibly disassociate from the metal center and coordinate to MAO. Scheme 18 depicts **19** in both the ‘open’ form and one of six possible coordination isomers of the ‘closed’ form. The open configuration polymerizes in an atactic manner, and reassociation of the ligands to the active center effects isotactic propagation, resulting in an atactic-isotactic block structure. While this system featured long catalyst lifetimes (up to 20 h) and the material was of uniform crystallinity, the molecular weight distributions were quite broad ( $M_n = 10,200\text{-}62,400$ ,  $\text{PDI} = 2.0\text{-}4.7$ ), increasing linearly with polymerization time.

**Scheme 18:** Eisen’s dynamic polymerization system.



### 1.5 Reversible Chain Transfer

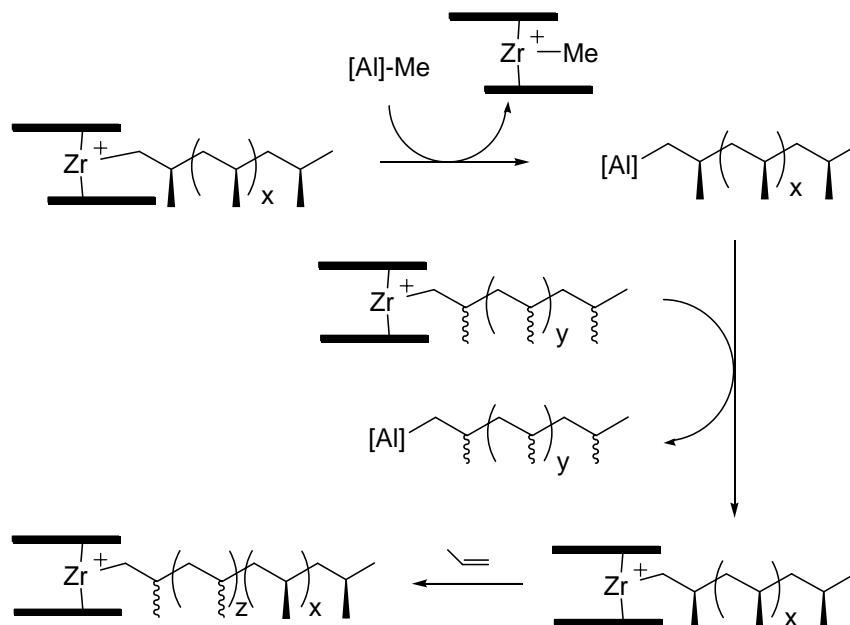
In systems activated by MAO, irreversible chain transfer to alkyl aluminum impurities is a common termination event. However, some systems have been found to undergo *reversible* chain transfer reactions, in which a polymer chain is transferred to another active metal center. In some cases, reversible chain transfer has been observed between active species that produce polymers of different microstructures or different comonomer incorporation levels to yield novel materials.

### 1.5.1 Chain Transfer via Transfer Agents

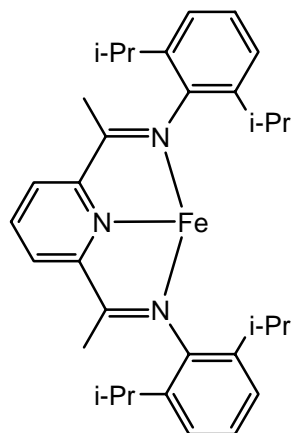
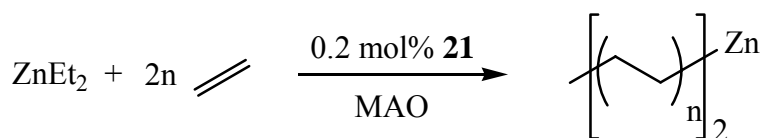
In 1997, Chien<sup>89</sup> reported using a binary system containing a C<sub>2</sub>-symmetric zirconocene and a C<sub>2v</sub>-symmetric zirconocene activated by [Ph<sub>3</sub>C][B(C<sub>6</sub>F<sub>5</sub>)<sub>4</sub>] (**20**) to polymerize propylene. The material produced was found to contain *iso*-PP (from the C<sub>2</sub> species), *a*-PP (from the C<sub>2v</sub> species), and about 7% isotactic-atactic *sb*-PP. This material, unlike a blend of pure *a*-PP and pure *iso*-PP, displayed elastomeric properties, which were attributed to the small amounts of *sb*-PP serving as a compatibilizer for the *a*-PP and *iso*-PP homopolymers. Subsequently, Chien<sup>90</sup> also reported a binary system which produces a mixture of *iso*-PP and *syn*-PP, once again with some amounts of stereoblock polymer.

Chien<sup>89, 90</sup> proposed several possible mechanisms for the formation of *sb*-PP in the binary system. One is that the vinyl end group of a chain that has terminated via  $\beta$ -hydride elimination has inserted into an active chain as a macromonomer, however, Chien is quick to point out that the metallocene catalysts employed in his studies are not active for higher  $\alpha$ -olefins. Another possibility is that the polymers are being transferred to the trialkyl aluminum scavenger, and then transferred from the aluminum to an active center of different symmetry (Scheme 19). In 2000, Brintzinger<sup>91</sup> reported his results with binary systems combining catalysts of atactic with either syndiotactic or isotactic selectivities, and also observed the formation of *sb*-PP (as much as 20%). He attributed this to reversible polymer exchange between the zirconium centers and the aluminum centers of MAO.

**Scheme 19:** Stereoblock-PP via reversible chain transfer to aluminum.



As another example of reversible chain transfer, in 2002, Gibson<sup>92</sup> reported iron-catalyzed PE chain growth on zinc (Figure 12). When a bis(imino)pyridineiron precatalyst (**21**) was activated with MAO, it provided high MW PE of broad PDI ( $M_n = 10\,000$ , PDI = 19.2). However, in the presence of 500 equivalents of  $\text{Et}_2\text{Zn}$ , the system produced PE with low MW and narrow PDI ( $M_n = 700$ , PDI = 1.1). It was determined that the polymer chains were undergoing extremely rapid and reversible transfer between the Fe and Zn centers, such that all chains were growing at the same rate. The final molar yield of the product, upon hydrolysis, corresponded to two polymer chains per Zn center, or 1000 equivalents of PE per equivalent of **21**. Subsequent reports from Gibson<sup>93, 94</sup> detailed the extension of this reaction to other metal-alkyl chain transfer agents and other catalysts.



**21**

**Figure 12:** Gibson's catalyst for PE growth on zinc.

Researchers at Dow Chemical<sup>95</sup> recently combined the use of a binary system with chain transfer agents to make novel PE materials. Using high-throughput screening techniques, it was found that **17** ( $R = \textit{iso}$ -butyl, 2-methylcyclohexyl;  $R' = R'' = \textit{t}$ Bu) and a hafnium pyridylamide catalyst (**22**, Figure 13) together provided a PE material with bimodal MW and broad PDI (13.6). However, when this binary system was run in the presence of  $\text{Et}_2\text{Zn}$ , the MW became monomodal with a narrow PDI (1.33), indicating that the polymer chains were being reversibly transferred between the Zn centers and both of the catalytic species. Furthermore, since each of these catalysts have different selectivities for comonomer incorporation (low incorporation of 1-octene for **21**, high incorporation for **22**), the chain transfer agents allowed the synthesis of polymers with blocks of linear high density polyethylene (HDPE) and blocks of linear low density polyethylene (LLDPE). These materials were found to combine the flexibility and

transparency of LLDPE with the high melting point of HDPE, and exhibited elastomeric properties at temperatures significantly higher than LLDPE of comparable density.

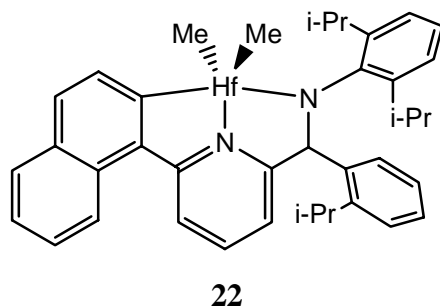


**Figure 13:** Precatalyst used in combination with **17** ( $R = \textit{iso}$ -butyl, 2-methylcyclohexyl;  $R' = R'' = \textit{t}$ Bu) by Dow Chemical to synthesize polyethylene elastomers via chain exchange using  $\text{ZnEt}_2$  as a chain-shuttling agent.

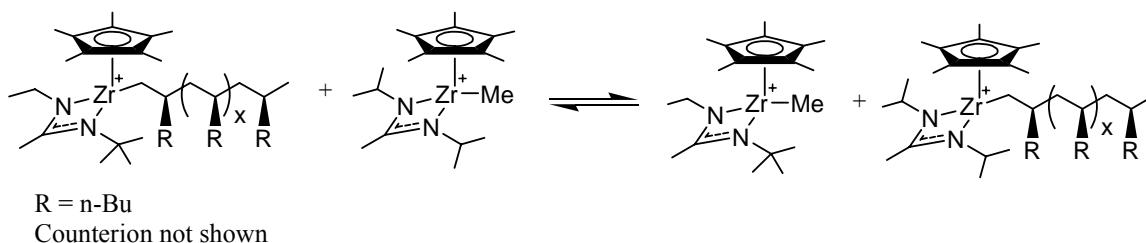
### 1.5.2 Direct Site Transfer

A third possible mechanism of chain transfer is direct exchange between two active centers. Although Chien notes this as a possibility in his report of the atactic/isotactic binary system,<sup>89</sup> in a subsequent publication he remarks that the transfer most likely involves the aluminum species.<sup>90</sup>

One system that has displayed this behavior is Sita's<sup>78</sup> zirconium acetamidinate initiator. As mentioned above,  $C_1$ -symmetric **12** produces *iso*-PH at  $-10^\circ\text{C}$  when activated by a stoichiometric amount of **13** to produce the active species, **16**. A  $C_5$ -symmetric derivative,  $\text{Cp}^*\text{ZrMe}_2[\text{N}(\textit{i}\text{Pr})\text{C}(\text{Me})\text{N}(\textit{i}\text{Pr})]$  (**23**), is also active for living 1-hexene polymerization, although in this case atactic polymer is produced. When a portion of the activated  $C_5$ -symmetric species,  $\{\text{Cp}^*\text{ZrMe}[\text{N}(\textit{i}\text{Pr})\text{C}(\text{Me})\text{N}(\textit{i}\text{Pr})]\}[\text{B}(\text{C}_6\text{F}_5)_4]$  (**24**), is added to a sample of living *iso*-PH derived from **16** (**16-PH**), direct methyl-polymeryl exchange between **24** and **16-PH** is observed, producing **16** and **24-PH**

(Scheme 20).<sup>96</sup> If a second portion of 1-hexene is then added to the system after equilibrium is reached, a polymer of bimodal MW is produced in which the low MW polymer is a mixture of homotactic *a*-PH and homotactic *iso*-PH, and the high MW polymer is a mixture of homotactic *iso*-PP, atactic-isotactic *sb*-PP, and isotactic-isotactic *sb*-PP.

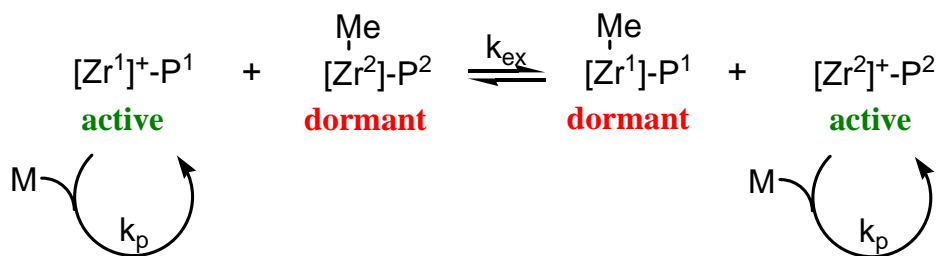
**Scheme 20:** Polymer, methyl exchange in CPZA initiators.



### 1.6 Degenerative Group Transfer

Another dynamic process demonstrated by the Sita system is degenerative group transfer. It was discovered that when the precatalyst **12** was activated by only 0.5 equivalents of **13** and then used to initiate the polymerization of 1-hexene, the molecular weight of the polymer was consistent with *all* of the zirconium centers being active for polymerization.<sup>97</sup> The reason for this was found to be the rapid, reversible transfer of a methyl group from the dormant dimethyl (or alkyl, methyl) species to the active cationic species, thereby reversing the dormant/active roles (Scheme 21). Since this transfer occurs much faster than propagation, all centers propagate at the same rate and the PDI remains as narrow as the fully activated system ( $\leq 1.05$ ).

**Scheme 21:** Degenerative methyl group transfer.



Another interesting outcome of the degenerative transfer (DT) process is that the PH materials produced at partial activation are atactic,<sup>97</sup> despite the fact that the  $C_1$ -symmetric **12** produces isotactic polymers when fully activated. It was determined that the loss of stereocontrol was due to the configurational instability of the neutral species, and *not* due to any kind of chain transfer reaction. 2-D  $^1\text{H}$  EXSY NMR techniques were used to verify that alkyl, methyl derivatives of **12** undergo rapid racemization through amidinate ring-flipping in solution, while the cationic monoalkyl derivatives are configurationally static on the polymerization time scale (Figure 14). Since this racemization occurs much faster than the methyl group transfer, and the transfer occurs much faster than propagation, the active species are effectively being continuously racemized during the polymerization. This unique feature of the CPZA system was exploited by initiating the polymerization of a portion of 1-hexene under DT conditions, producing living *a*-PH, and then activating the system with another 0.5 equivalents of cocatalyst before a portion of 1-octene was added to produce *a*-PP-*block-iso*-PO ( $M_n = 12,400$ , PDI = 1.04). This was the first example of a homogeneous, discrete atactic-isotactic stereoblock polyolefin.

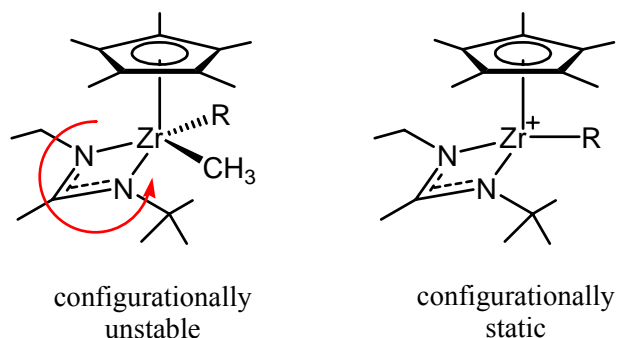


**Figure 14:** The configurational instability of alkyl, methyl CPZA complexes, coupled with the degenerative methyl group transfer process, results in atactic polymers from substoichiometrically activated **12**.

It was also found that the combination of alkyl, chloro CPZA complexes with alkyl CPZA cations would also result in rapid degenerative transfer of the chloride atom, and once again all zirconium centers were found to be active for polymerization.<sup>98</sup> In this case the PH obtained was isotactic ( $M_n = 24,100$ , PDI = 1.02), due to the fact that the alkyl, chloro derivatives are also configurationally static.

### 1.7 Living Polymerization

Since the living nature of some CPZA polymerization systems is key to much of what will be discussed in this dissertation, an appropriate understanding of living Ziegler-Natta polymerization is necessary. While the exact definition of the term “living polymerization” has been the subject of some debate,<sup>99</sup> it is typically used to describe a system in which irreversible termination events are negligible. Living polymerizations were first discovered by Szwarc<sup>100, 101</sup> in 1956 in the context of anionic polymerization. Since then, Quirk<sup>102</sup> has outlined common characteristics of a living system. They include: (1) polymerization proceeds until 100% of monomer is consumed; (2) molecular weight ( $M_n$ ) increases linearly with monomer conversion; (3) the number of polymer

molecules is equal to the number of active initiator molecules, and remains constant; (4) the degree of polymerization (DP) is equal by the initial monomer concentration ( $[M]_0$ ) divided by the initial initiator concentration ( $[I]_0$ ), or  $DP = [M]_0/[I]_0$ ; (5) the rate of activation is much greater than the rate of polymerization, ( $R_a \gg \gg R_p$ ), such that polymers of narrow PDI ( $<1.1$ ) are produced; (6) block copolymers are quantitatively produced by sequential monomer additions; and (7) telechelic polymers are quantitatively produced when the polymerization is quenched with functional group containing reagents.

The first example of living Ziegler-Natta polymerization was demonstrated by Doi and co-workers<sup>103</sup> in 1979 using  $V(acac)_3-AlEt_2Cl$  (**25**), which had previously been shown by Natta<sup>104</sup> to produce PP with a predominantly syndiotactic microstructure. The syndiotacticity of the polymer is formed under chain-end control via 2,1-insertions of the propylene into the vanadium-carbon bonds. Doi discovered that when polymerizations were conducted with **25** below  $-65\text{ }^\circ\text{C}$ , the PDI of the samples were narrow (1.07-1.18) with  $M_n$  as high as 91,300. Further evidence of a living system was obtained through kinetic analysis, which revealed a linear increase of yield and molecular weight with time at constant propylene concentration. Since then, many systems capable of living Ziegler-Natta polymerization of  $\alpha$ -olefins have been reported,<sup>105</sup> providing a wide variety of unique polymers. Several of these systems are discussed where appropriate.

## Chapter 2: Discrete Cationic CPZA Alkyl Complexes as Models for Living Polymers

### 2.1 Mechanistic Studies in Living Ziegler-Natta Polymerization

Given the advantages offered by a living polymerization system over non-living systems, it is surprising that more mechanistic studies taking advantage of the ability to directly observe the active species, have not been conducted. Indeed, an understanding of the factors that control termination under certain conditions would provide insight into the rational design of the next generation of living polymerization systems. Schrock and co-workers<sup>106-109</sup> have suggested that the steric environment around the metal center of their {[NON]ZrMe}[B(C<sub>6</sub>F<sub>5</sub>)<sub>4</sub>] (**26**, [NON]<sup>2-</sup> = [tBu-d<sub>6</sub>-N-o-C<sub>6</sub>H<sub>4</sub>)<sub>2</sub>O]<sup>2-</sup>) initiator prevent formation of β-agostic interactions, and therefore prevent β-hydride elimination and transfer reactions. This theory appeared to be validated in another of their living systems, when the direct observation by <sup>1</sup>H NMR spectroscopy of the *iso*-butyl initiators, {[MesNpy]M(tBu)}[B(C<sub>6</sub>F<sub>5</sub>)<sub>4</sub>] (M = Zr (**27**) and Hf (**28**); [MesNpy]<sup>2-</sup> = [H<sub>3</sub>CC(2-C<sub>5</sub>H<sub>4</sub>N)(CH<sub>2</sub>Nmesityl)<sub>2</sub>]<sup>2-</sup>), did not reveal any evidence for an agostic interaction between the metal and the β-hydrogen of the *iso*-butyl group.<sup>110, 111</sup> Both initiators **27** and **28** were found to decompose only very slowly at 0° C in a strictly first-order fashion via assumed β-hydride elimination; with t<sub>1/2</sub> = 40 min for **27** and t<sub>1/2</sub> = 21 h for **28**.

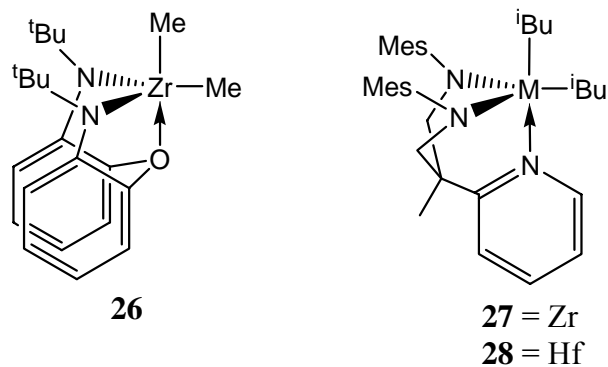


**Figure 15:** Schrock's initiators for living  $\alpha$ -olefin polymerization.

Fujita and co-workers<sup>112, 113</sup> have recently proposed a different hypothesis for their surprisingly robust titanium bis(phenoxyimine) catalyst,  $\text{TiCl}_2(\eta^2\text{-1-[C\{H\}=NAr]-2-O-3-tBu-C}_6\text{H}_3)_2$  (**29**, Ar = fluorinated phenyl), capable of living polymerization of ethylene and propylene at 50 °C. On the basis of DFT calculations, Fujita attributed this remarkable stability to an attractive force between an *ortho*-fluorine and the  $\beta$ -hydrogen of the polymer chain, claiming that this interaction is strong enough to mitigate reactivity of the  $\beta$ -hydrogen towards  $\beta$ -hydride elimination and transfer to monomer reactions. Independently, Chan and co-workers<sup>114</sup> reported a neutral (phenoxy-pyridine)Zr-benzyl model complex (**30**) that displays a weak  $\text{H}\cdots\text{F}$  interaction between a fluorine atom of an *ortho*- $\text{CF}_3$  group and the  $\alpha$ -hydrogen of a benzyl group (Figure 16), observable by  $^1\text{H}$  and  $^{19}\text{F}$  NMR. Chan and Fujita<sup>113</sup> both claim that **30** serves as a model for the direct observation of the  $\text{H}\cdots\text{F}$  interaction proposed in **29**. However, detailed computational investigations by Busico and co-workers<sup>115</sup> suggest that the effects of the *ortho*-F atoms are primarily *steric* in nature, destabilizing the transition state of  $\beta$ -hydride transfer to monomer by coming in close contact with *the monomer*. Furthermore, the presence of the *ortho*-F atoms prevents the phenyl groups from rotating to reduce these steric

interactions. Similar transition state energies were found when the *ortho*-F atoms were replaced with methyl groups. Interestingly, this study also suggests that the transition state of  $\beta$ -hydride transfer to monomer is slightly *stabilized* by a weak attractive force between the *ortho*-F atom and the closest  $\alpha$ -hydrogen of the polymer chain, an interaction that might be more appropriately modeled by Chan's complex.

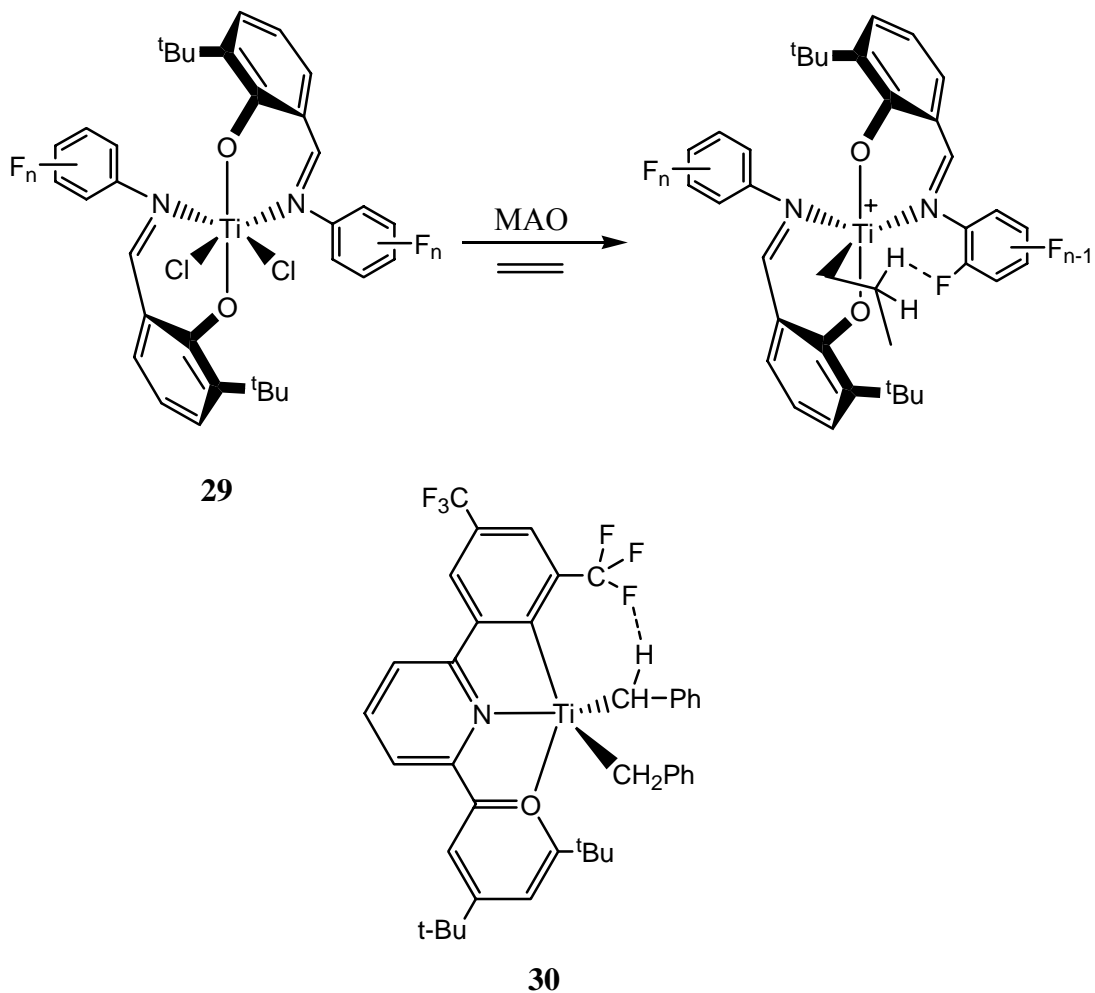
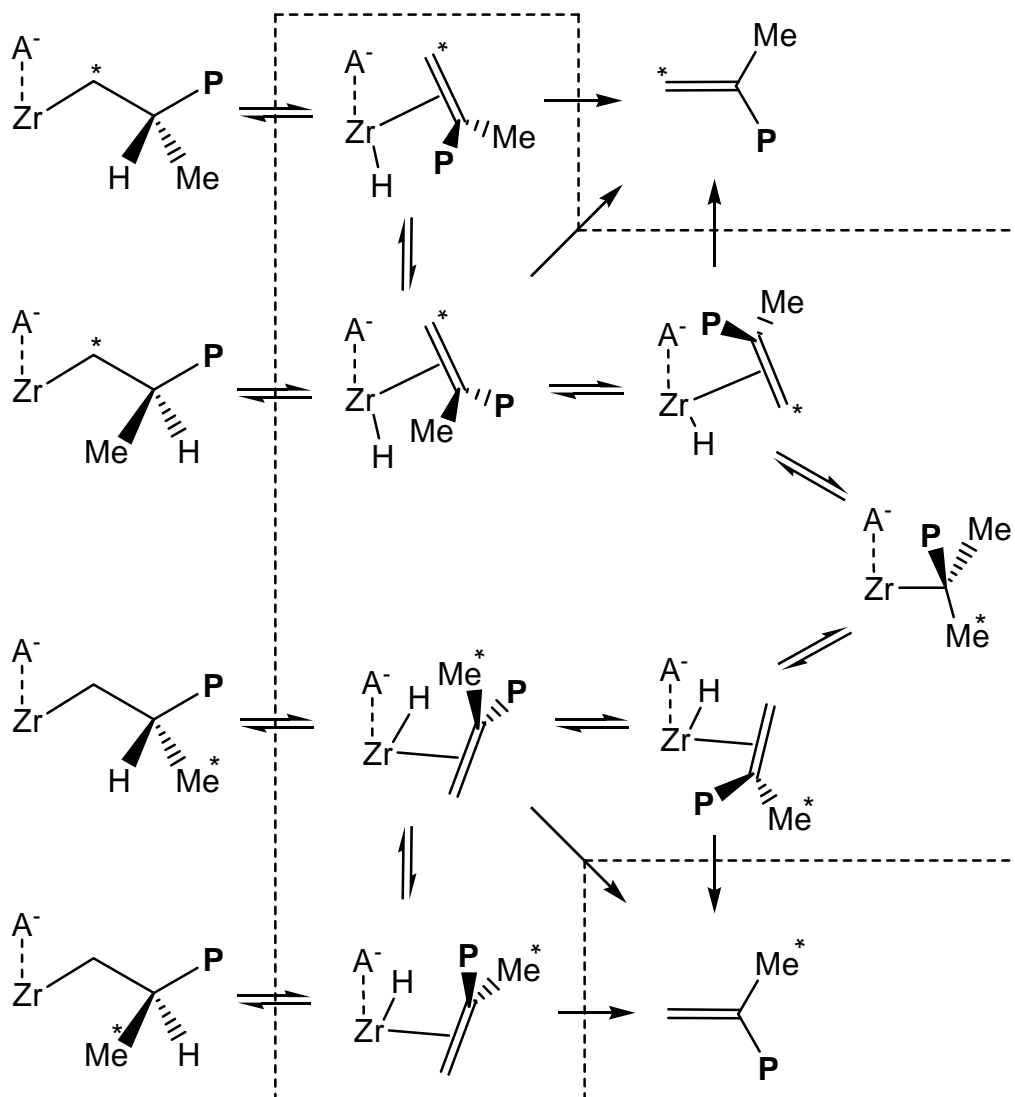


**Figure 16:** Top: Fujita's preinitiator for living propylene and ethylene polymerization and the activated ethylene insertion product modeled by DFT calculations. Bottom: Chan's model complex displaying a weak F $\cdots$ H interaction.

**Scheme 22:** Chain-end epimerization products observed by Landis. Species inside box were not observed.

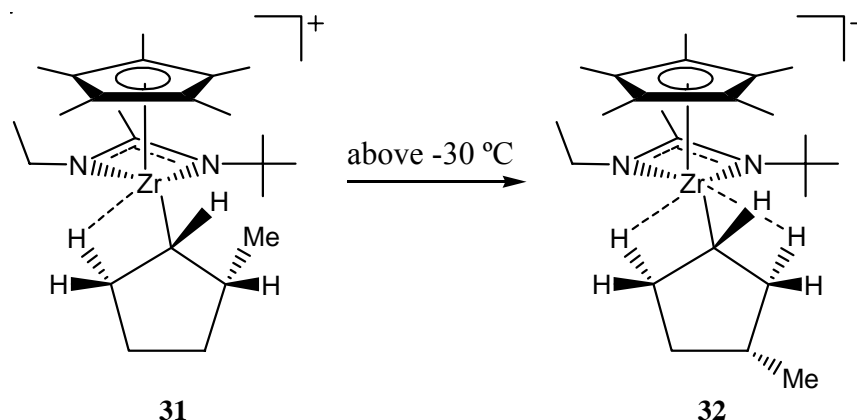


Landis and co-workers<sup>116-121</sup> have reported extensive investigations analyzing initiation and propagation events of 1-hexene, propylene and ethylene polymerizations by *rac*-(EBI)ZrMe<sub>2</sub>, activated via methyl-group abstraction by B(C<sub>6</sub>F<sub>5</sub>)<sub>3</sub>, at -40 °C using <sup>13</sup>C NMR.<sup>117</sup> These studies, combined with previously conducted kinetic investigations<sup>119</sup> and kinetic isotope effects,<sup>121</sup> indicate that propagation begins with reversible olefin coordination and displacement of the anion, followed by the rate-limiting insertion of the alkene into the metal-polymer bond. Further studies with this system were conducted

in an attempt to observe the chain-end epimerization process using (1-<sup>13</sup>C)-propylene.<sup>118</sup> All expected primary polymeryl species, including those only accessible through the proposed non-dissociative alkene enantioface exchange, were observed (Scheme 22). However, the tertiary alkyl and coordinated alkene intermediates remained elusive.

Through extensive low temperature 1- and 2-D <sup>13</sup>C, <sup>1</sup>H NMR experiments, Sita and co-workers<sup>122</sup> reported the observation of cyclopentene insertion into the Zr-Me bond of **16**. At -30 °C, the *cis*-1,2-product of insertion (**31**) is indefinitely stable, and possesses a single strong β-agostic interaction. However, above -30 °C, this complex undergoes rearrangement to the *cis*-1,3-isomer (**32**) in a strictly first-order process, possibly driven by steric interactions between the methyl group on the cyclopentyl unit and the amidinate *N-tert*-butyl group. No intermediates of any kind are observed, including alkene, hydride complexes as required by the Busico mechanism for chain-end epimerization. If the isomerization is occurring through this mechanism, the alkene rotation step brings the bulk of the alkyl ring into close contact with the Cp\* ligand, which should be a highly unfavorable conformation. In this regard it is fairly surprising that the isomerization proceeds readily at such low temperatures, although additional driving force for the isomerization might be found in the two separate β-agostic interactions that **32** was observed to be engaged in (Scheme 23). Formation of a double β-agostic interaction has previously been proposed as a possible stabilizing interaction in the tertiary alkyl intermediate during chain-end epimerization,<sup>123, 124</sup> and so this observation in **32** is of particular significance.

**Scheme 23:** Isomerization of cyclopentene insertion product.



This dissertation focuses on investigations into dynamic processes present in the CPZA living polymerization system towards the development of a method for precise control of polyolefin stereochemistry. The work described in Chapter 2 can be found in Harney, M. B.; Keaton, R. J.; Sita, L. R. *J. Am. Chem. Soc.* **2004**, *126*, 4536-4537 and Harney, M. B.; Keaton, R. J.; Fettinger, J. C.; Sita, L. R. *J. Am. Chem. Soc.* **2006**, *128*, 3420-3432. The work described in Chapter 3 can be found in Harney, M. B.; Zhang, Y.; Sita, L. R. *Angew. Chem. Int. Ed.* **2006**, *45*, 2400-2404, and the work described in Chapter 4 can be found in Harney, M. B.; Zhang, Y.; Sita, L. R. *Angew. Chem. Int. Ed.* **2006**, *45*, 6140-6144.

## 2.2 Chain Walking and Cationic CPZA Model Complexes

The isomerization mechanism proposed by Busico<sup>61, 62</sup> and apparently validated by Bercaw's<sup>72</sup> doubly labeled propylene experiment (see Section 1.3), might be responsible for the observed isomerization in **31**. However, there are several unsettling aspects of the Busico mechanism: (1) a relatively large number of *reversible* steps must occur within an extremely short amount of time in order for the process to compete with propagation; (2) none of the six unique alkene, hydride intermediates, which avoid alkene

displacement by monomer, have ever been observed; (3) the tertiary alkyl intermediate has never been observed; (4) the alkene enantiofacial exchange would appear to require at least partial dissociation and reassociation of the olefinic polymer end-group, and yet termination through alkene release or displacement by free monomer is avoided.

The living nature of polymers derived from **16** and other CPZA derivatives, as well as the unique stability of alkyl CPZAs,<sup>125</sup> offers a unique opportunity for in-depth analysis of isomerization mechanisms through direct observation of cationic species. As such, in order to observe the effects of any isomerization reactions in the living polymer, which, under normal conditions are not competitive with propagation, an oligomeric sample of poly(1-butene) initiated by **16** (**16-PB**) with DP  $\approx$  20 was maintained at  $-10$  °C for an extended period of time.<sup>126</sup> While higher molecular weight polymers (DP  $\geq$  100) show virtually no alkene resonances from  $\beta$ -hydride elimination using standard acquisition parameters, samples of **16-PB** that were quenched and analyzed by  $^1\text{H}$  NMR show alkene resonances that grow steadily over the course of several days (Figure 17). Aside from the expected resonances of the endgroup **I** ( $\delta$  4.69 and 4.76) from the direct  $\beta$ -hydride elimination of unchanged **16-PB**, those of a mixture of E and Z isomers of the trisubstituted alkene endgroup **II** ( $\delta$  5.18 and 5.27) as well as the terminal alkene endgroup **III** ( $\delta$  4.90, 4.96 and 5.68) are observed. This suggests isomerization of the living polymer before decomposition, resulting in the cationic zirconium center chain-walking down the pendant group of the last inserted monomer (Scheme 24). The initial isomer of **16-PB**, **IV**, presumably isomerizes into intermediates **V-VII**, all of which undergo  $\beta$ -hydride elimination to account for **I-III**. At no time are resonances observed attributable to **VIII**, resulting from  $\beta$ -hydride elimination of **V** into

the polymer backbone, which may be inaccessible for steric reasons. Unfortunately, we have not yet been able to directly spectroscopically observe **V-VII**.

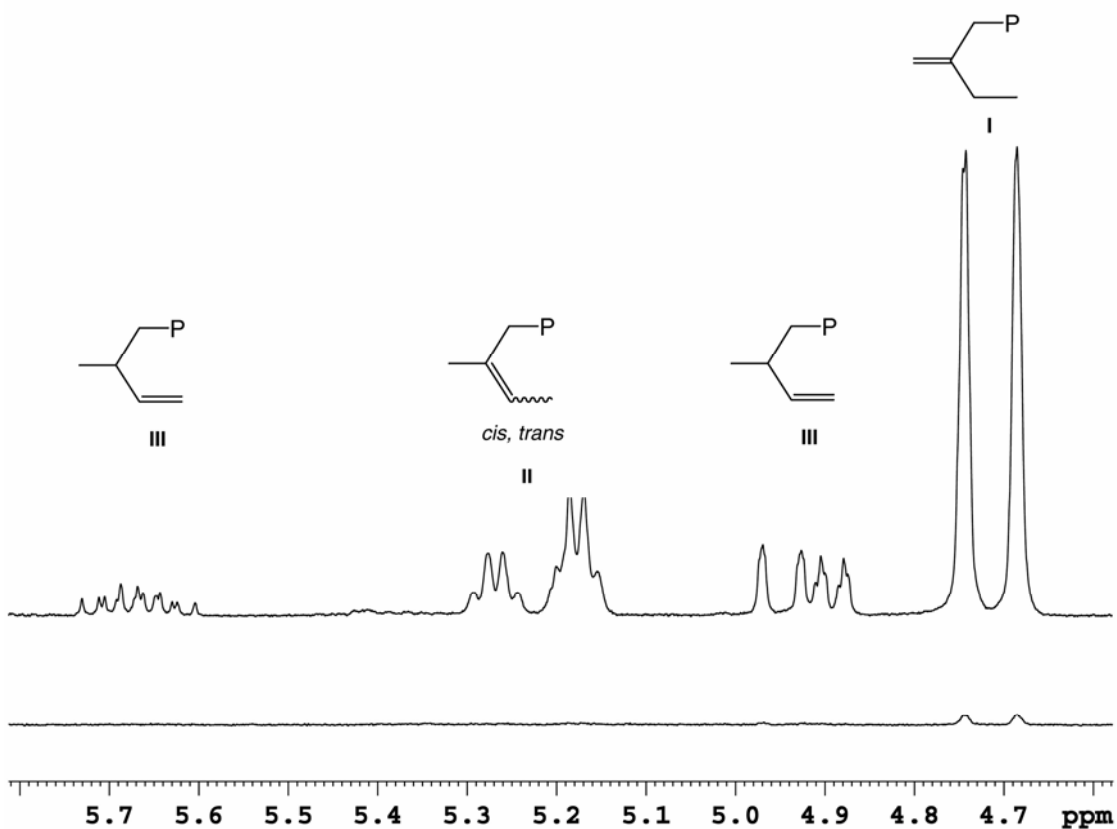
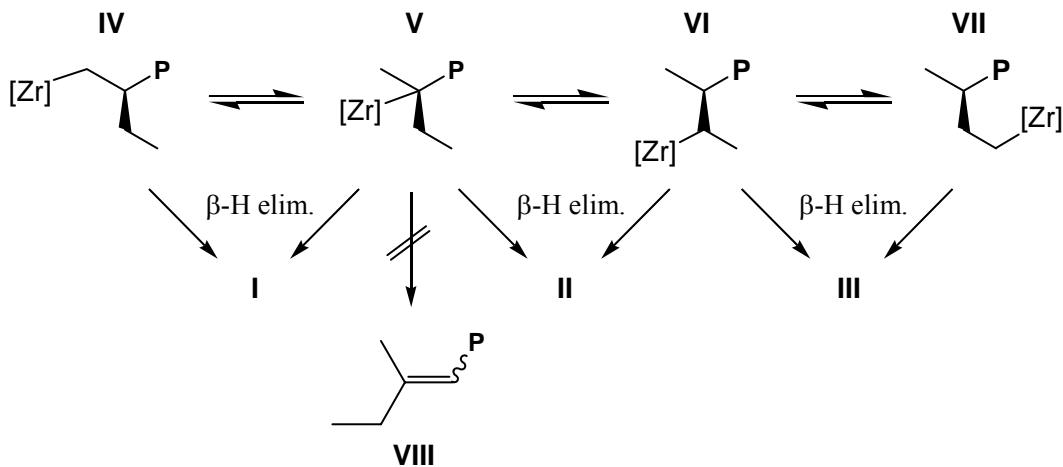


**Figure 17:**  $^1\text{H}$  NMR (400 MHz,  $\text{CDCl}_3$ , 25  $^\circ\text{C}$ ) spectra of the alkene region of oligomeric poly(1-butene) quenched immediately (bottom) and after 72 h at  $-10$   $^\circ\text{C}$  (top). **P** = isotactic poly(1-butene).

**Scheme 24:** Mechanism of formation of end groups **I-III**.



Using low MW alkyl complexes as models for a living active center could permit the direct observation of isomerization events. As depicted in Figure 18, the pendant alkyl groups of  $\{\text{Cp}^*\text{Zr}(\text{R})[\text{N}(\text{Et})\text{C}(\text{Me})\text{N}(\text{tBu})]\}\text{[B}(\text{C}_6\text{F}_5)_4]$  (**33-R**, R = varied alkyl group) can be tailored to mimic different types of polyolefin chains. For example, an *n*-propyl group can be viewed as a model for a living polyethylene chain, while an *iso*-butyl group can be viewed as a model for polypropylene. Further increasing the size of the alkyl group improves the ability of the complex to model living polyolefins obtained from higher  $\alpha$ -olefins. The decomposition and potential structural rearrangements of these models can be easily monitored by  $^1\text{H}$  and  $^{13}\text{C}$  NMR spectroscopy, whereas the complexity of spectra of living polymers hinders straightforward analysis.

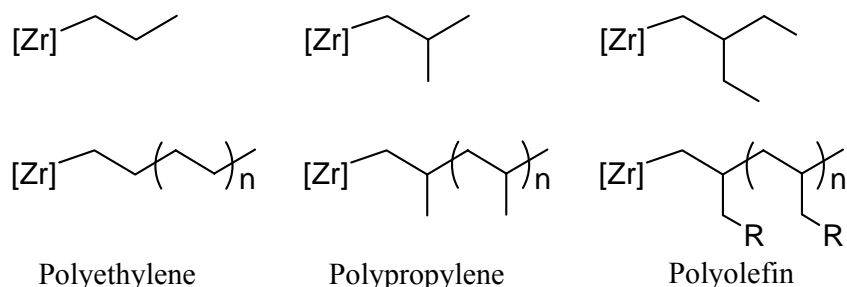
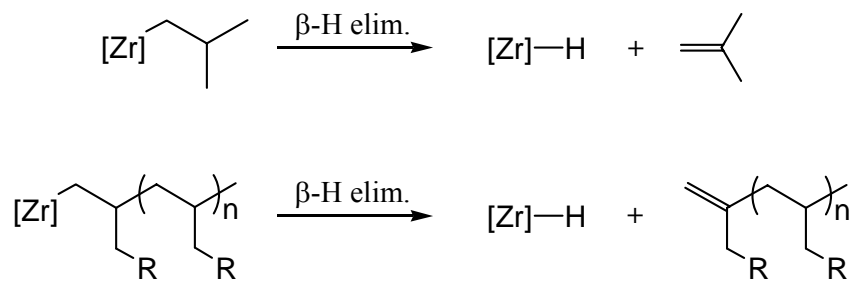


**Figure 18:** Low molecular weight alkyl groups as models for living polymers

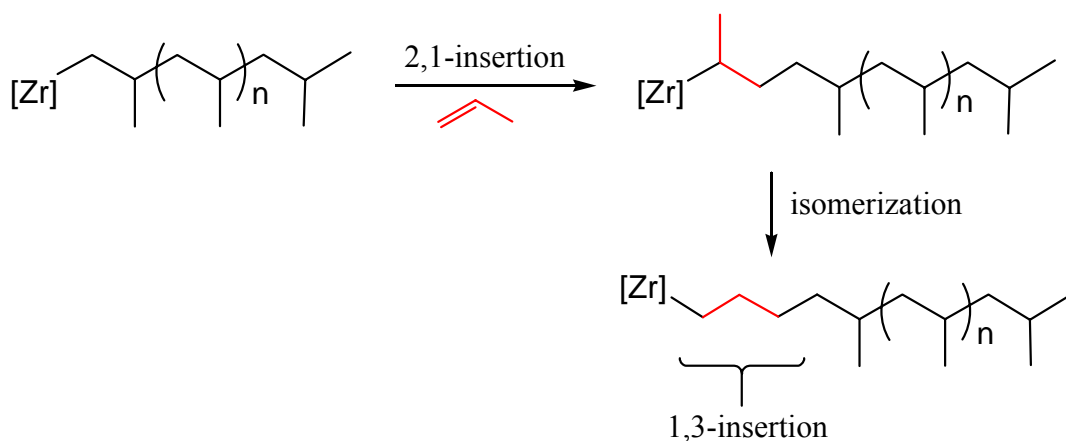
It is intuitive to think that the rates of decomposition of the models and living polymers should be relatively similar given the nearly identical environments around the zirconium center (Scheme 25). However, a model complex clearly cannot accurately reproduce the extended steric interactions of a polymer chain, and it is unclear what kind of ramifications this will have on the stability of the complex. Due to this, a comparison of stabilities between the model complexes and a living polymer must be conducted to reveal the magnitude of this effect.

**Scheme 25:** Comparison of the  $\beta$ -hydride elimination of a low molecular weight alkyl group to that of a living polymer.



Secondary alkyl groups can also provide valuable information as models. Several systems have been found to polymerize propylene via 2,1-insertion, which results in a secondary polymeryl group bound to the metal. In addition, regioerrors during propylene polymerizations with metallocenes, which propagate via 1,2-insertion, also result in a secondary polymeryl species, which has been described as a ‘dormant state’ on the basis of an excessive number of *n*-butyl end groups relative to the occurrence of regio-misinsertions.<sup>127-131</sup> However, Landis<sup>120</sup> has recently determined that the *n*-butyl end group enrichment may be more accurately attributed to the higher reactivity of secondary alkyls with molecular hydrogen, which is commonly used as an irreversible chain transfer agent. Secondary polymeryl complexes can also isomerize to the primary position and continue monomer propagation, resulting in a 1,3-insertion (Scheme 26). Therefore, it was of interest to observe the stability of a cationic CPZA secondary alkyl model with respect to isomerization vs. direct decomposition given the unique stability of our secondary and tertiary alkyl/chloro CPZA derivatives, which do not undergo isomerization to primary alkyls even at temperatures as high as 60 °C.<sup>132</sup>

**Scheme 26:** Formation of 1,3-insertions through the isomerization of 2,1-insertions.



### 2.3 Synthesis and Structure

The synthesis of discrete cationic CPZA alkyl complexes can be achieved through protonolysis of alkyl, methyl complexes with **13**, in the same way that the methyl cation **16** is generated through protonolysis of the dimethyl **12**.<sup>133</sup> Alkyl, methyl complexes can be synthesized through methylation of alkyl, chloro complexes, which in turn can be synthesized from the previously reported dichloride complex,  $\text{Cp}^*\text{ZrCl}_2[\text{N}(\text{Et})\text{C}(\text{Me})\text{N}(\text{tBu})]$  (**34**).<sup>125</sup>

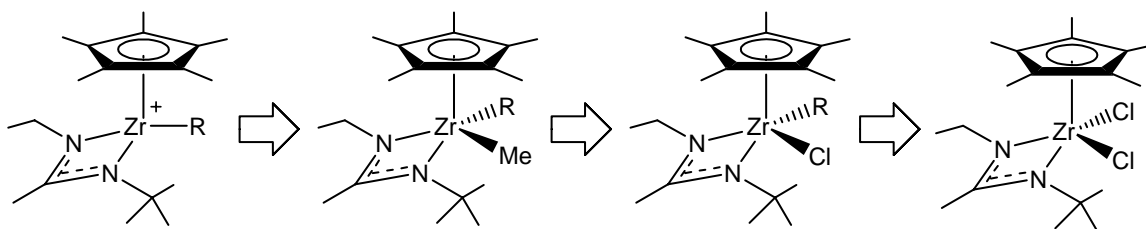


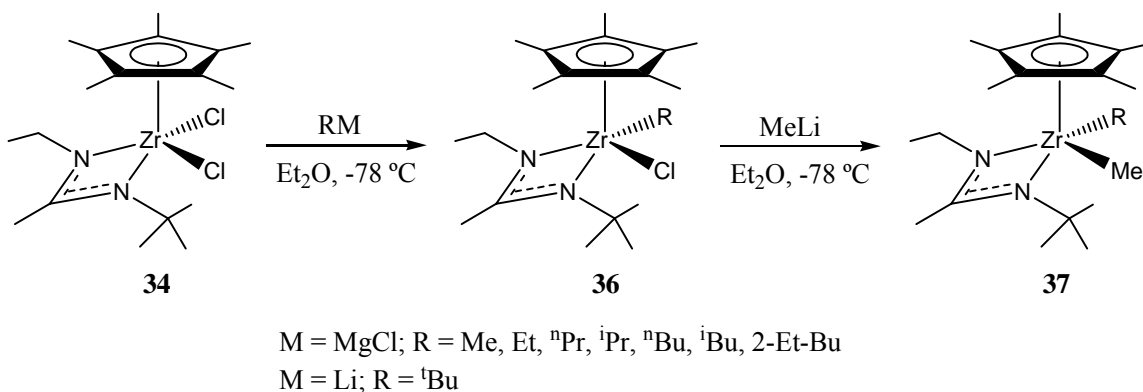
**Figure 19:** Retrosynthetic strategy for **33**.

#### 2.3.1 CPZA Alkyl, Chloro Complexes

The dichloride starting material **34** is easily prepared in large quantities from the lithium amidinate salt and commercially available  $\text{Cp}^*\text{ZrCl}_3$  (**35**) at  $-78\text{ }^\circ\text{C}$  in diethyl

ether (Et<sub>2</sub>O). This compound is then reacted with alkylmagnesium chlorides, or alkyllithium reagents in the cases of the sterically demanding *tert*-butyl and neopentyl groups, under similar conditions to provide the monoalkylated product Cp\*ZrRCl[N(Et)C(Me)N(<sup>t</sup>Bu)] (**36-R**, R = varied alkyl group), as shown in Scheme 27. The *tert*-butyl derivative, **36-<sup>t</sup>Bu**, requires extended reaction times (18 h) at -55 °C to avoid isomerization to the *iso*-butyl derivative, **36-<sup>i</sup>Bu**, which occurs in the presence of unreacted *tert*-butyl lithium if the reaction is warmed to room temperature before completion. If alkylmagnesium bromides are employed instead of chlorides, transhalogenation at zirconium takes place, yielding the product as a mixture of alkyl, chloro and alkyl, bromo (**36'-R**) derivatives.

**Scheme 27:** Synthesis of CPZA alkyl, chloro and alkyl, methyl derivatives.



Several derivatives of **36-R** and **36'-R** have had their structures determined by single crystal x-ray diffraction, and each was found to exist as a single diastereomer with the chloride (or bromide) residing adjacent to the amidinate N-*tert*-butyl group.<sup>132</sup> Importantly, no derivative of **36-R** exhibited a close interaction between  $\beta$ -hydrogens and the metal center. Examining the structure of **36'-(2-Et-Bu)** (Figure 20), the largest of the alkyl models examined, reveals that the bond angles around the  $\alpha$ -carbon are not

significantly distorted from tetrahedral geometry, aside from the Zr-C<sub>α</sub>-C<sub>β</sub> bond angle of 117.72(8)° (*cf.* 109° for ideal tetrahedral). Likewise, the angles around the β-carbon are only slightly ‘flattened’ towards the β-hydrogen, most likely due to steric effects. It is interesting to note that part of the 2-ethyl-butyl group is accommodated in the open area ‘beneath’ the amidinate ligand and opposite to the Cp\* ligand. It is not then unreasonable to presume that the living polymer might also take advantage of this space for accommodation of the β-alkyl groups of a poly(α-olefin) chain.

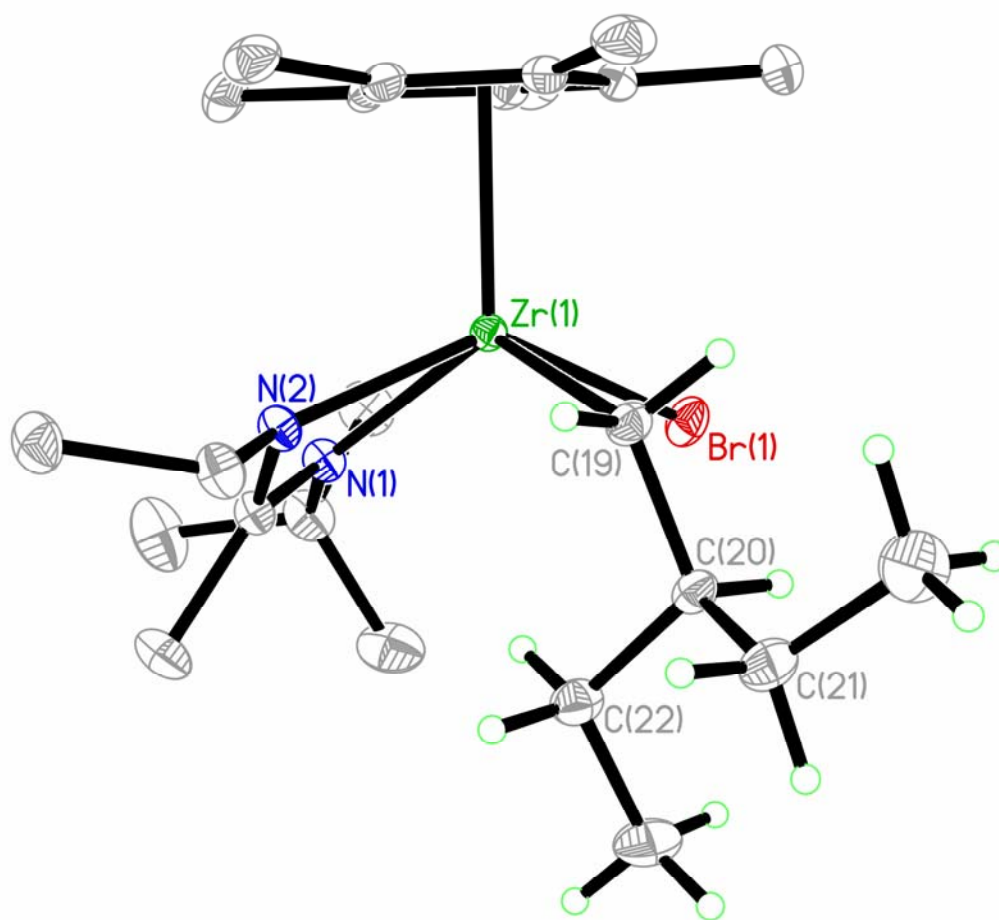


**Figure 20:** Molecular structure (30% thermal ellipsoids) of **36'-(2-Et-Bu)**. All hydrogens, aside from those on the 2-ethyl-butyl group, have been removed for the sake of clarity.

**Table 1:** Bond angles of the  $\alpha$ - and  $\beta$ -carbons of **36'**-(**2-Et-Bu**).

Bond	Angle (degrees)
C(20)-C(19)-Zr(1)	117.72(8)
C(20)-C(19)-H(19)	106.7(10) 109.7(10)
Zr(1)-C(19)-H(19)	107.8(10) 107.3(10)
H(19)-C(19)-H(19')	107.2(14)
C(22)-C(20)-C(21)	110.30(11)
C(22)-C(20)-C(19)	113.06(10)
C(21)-C(20)-C(19)	111.85(11)
C(22)-C(20)-H(20)	105.8(9)
C(21)-C(20)-H(20)	108.2(9)
C(19)-C(20)-H(20)	107.2(9)

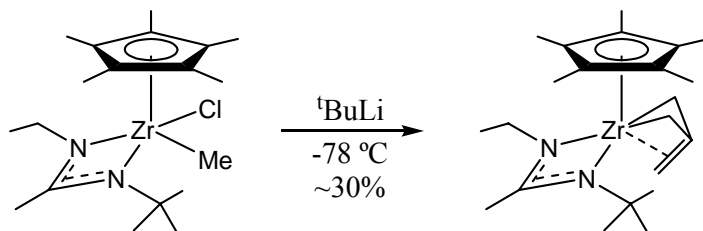
In solution,  $^1\text{H}$  NMR confirms the presence of a single diastereomer for each derivative, presumably the same as that determined from x-ray crystallography. Further, variable temperature NMR confirmed that each derivative of **36-R** is stable with respect to decomposition, isomerization and racemization through amidinate ring-flipping at all temperatures examined (as high as 80 °C).<sup>132</sup>

### 2.3.2 CPZA Alkyl, Methyl Complexes

With the chloro, alkyl complexes in hand, the synthesis of alkyl, methyl derivatives,  $\text{Cp}^*\text{ZrRMe}[\text{N}(\text{Et})\text{C}(\text{Me})\text{N}(\text{tBu})]$  (**37-R**, R = varied alkyl group), was accomplished by treating **36-R** with methyl lithium (Scheme 27). The only unsuccessful attempt was in the case of R = *tert*-butyl. While the chloro derivative **36-tBu** was synthesized from *tert*-butyl lithium with extended reaction times at -55 °C, all subsequent

attempts at methylation failed.<sup>132</sup> Presumably, shielding of the metal center by the bulky *tert*-butyl group prevented alkylation, with the reaction resulting only in formation of **37-Bu** when attempted at room temperature. Reversing the steps and attempting to react the methyl, chloro derivative **36-Me** with *tert*-butyl lithium also proved unsuccessful. The major product of this reaction (ca. 30% by <sup>1</sup>H NMR) was a previously characterized trimethylenemethane (TMM) complex (Scheme 28).<sup>134</sup>

**Scheme 28:** Treating **36-Me** with *tert*-butyl lithium produced the TMM derivative in low yield.



Once again, the solid state structures of several derivatives of **37-R**, synthesized by Richard J. Keaton,<sup>132</sup> were determined by x-ray diffraction. Similar to derivatives of **36-R**, each of the alkyl methyl complexes were found to have their methyl group adjacent to the amidinate *N-tert*-butyl group, and there were no close  $\beta$ -hydrogen-zirconium interactions observed. However, the <sup>1</sup>H NMR revealed the two sets of peaks, indicating the presence of two diastereomers. As mentioned above, 2-D <sup>1</sup>H EXSY NMR experiments conducted by Yonghui Zhang<sup>135</sup> confirmed that in solution, the amidinate ligand is configurationally unstable and undergoes rapid racemization for all derivatives of **37-R**.<sup>97</sup> This disparity between the configurational stability in the alkyl, chloro (or alkyl, bromo) complexes vs. the alkyl, methyl complexes is most likely an electronic effect caused by the electron withdrawing nature of the halide. Indeed, close examination

of the crystal structures reveals that derivatives of **36-R** uniformly have slightly shorter N-Zr bond lengths than analogous derivatives of **37-R** (Table 2).<sup>133</sup>

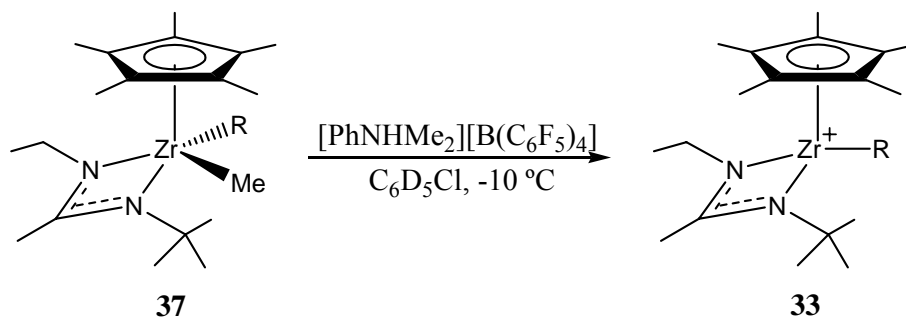
**Table 2:** Comparison of Zr-N bond lengths of **36-R** and **37-R** for R = <sup>i</sup>Pr and <sup>i</sup>Bu.

	<b>36-<sup>i</sup>Pr</b>	<b>37-<sup>i</sup>Pr</b>	<b>36-<sup>i</sup>Bu</b>	<b>37-<sup>i</sup>Bu</b>
Zr-N(Et)	2.2419(11)	2.2594(9)	2.2284(15)	2.2601(12)
Zr-N(t-Bu)	2.2528(11)	2.2808(9)	2.2587(16)	2.2821(12)

### 2.3.3 Cationic CPZA Alkyl Complexes

Activation of **37-R** with [PhNMe<sub>2</sub>H][B(C<sub>6</sub>F<sub>5</sub>)<sub>4</sub>] in chlorobenzene at -10 °C results in the cationic CPZA alkyl species **33-R** (Scheme 29) via protonolysis of the methyl group. Competitive protonolysis of the alkyl groups is not observed. In work done by Keaton,<sup>132</sup> cationic CPZA alkyl complexes were found to possess a strong β-agostic interaction in solution. To further clarify the solution structure, a series of difference-1D NOE <sup>1</sup>H NMR experiments were carried out. For the derivatives of **33-R** in which R contains β-hydrogens, it was found that the agostically bound β-hydrogen resides in close proximity to the N-ethyl group. As presented in Table 3, proof of the agostic interaction was evident in the <sup>1</sup>J<sub>CH</sub> coupling values, which were reduced at the β-position (85-110 Hz) and increased at the α-position (133-155 Hz), as determined by Keaton using 2D <sup>13</sup>C, <sup>1</sup>H J-resolved HSQC NMR techniques. No such interaction was found in a sample of oligomeric **16-PB**. Much like the alkyl chloro derivatives, the cations exhibit configurational stability with respect to amidinate ring flipping and do not racemize in solution.

**Scheme 29:** Activation of **37-R** via methyl group protonolysis.



R = Et, <sup>n</sup>Pr, <sup>i</sup>Pr, <sup>n</sup>Bu, <sup>i</sup>Bu, 2-Et-Bu.

[B(C<sub>6</sub>F<sub>5</sub>)<sub>4</sub>] counterion of **33** not shown.

**Table 3:** <sup>1</sup>J(<sup>13</sup>C-<sup>1</sup>H) coupling constants for **33-R**.<sup>a</sup>

R	<sup>1</sup> J( <sup>13</sup> C <sub>α</sub> - <sup>1</sup> H <sub>α</sub> ) <sup>b</sup>		<sup>1</sup> J( <sup>13</sup> C <sub>β</sub> - <sup>1</sup> H <sub>β</sub> ) <sup>b</sup>	
Et	140	135	123	
<sup>n</sup> Pr	144	133	110	n.o.
<sup>i</sup> Pr	155		126	85
<sup>n</sup> Bu	140	133	121	109
<sup>i</sup> Bu	138	128	92	
2-Et-Bu	140	120	86	

<sup>a</sup> Obtained from 2D <sup>13</sup>C, <sup>1</sup>H HSQC NMR in chlorobenzene-*d*<sub>5</sub> at -10 °C.

<sup>b</sup> Two values denote that two distinct resonances for diastereotopic protons were observed.

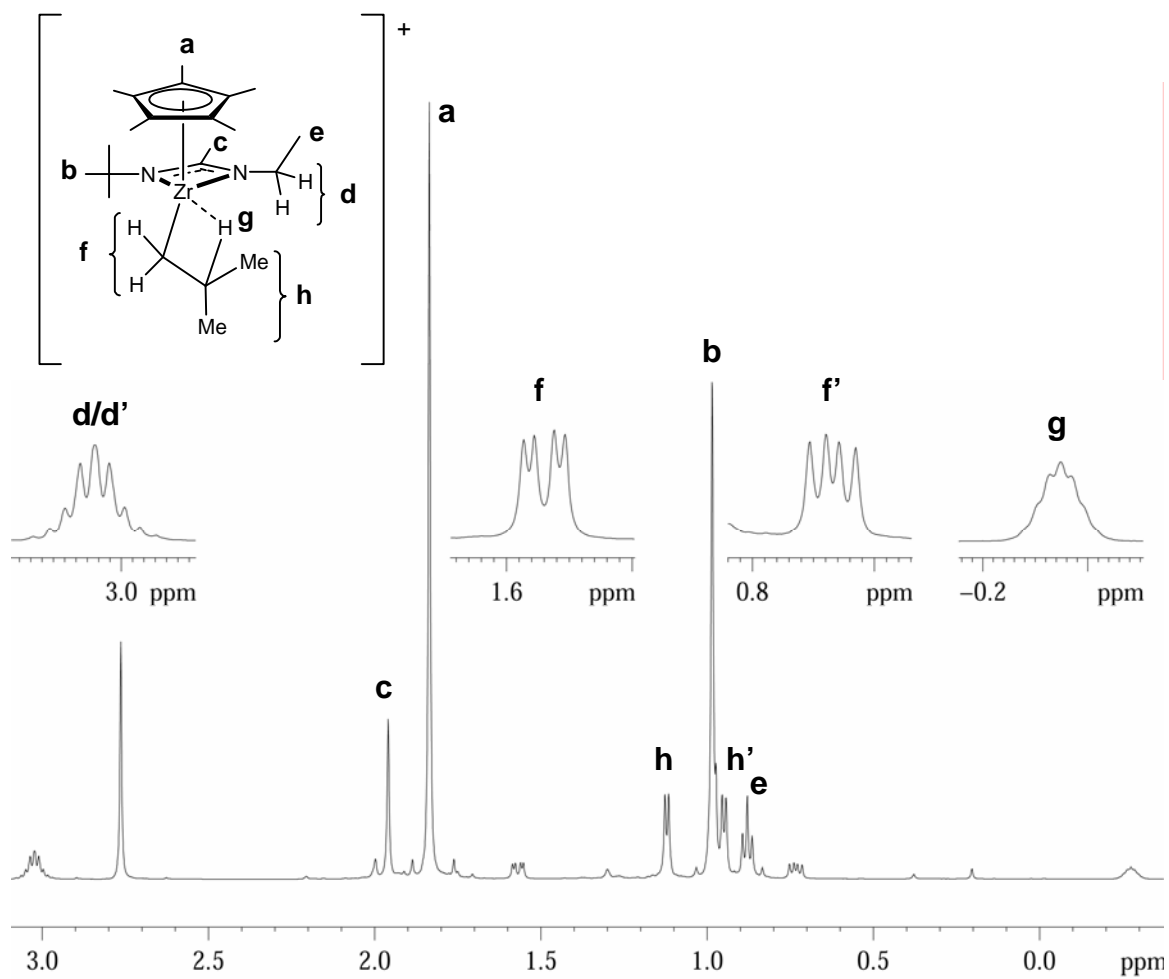


**Figure 21:**  $^1\text{H}$  NMR (400 MHz,  $-10\text{ }^\circ\text{C}$ ,  $\text{C}_6\text{D}_5\text{Cl}$ ) of **33-Bu**. Note the agostically bound  $\beta$ -hydrogen, which occurs as a broad multiplet at  $-0.13$  ppm. Resonance at  $2.77$  ppm is due to  $\text{N}_2\text{N}'$ -dimethylaniline.

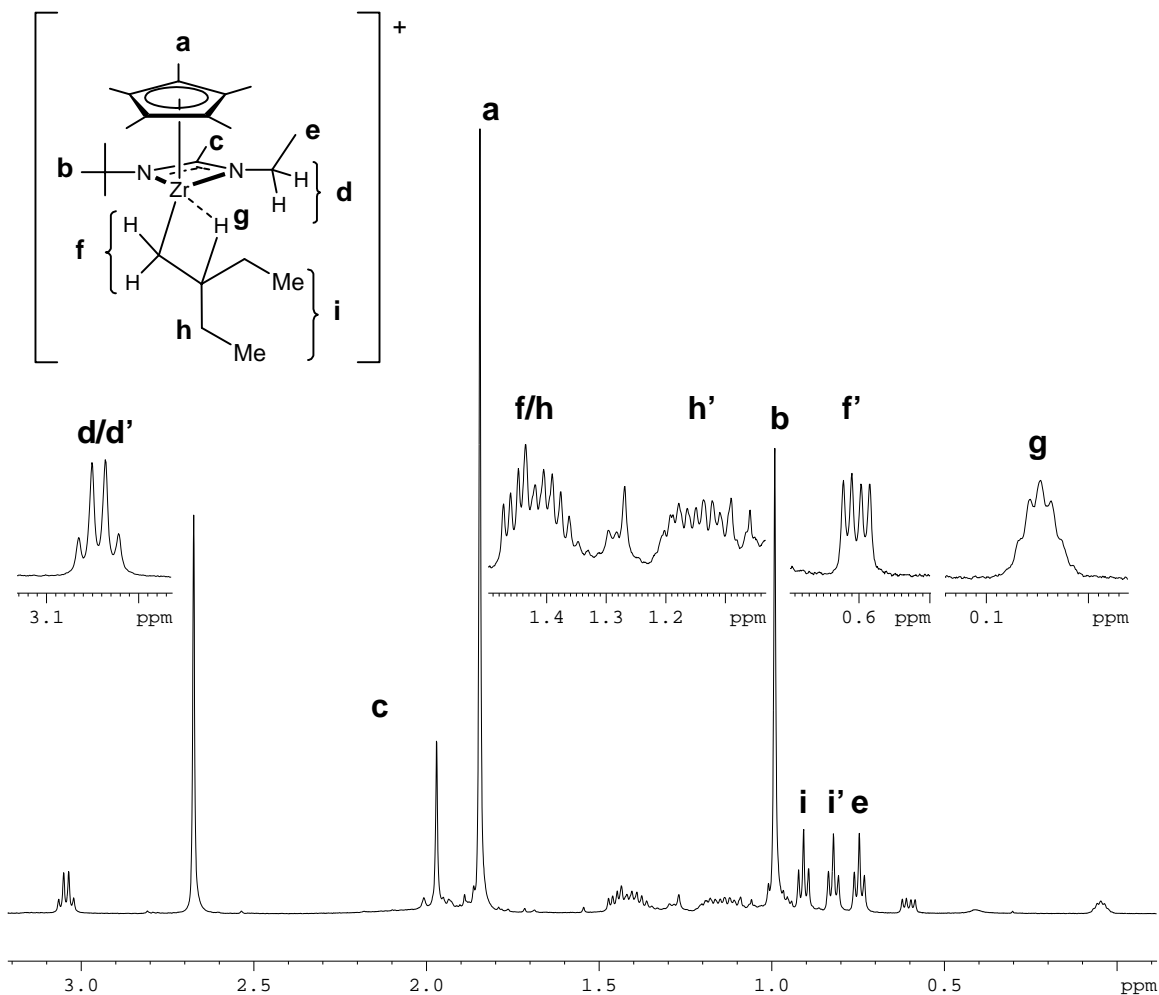


**Figure 22:** <sup>1</sup>H NMR (400 MHz, -10 °C, C<sub>6</sub>D<sub>5</sub>Cl) of **33**-(2-Et-Bu). Note the agostically bound β-hydrogen, which occurs as a broad multiplet at -0.13 ppm.

While several attempts have been made for each derivative of **33**, only the *iso*-butyl derivative provided crystals sufficient for x-ray analysis, as shown in Figure 23. The borate counterion (not shown) is well displaced from the zirconium cation and there are no close Zr-F interactions between the ion pair. The existence of a β-agostic interaction as revealed by solution <sup>1</sup>H NMR data is confirmed by the position of the crystallographically located β-hydrogen atom [*cf.* Zr(1)-H(20A) distance of 2.25(3) Å].<sup>136</sup> Additional evidence for this β-hydrogen agostic interaction is provided by bond angles

around the  $\alpha$ - and  $\beta$ -carbons (Table 4). The geometry of the  $\alpha$ -carbon is quite distorted, with a Zr-C<sub>a</sub>-C<sub>b</sub> bond of only 88.06(16)°. It is also interesting to note that the zirconium-nitrogen bonds in the cation **33**-<sup>i</sup>Bu are very short at 2.1376(18) and 2.1882(18) Å, and so it would appear that this geometric parameter is indeed a good measure of the electron deficiency of the metal center as now established by the zirconium-nitrogen bond length trend: **37**-<sup>i</sup>Bu > **36**'-<sup>i</sup>Bu > **33**-<sup>i</sup>Bu.<sup>137</sup>

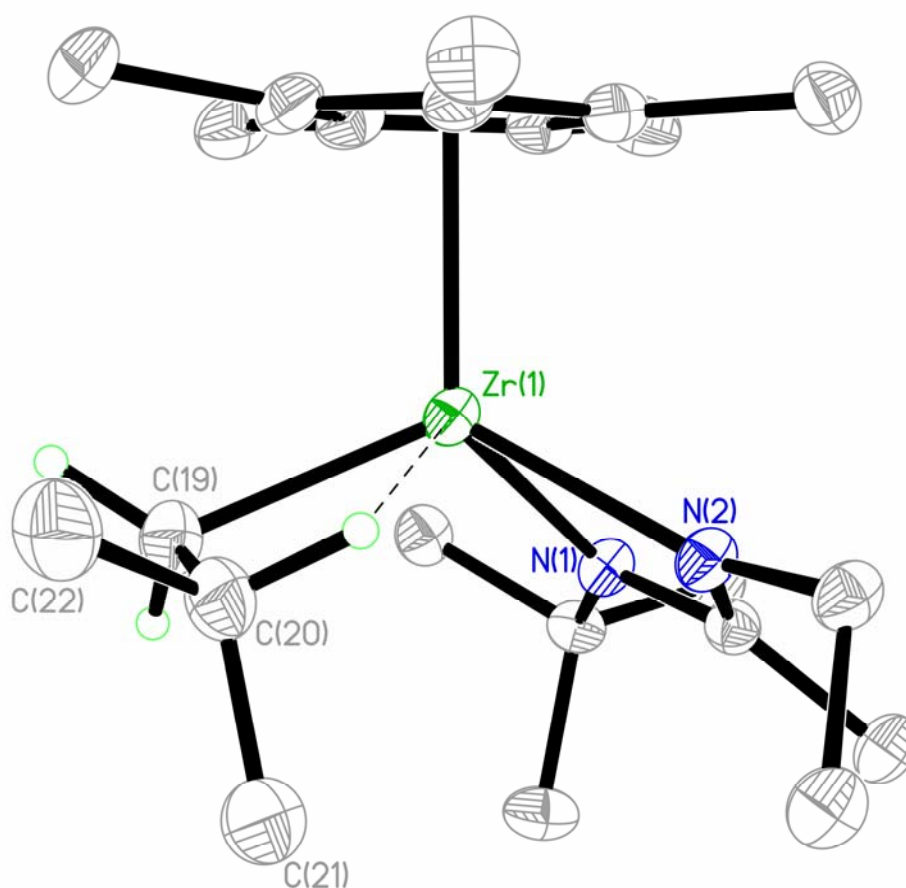


**Figure 23:** Molecular structure (30% thermal ellipsoids) of **33**-<sup>i</sup>Bu. The B(C<sub>6</sub>F<sub>5</sub>)<sub>4</sub> counterion and all hydrogens, aside from the  $\alpha$ - and  $\beta$ -hydrogens of the *iso*-butyl group, have been removed for the sake of clarity.

**Table 4:** Bond angles of the  $\alpha$ - and  $\beta$ -carbons of **33-<sup>i</sup>Bu**.

Bond	Angle (degrees)
C(20)-C(19)-Zr(1)	88.06(16)
C(20)-C(19)-H(19)	116(2) 124(2)
Zr(1)-C(19)-H(19)	122(2) 110(2)
H(19)-C(19)-H(19')	98(3)
C(21)-C(20)-C(19)	112.1(3)
C(21)-C(20)-C(22)	111.6(3)
C(19)-C(20)-C(22)	114.0(3)
C(19)-C(20)-H(20)	113.6(14)
C(21)-C(20)-H(20)	102.9(14)
C(22)-C(20)-H(20)	101.8(14)

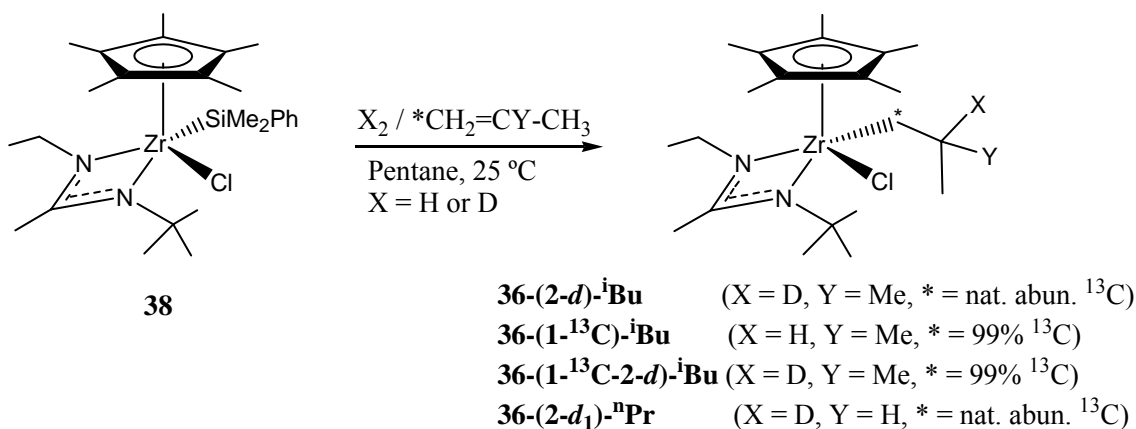
### 2.3.4 Isotopically Labeled Derivatives

As detailed above, the incorporation of isotopic labels into polypropylene, through the polymerization of isotopically labeled monomer, has been useful in elucidating the mechanisms of isomerization reactions. If derivatives of **33-R** undergo isomerization prior to decomposition in a manner similar to that observed during decomposition **16-PB**, the Busico mechanism would dictate that a deuterium label in the  $\beta$ -position would, upon isomerization, necessarily be relocated to what was formerly the  $\alpha$ -carbon. As such, derivatives of **33-R** with isotopic labels in either the  $\alpha$ - or  $\beta$ -position (or both) were desirable.

In order to synthesize isotopically labeled derivatives of **33-R**, the hydrozirconation techniques developed in our lab were utilized.<sup>138</sup> Hydrogenolysis of Cp\*ZrCl(SiMe<sub>2</sub>Ph)[N(Et)C(Me)N(<sup>t</sup>Bu)] (**38**) under an atmosphere of D<sub>2</sub> allowed the hydrozirconation of isobutylene or propylene to provide  $\beta$ -deuterium labeled *iso*-butyl and *n*-propyl compounds **36-(2-*d*)-<sup>i</sup>Bu** and **36-(2-*d*<sub>1</sub>)-<sup>n</sup>Pr** through insertion of the olefin

into the Zr-D bond of the in-situ generated CPZA chloro deuteride species (Scheme 30). Also, the hydrozirconation of (1-<sup>13</sup>C)-isobutylene, synthesized via Wittig reaction between acetone and (<sup>13</sup>C-methyl)triphenylphosphonium iodide, under either H<sub>2</sub> or D<sub>2</sub> provided the <sup>13</sup>C labeled **36-(1-<sup>13</sup>C)-<sup>i</sup>Bu** and the doubly labeled **36-(1-<sup>13</sup>C-2-*d*)-<sup>i</sup>Bu**. Cationic versions of these isotopically labeled compounds, **33-(2-*d*)-<sup>i</sup>Bu**, **33-(1-<sup>13</sup>C)-<sup>i</sup>Bu**, **33-(1-<sup>13</sup>C-2-*d*)-<sup>i</sup>Bu** and **33-(2-*d*<sub>1</sub>)-<sup>n</sup>Pr**, were then obtained in the same fashion as the unlabeled derivatives as detailed above.

**Scheme 30:** Synthesis of isotopically labeled compounds via hydrozirconation.



It is important to note that neither the hydrozirconation reaction nor any of the steps leading to the cationic species resulted in any detectable amount of scrambling of the isotopic labels. Furthermore, none of the isotopically labeled alkyl, chloro or alkyl, methyl derivatives showed scrambling upon heating to 60 °C for several hours. This stands in sharp contrast to the isomerization of neutral alkyl, chloro zirconocene resulting from hydrozirconation of internal olefins.<sup>63</sup>

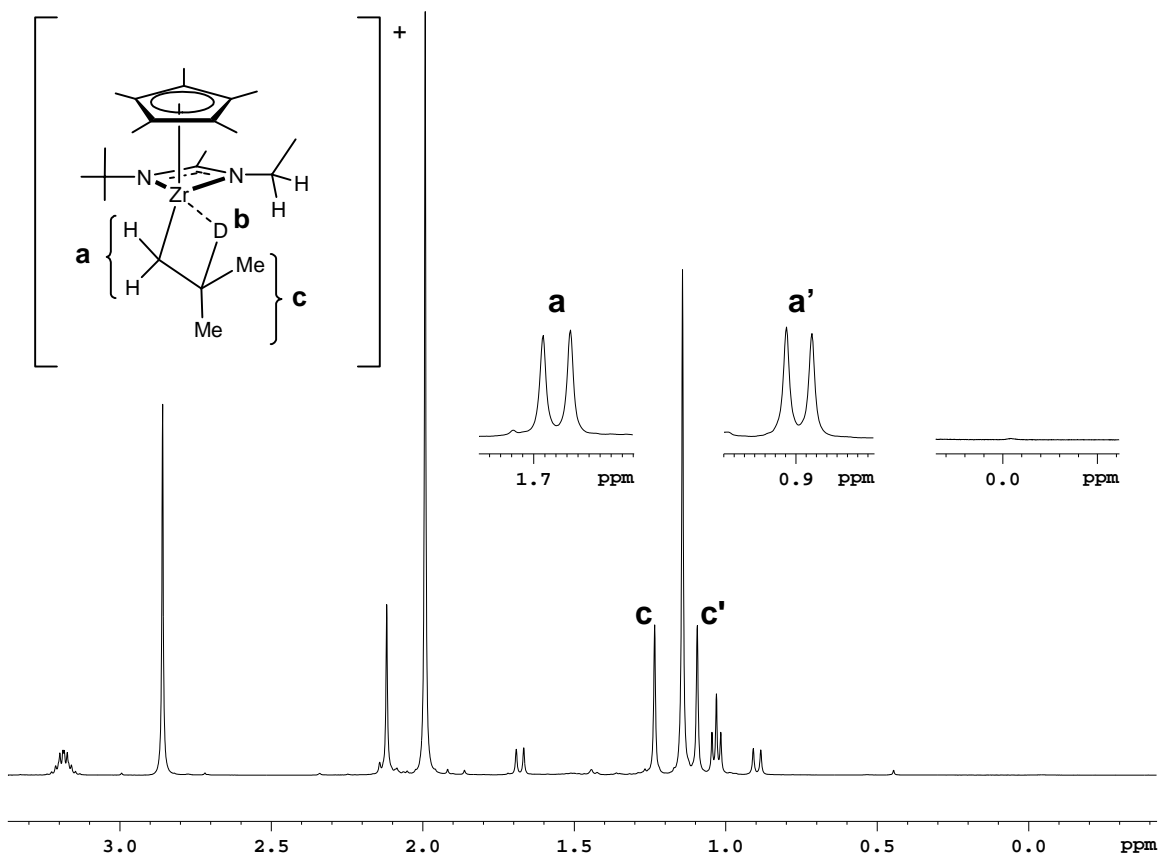


**Figure 24:**  $^1\text{H}$  NMR (500 MHz,  $0\text{ }^\circ\text{C}$ ,  $\text{C}_6\text{D}_5\text{Cl}$ ) of  $33\text{-(2-d)-iBu}$ . Note that the  $\beta$ -hydrogen resonance has disappeared as compared to  $33\text{-iBu}$  (Figure 21).

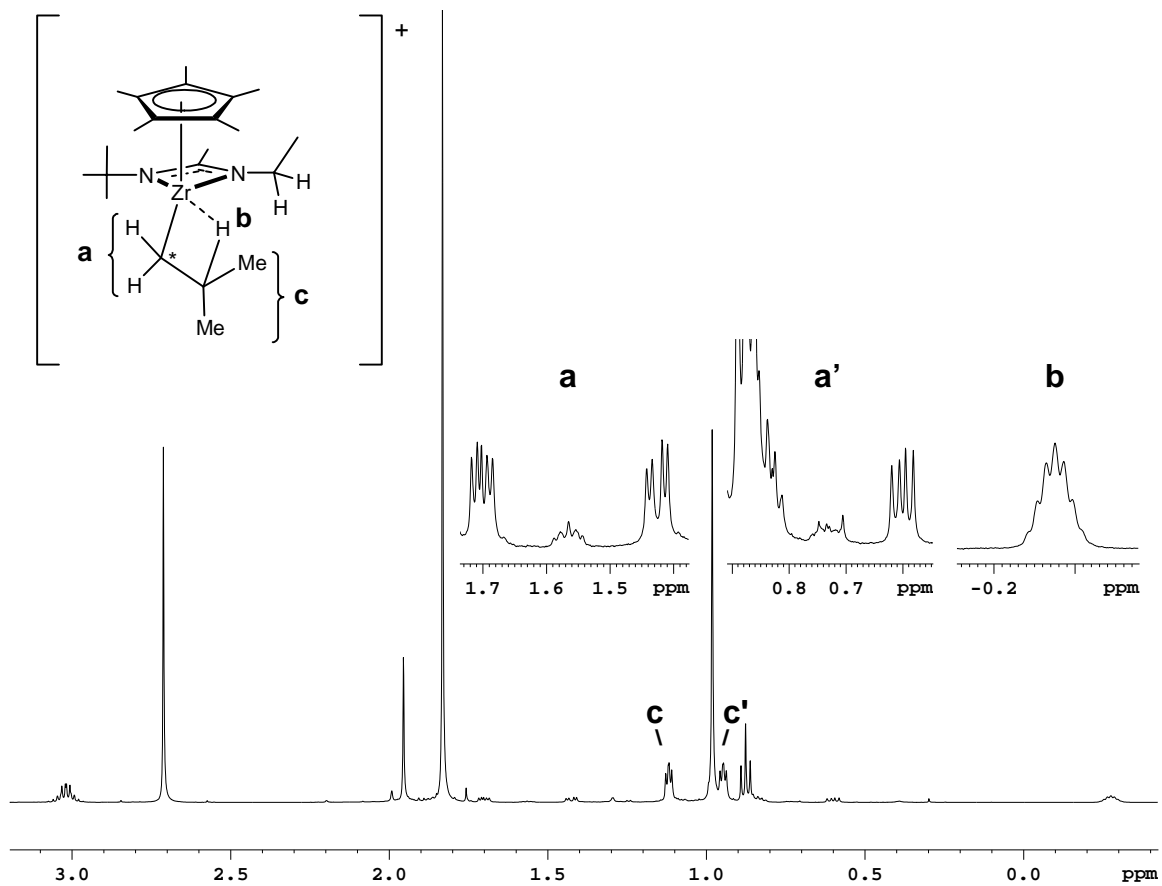


**Figure 25:**  $^1\text{H}$  NMR (500 MHz,  $-10\text{ }^\circ\text{C}$ ,  $\text{C}_6\text{D}_5\text{Cl}$ ) of  $33\text{-}(1\text{-}^{13}\text{C})\text{-iBu}$ . Note that the  $\alpha$ -hydrogen resonances have been split by the  $^{13}\text{C}$ -label as compared to  $33\text{-iBu}$  (Figure 21).

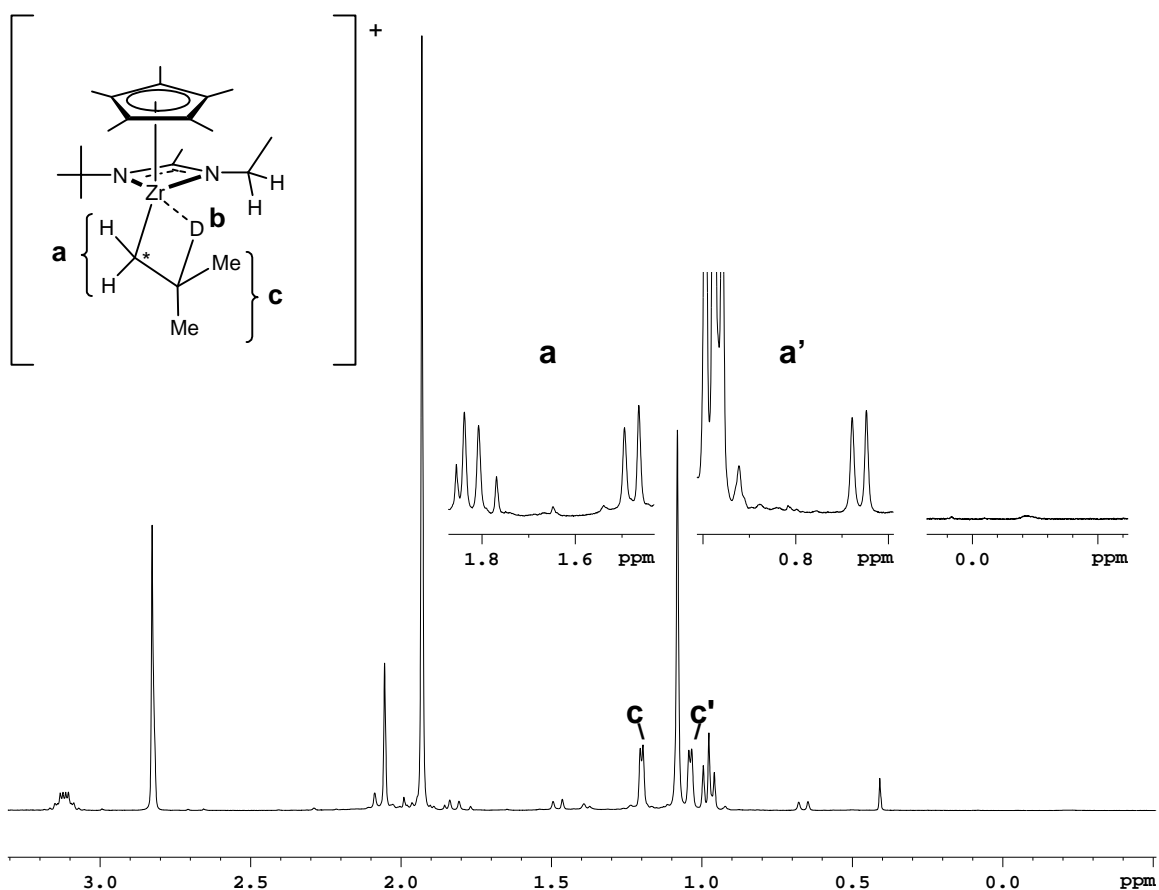


**Figure 26:**  $^1\text{H}$  NMR (500 MHz,  $-10\text{ }^\circ\text{C}$ ,  $\text{C}_6\text{D}_5\text{Cl}$ ) of **33**-(1- $^{13}\text{C}$ -2- $d$ )- $i$ -Bu. Note that the  $\alpha$ -hydrogen resonances have been split by the  $^{13}\text{C}$ -label and the  $\beta$ -hydrogen resonance has disappeared as compared to **33**- $i$ Bu (Figure 21).

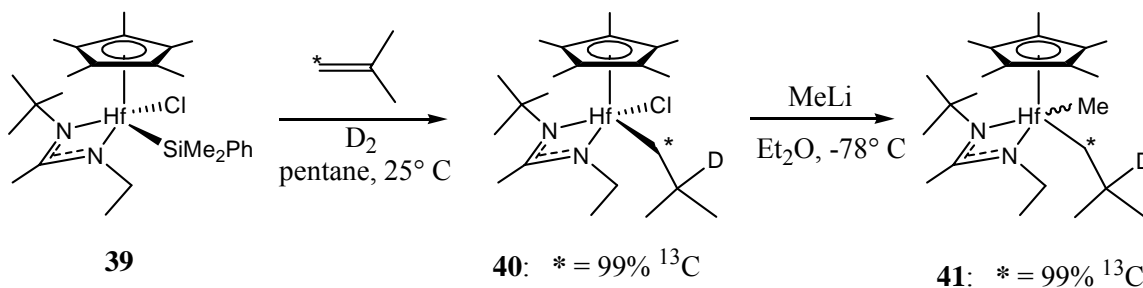
### 2.3.5 Hafnium Derivatives

Given that the cationic cyclopentadienyl hafnium acetamidinate (CPHA) methyl and *iso*-butyl analogs of **33-R** can also serve as initiators for the isospecific living polymerization of 1-hexene,<sup>139</sup> albeit with a rate of propagation that is  $\sim 60$  times slower than their second row cousins, it was decided to expand the range of the present studies to include isotopically labeled hafnium derivatives. A neutral base-stabilized hafnocene isobutylene complex has been isolated, although not in the context of chain-end epimerization studies.<sup>140</sup> In addition, considering all the previous failed attempts to

prepare a cationic *tert*-butyl derivative of **33-R**, it was felt that better success might be achieved in efforts to synthesize the corresponding cationic hafnium *tert*-butyl species.

The synthesis of double isotopically labeled hafnium *iso*-butyl was achieved in analogous fashion to the synthetic protocol used to prepare the zirconium analog **33-(1-<sup>13</sup>C-2-*d*-<sup>i</sup>Bu)**. Thus, as Scheme 31 reveals, hydrogenolysis of Cp\*HfCl(SiMe<sub>2</sub>Ph)[N(Et)C(Me)N(<sup>t</sup>Bu)] (**39**) under a D<sub>2</sub> atmosphere resulted in the hydrohafnation<sup>141</sup> of (1-<sup>13</sup>C)-*iso*butylene to provide the desired isotopically labeled chloro, *iso*-butyl hafnium compound **40**; albeit in only moderate yield as compared to the analogous hydrozirconation reaction (*cf* 70% yield for **36-(1-<sup>13</sup>C-2-*d*-<sup>i</sup>Bu)** vs. 48% for **40**). Methylation of **40** using the standard procedure successfully provided the isotopically labeled methyl, *iso*-butyl hafnium compound **41**. Finally, treatment of **41** with 1 equiv of [PhNMe<sub>2</sub>H][B(C<sub>6</sub>F<sub>5</sub>)<sub>4</sub>] in chlorobenzene at -10° C provided the desired cationic species Cp\*Hf[(1-<sup>13</sup>C-2-*d*-<sup>i</sup>Bu)[N(Et)C(Me)N(<sup>t</sup>Bu)]]{[BC<sub>6</sub>F<sub>5</sub>]} (**42**) in quantitative fashion as determined by <sup>1</sup>H NMR. In this respect, it is important to note that it was previously reported that *no evidence for a β-hydrogen agostic interaction* could be found for an analogous, unlabeled CPHA *iso*-butyl cation (**43**, Figure 27) in solution using 1-D and 2-D NMR techniques.<sup>139</sup>

**Scheme 31:** Synthesis of isotopically labeled hafnium derivatives.



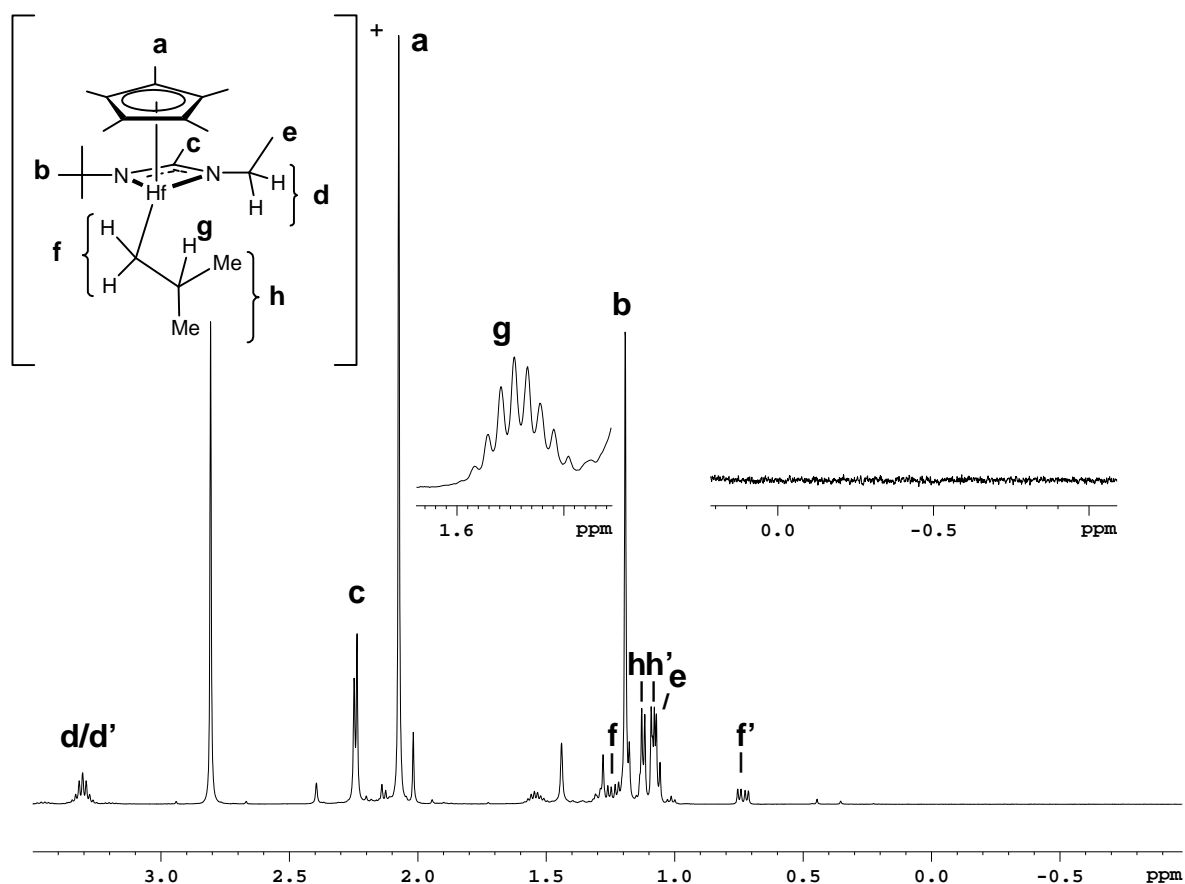


**Figure 27:**  $^1\text{H}$  NMR (500 MHz,  $0\text{ }^\circ\text{C}$ ,  $\text{C}_6\text{D}_5\text{Cl}$ ) of **43**. Note the well-defined coupling pattern of the  $\beta$ -hydrogen resonance as compared to the broad multiplet of **33-<sup>i</sup>Bu** (Figure 21).

Regarding the synthesis of a cationic CPHA *tert*-butyl complex (**44**), the first attempt involved alkylation of the hafnium dichloride starting material **45**<sup>139</sup> with *tert*-butyl lithium to provide the chloro, *tert*-butyl product **46** in an analogous manner to the zirconium derivatives as depicted in Scheme 27. Single crystal X-ray analysis confirmed the structure of **46** (Figure 28), which has uniformly shorter metal-ligand bond lengths than the previously reported zirconium analog **36-<sup>t</sup>Bu** (Table 5).<sup>125</sup> This is commonly observed when comparing isostructural hafnium and zirconium derivatives due to the effect of the lanthanide contraction.<sup>142</sup> Note that in each, the bulky *tert*-butyl group causes the acetamidinate ligand to take on a canted conformation.

**Table 5:** Comparison in selected bond lengths of **46** and **36-<sup>t</sup>Bu**.

Bond	M = Hf ( <b>46</b> )	M = Zr ( <b>36-<sup>t</sup>Bu</b> )
M-N(2)	2.211(2)	2.2360(17)
M-N(1)	2.254(2)	2.2928(18)
M-C(CH <sub>3</sub> ) <sub>3</sub>	2.298(3)	2.316(2)
M-Cl(1)	2.4389(7)	2.4732(6)
	2.485(3)	2.501(2)
	2.492(3)	2.503(2)
M-Cp*	2.530(3)	2.548(2)
	2.534(3)	2.554(2)
	2.573(3)	2.591(2)

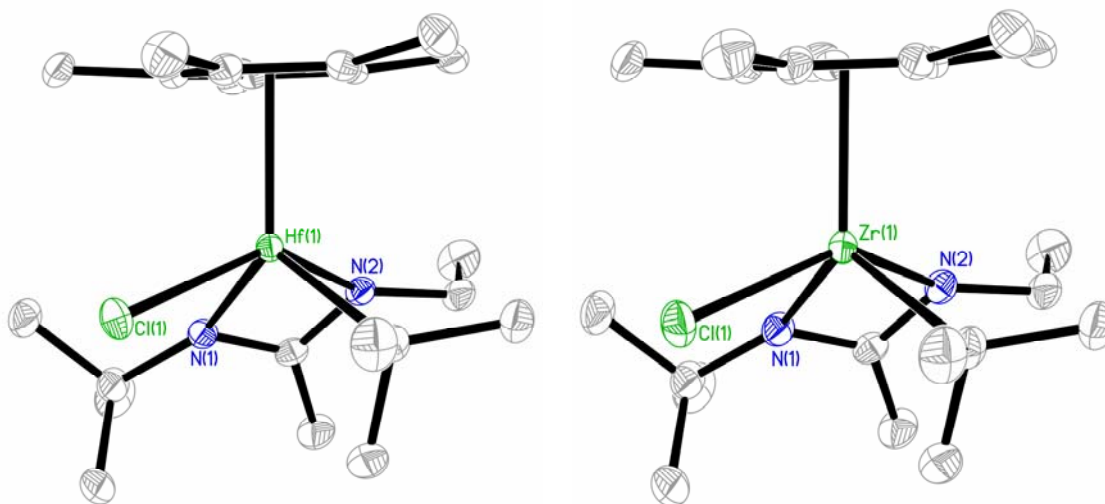
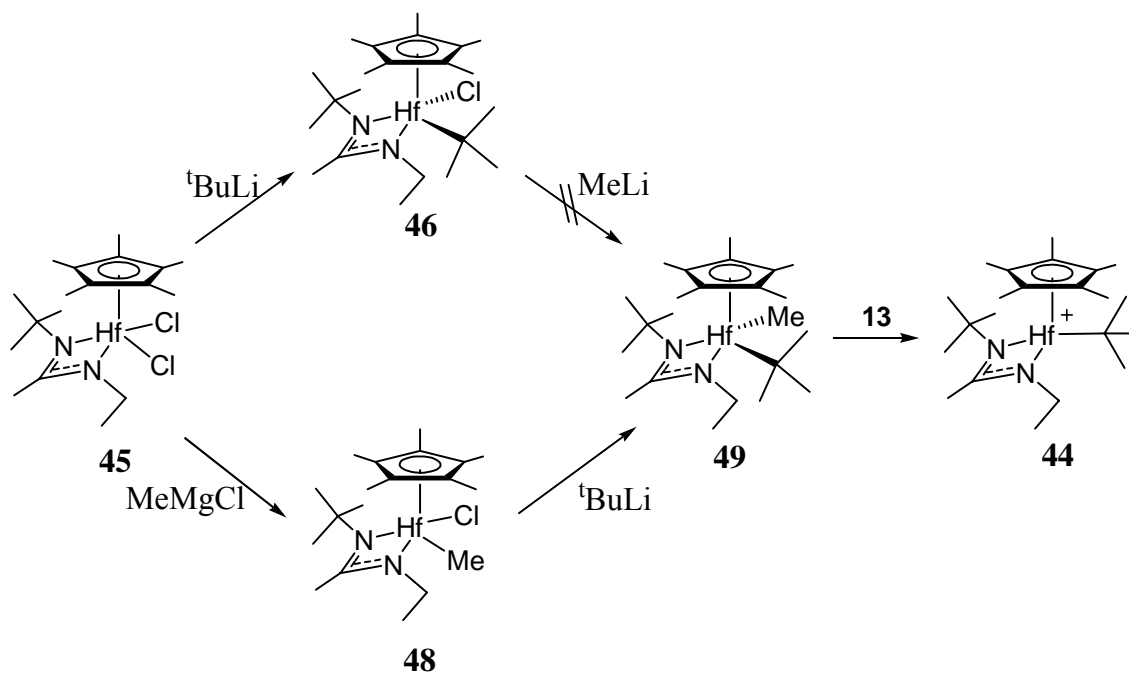


**Figure 28:** Molecular structure (30% thermal ellipsoids) of **46** (left) and **36-<sup>t</sup>Bu** (right). All hydrogens have been removed for the sake of clarity.

Unfortunately, in the same manner as the zirconium derivative, attempts to methylate **46** produced only the unlabeled derivative of the methyl, *iso*-butyl compound, Cp\*HfMe(*i*Bu)[N(Et)C(Me)N(*t*Bu)] (**47**). However, success was at last realized in reversing the order of alkylation of **45**. As depicted in Scheme 32, methylation of **45** using methylmagnesium chloride first provided the chloro, methyl compound **48**, which

was then reacted with *tert*-butyl lithium overnight at  $-55\text{ }^{\circ}\text{C}$  to afford the elusive methyl, *tert*-butyl complex **49**. Finally, upon treatment of **49** with 1 equiv. of **13**, the desired cationic *tert*-butyl hafnium complex **44** was quantitatively generated as determined by  $^1\text{H}$  NMR spectroscopy. It is important to note that the resonance of the  $\beta$ -hydrogens appears as a single sharp singlet with no evidence for any  $\beta$ -agostic interactions, as shown in Figure 29.

**Scheme 32:** Synthesis of the hafnium *tert*-butyl cation.



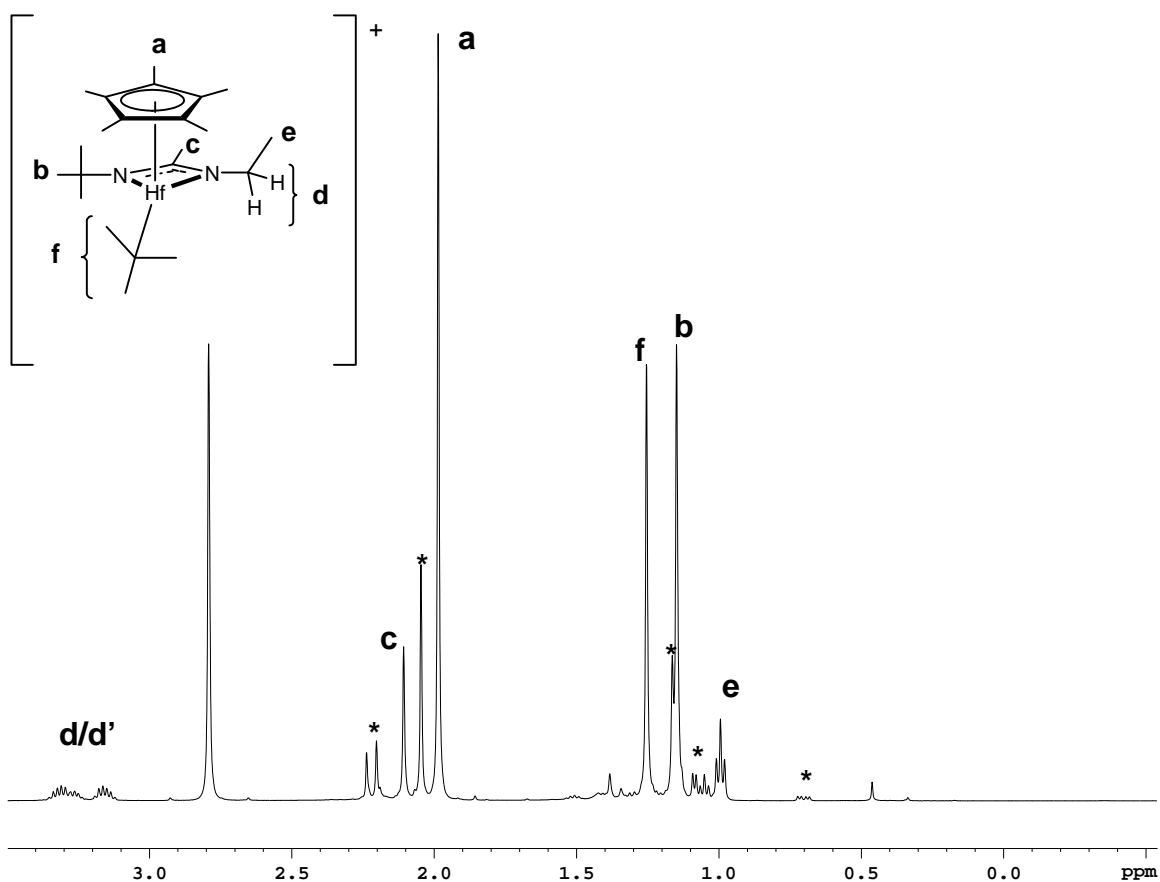


**Figure 29:**  $^1\text{H}$  NMR (500 MHz,  $-25\text{ }^\circ\text{C}$ ,  $\text{C}_6\text{D}_5\text{Cl}$ ) of **44**. Note that isomerization to **43** (Figure 27) has already begun (resonances marked with \*).

## 2.4 Results

### 2.4.1 Stability of CPZA Alkyl Cations

All derivatives of **33-R** appeared quite stable at  $-10\text{ }^\circ\text{C}$  (no detectable decomposition or isomerization after  $\sim 18$  hours by  $^1\text{H}$  NMR). At the higher temperature of  $30\text{ }^\circ\text{C}$ , however, decomposition does ensue and an initial screening qualitatively determined a relative order of stability of **33-R** to be  $\text{R} = \text{Et} > {}^n\text{Pr} > {}^n\text{Bu} > {}^i\text{Pr} > {}^i\text{Bu} > 2\text{-ethylbutyl}$ .<sup>132</sup> Based on this observation, several of these complexes were targeted for more in-depth analysis, with the subset being comprised of: **33-<sup>n</sup>Pr**, **33-<sup>i</sup>Pr**, **33-<sup>i</sup>Bu**, and **33-(2-Et-Bu)** (Figure 30).

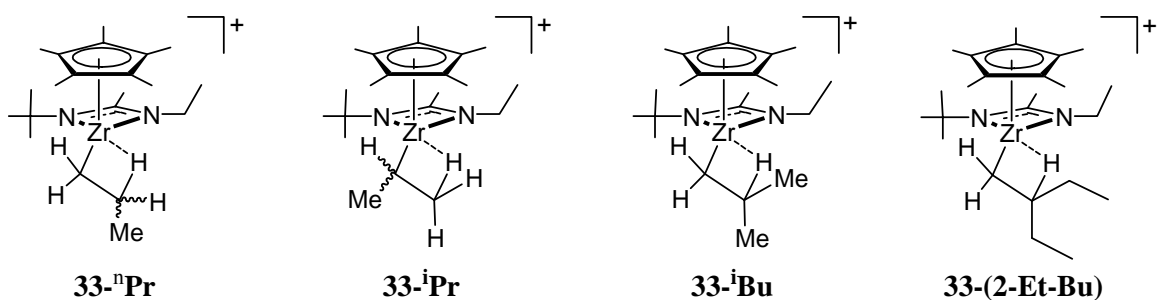


**Figure 30:** Subset of CPZA cations chosen for detailed low-temperature studies.

All derivatives of **33** appeared quite stable by  $^1\text{H}$  NMR at  $-10\text{ }^\circ\text{C}$ , with no detectable decomposition or isomerization after  $\sim 18$  hours. At  $0\text{ }^\circ\text{C}$ , **33-<sup>i</sup>Bu** and **33-(2-Et-Bu)** decomposed in a first-order fashion while **33-<sup>n</sup>Pr** and **33-<sup>i</sup>Pr** remained stable. Surprisingly, the 2-ethyl-butyl derivative **33-(2-Et-Bu)** decomposed approximately twice as fast as the *iso*-butyl derivative **33-<sup>i</sup>Bu** ( $k_d = 0.066\text{ h}^{-1}$ ;  $t_{1/2} = 10.3\text{ h}$  vs.  $0.035\text{ h}^{-1}$ ;  $20.4\text{ h}$ , respectively). In order to put this disparity into proper perspective, the rate of decomposition of a living polymer derived from **16** was also measured at  $0\text{ }^\circ\text{C}$ . This was done by polymerizing  $\sim 15$  equivalents of  $(1-^{13}\text{C})$ -1-decene in chlorobenzene- $d_5$  at  $-10\text{ }^\circ\text{C}$  to provide oligomeric living poly( $1-^{13}\text{C}$ -decene) (**16-PD**), which was then allowed to equilibrate at  $0\text{ }^\circ\text{C}$  inside the NMR. Following the disappearance of the  $\alpha$ -carbon  $^{13}\text{C}$  resonance at  $82.3\text{ ppm}^{96}$  using inverse gated  $^{13}\text{C}$  NMR allowed determination of  $k_d$  to be  $0.212\text{ h}^{-1}$  ( $t_{1/2} = 3.2\text{ h}$ ), more than six times greater than that of **33-<sup>i</sup>Bu**.

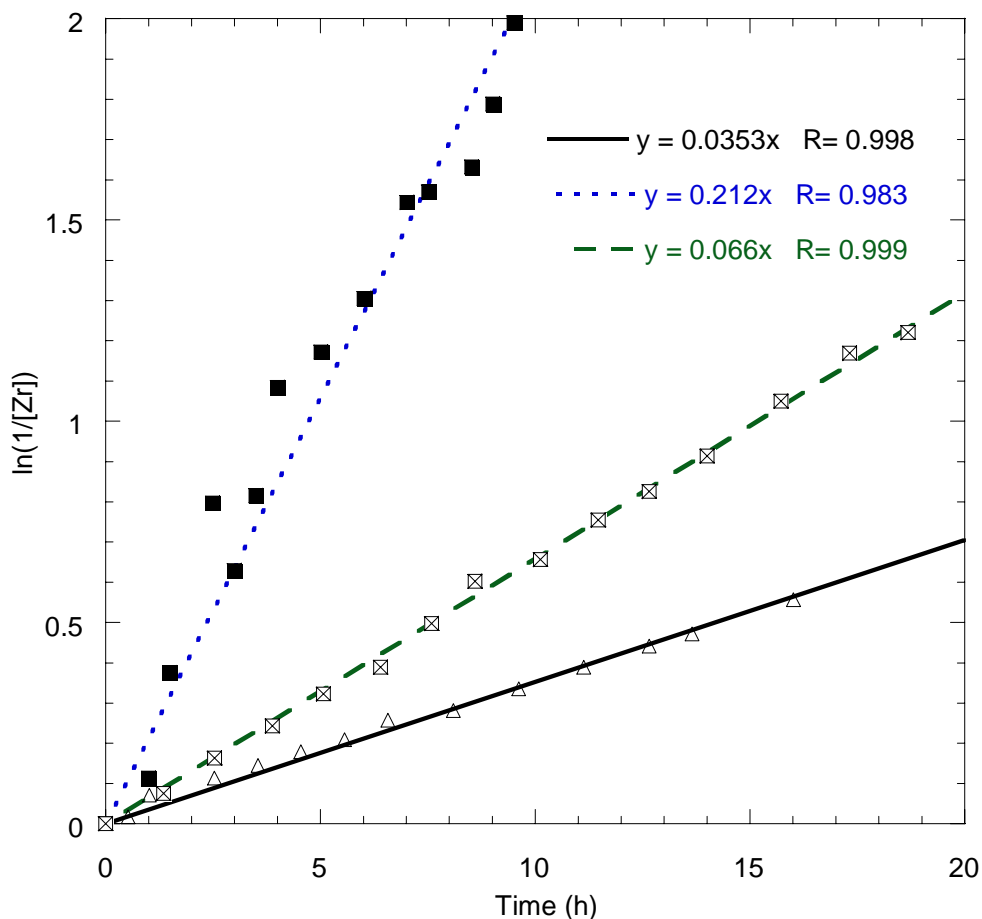


**Figure 31:** Decomposition of **33-iBu** (solid line), **33-(2-Et-Bu)** (dashed line) and **16-PD** (dotted line) at 0 °C in chlorobenzene- $d_5$ , as observed by  $^1\text{H}$  (**33-iBu**, **33-(2-Et-Bu)**) or  $^{13}\text{C}$  (**16-PD**) NMR.

The pathway by which **33-iBu** decomposes was probed by observing the course of decomposition of the single deuterium labeled derivative **33-(2-d)-iBu** and the double isotopically labeled derivative **33-(1- $^{13}\text{C}$ -2-d)-iBu** through  $^1\text{H}$  and  $^{13}\text{C}$  NMR. Upon warming **33-(2-d)-iBu** from -10 to 0 °C, the original  $\beta$ -positioned deuterium label began to undergo scrambling almost immediately, concurrently with decomposition, reaching apparent equilibrium in approximately 11 hours (Figure 32). In following the decomposition of **33-(1- $^{13}\text{C}$ -2-d)-iBu**, by  $^{13}\text{C}$  NMR, two 1:1:1 triplets for diastereotopic

$^{13}\text{CH}_2\text{D}$ -labeled methyl groups of the *iso*-butyl substituent were observed, with no evidence being obtained for the corresponding singlets that should arise from formation of single  $^{13}\text{C}$ -labeled methyl groups (Figure 33). The mechanism by which scrambling occurs always places a D and  $^{13}\text{C}$  label on the same carbon atom as shown in Scheme 33, and this is consistent with the multi-step sequence of events also shown in this scheme that is identical in nature to the mechanism proposed by Busico and co-workers for chain-end epimerization (*vide supra*).

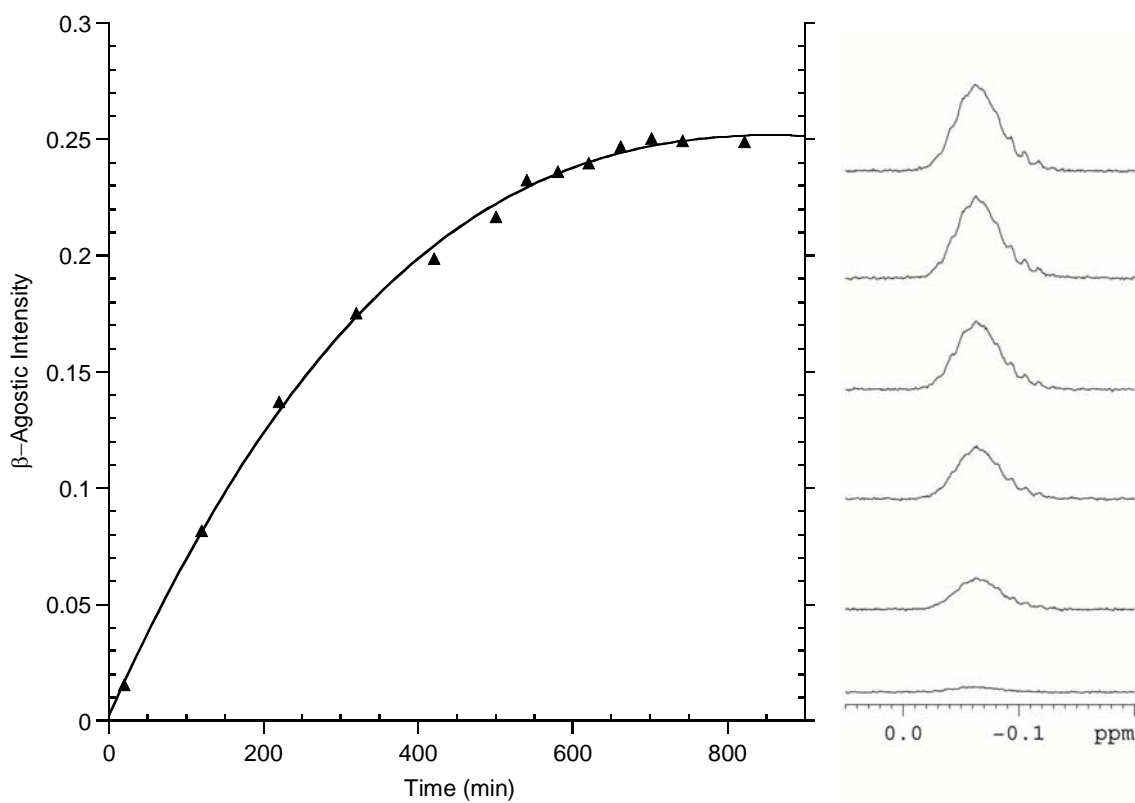


**Figure 32:** Left: graph of the intensity of the  $\beta$ -agostic peak (relative to amidinate ethyl  $\text{CH}_2$  peaks) vs. time. Trend line provided as a guide for the eye. Right: the  $\beta$ -agostic region of the  $^1\text{H}$  NMR (500 MHz, 0  $^\circ\text{C}$ ,  $\text{C}_6\text{D}_5\text{Cl}$ ) of **33-(2-*d*)-<sup>i</sup>Bu**. Spectra correspond to the first 6 data points on the graph, bottom to top.

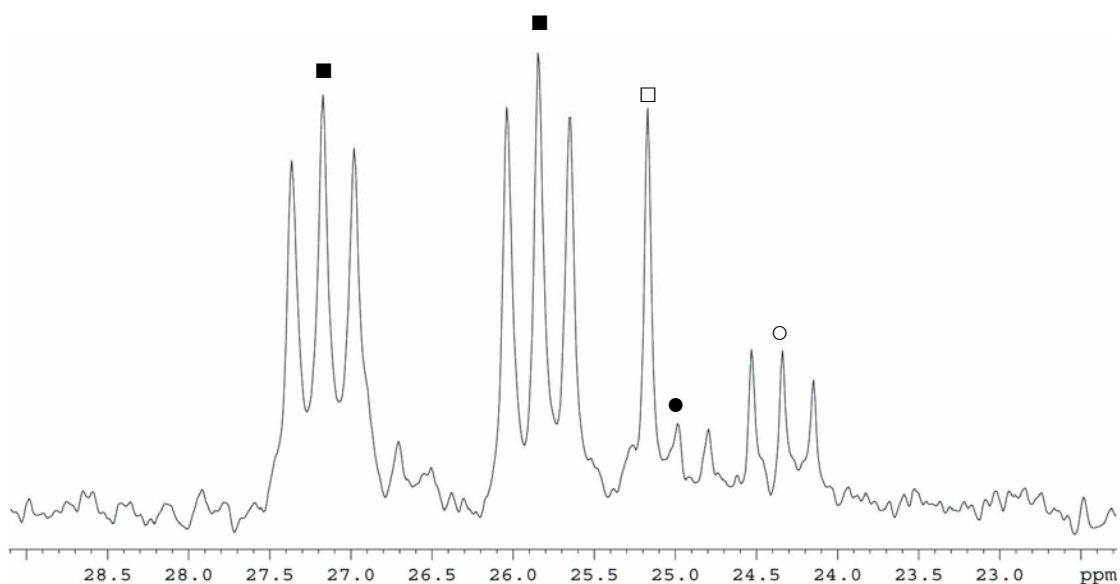
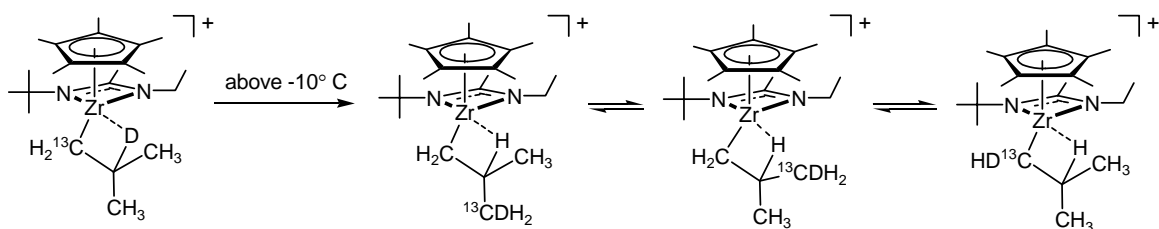


**Figure 33:**  $^{13}\text{C}\{^1\text{H}\}$  NMR (100 MHz,  $\text{C}_6\text{D}_5\text{Cl}$ ,  $0^\circ\text{C}$ ) of **33-(1- $^{13}\text{C}$ -2-*d*)-*i*Bu** after 15 hours at  $0^\circ\text{C}$ . ■ - diastereotopic doubly labeled methyl groups ( $^{13}\text{CH}_2\text{D}$ ) of the *iso*-butyl group of **33-(1- $^{13}\text{C}$ -2-*d*)-*i*Bu**. □ -  $\text{DC}(\text{CH}_3)_2(^{13}\text{CH}_3)$ . ● -  $\text{HC}(\text{CH}_3)_2(^{13}\text{CH}_2\text{D})$ . ○ -  $\text{H}_2\text{C}=\text{C}(\text{CH}_3)(^{13}\text{CH}_2\text{D})$ .

**Scheme 33:** Isotopic scrambling observed in **33-(1- $^{13}\text{C}$ -2-*d*)-*i*Bu**.



In addition to the isobutylene product expected from  $\beta$ -hydride elimination, formation of isobutane was also observed to occur continuously throughout decomposition, both appearing in a zero-order fashion. Initially, only resonances attributable to singly labeled methyl groups ( $^{13}\text{CH}_3$ ) of isobutane, presumably (1- $^{13}\text{C}$ -2-*d*)-2-methylpropane from the protonolysis of the unscrambled *iso*-butyl fragment, but as the quantity of scrambled **33-(1- $^{13}\text{C}$ -2-*d*)-*i*Bu** builds up, increasing amounts of (1- $^{13}\text{C}$ -1-*d*)-2-methylpropane are generated as observed in Figure 33. Schrock and co-workers<sup>111</sup> previously reported formation of isobutane during decomposition of their *iso*-butyl

hafnium initiator, but they attributed this product to the reaction of the initiator with dimethylaniline, which is a byproduct of activation using  $[\text{PhNHMe}_2][\text{B}(\text{C}_6\text{F}_5)_4]$  (**13**). No evidence of a reaction between any derivative of **33-R** and dimethylaniline was detected in the present study, and replacing this borate with  $[\text{Ph}_3\text{C}][\text{B}(\text{C}_6\text{F}_5)_4]$  (**19**), which can also be used to generate **33-R** from **37-R** through methide abstraction, albeit with lower chemoselectivity (a small amount of **16** is generated through competitive alkyl group abstraction), unfortunately did not prevent production of 2-methylpropane during decomposition of **33-<sup>i</sup>Bu**. Other attempts to remove obvious proton sources from the equation (e.g., use of silylated glassware) were likewise unsuccessful.

The decomposition products of **33-(2-Et-Bu)** also showed signs of isomerization in the form of several different alkene isomers, analogously to the alkene end groups observed for the oligomeric poly(1-butene) resulting from the decomposition of **16-PB**. As such,  $^1\text{H}$  NMR analysis of vacuum transferred volatiles from a sample of decomposed **33-(2-Et-Bu)** revealed not only the 2-ethyl-1-butene, as produced by  $\beta$ -hydride elimination without isomerization, was accompanied by lesser amounts of 2-ethyl-2-butene and 3-methyl-1-pentene, produced from the zirconium center chain-walking within the group before elimination. However, none of the discrete, cationic alkyl derivatives expected from isomerization, **33-R** with  $\text{R} = 3\text{-methyl-3-pentyl}$ ,  $3\text{-methyl-2-pentyl}$ , or  $3\text{-methyl-1-pentyl}$ , were observed. Once again, a significant amount of alkane (2-ethylbutane) was produced concurrently with the alkenes.

Since the cationic *tert*-butyl derivative has not yet yielded to synthesis, it has not been possible to investigate the stability of this species relative to that of the *iso*-butyl cation. However, a similar investigation was conducted with the *n*-propyl and *iso*-propyl

derivatives, in the hopes that comparable behavior would be observed. As stated previously, both **33-<sup>n</sup>Pr** and **33-<sup>i</sup>Pr** remained unchanged over extended periods of time at 0 °C in chlorobenzene solution, a temperature at which both **33-<sup>i</sup>Bu** and **33-(2-Et-Bu)** undergo isomerization and decomposition. At 5 °C, however, **33-<sup>i</sup>Pr** disappeared in a first order fashion ( $k = 0.010 \text{ h}^{-1}$ ,  $t_{1/2} = 68 \text{ h}$ ) with only a trace amount of decomposition being observed, while **33-<sup>n</sup>Pr** appeared in a zero-order fashion. This is consistent with slow  $\beta$ -hydride elimination of **33-<sup>i</sup>Pr** followed by rapid reinsertion or isomerization to **33-<sup>n</sup>Pr**. In order to determine if this isomerization process is reversible, decomposition of the deuterium labeled *n*-propyl derivative **33-(2-*d*<sub>1</sub>)-<sup>n</sup>Pr** was studied at elevated temperatures. Thus, at 20 °C, while **33-(2-*d*<sub>1</sub>)-<sup>n</sup>Pr** was observed to decompose in first order fashion ( $k = 0.012 \text{ h}^{-1}$ ,  $t_{1/2} = 59.8 \text{ h}$ ), the deuterium label in the  $\beta$ -position of the *n*-propyl group *did not* show any evidence of scrambling (see Figure 34 for <sup>1</sup>H NMR), and this remained true at all temperatures examined up to 50 °C. Curiously, propylene, the expected product of  $\beta$ -hydride elimination of **33-<sup>n</sup>Pr** and **33-<sup>i</sup>Pr**, was not observed in either case. Unfortunately, the alkane region of the <sup>1</sup>H NMR was not clear enough to verify propane as an alternate decomposition product, although it is possible that the volatility of propylene and propane produced is contributing to the difficulty in detection. Eyring analysis determined the activation parameters to be  $\Delta H^\ddagger = 22.0 \text{ kcal/mol}$ ,  $\Delta S^\ddagger = 3.3 \text{ eu}$  for **33-<sup>i</sup>Pr** and  $\Delta H^\ddagger = 21.6 \text{ kcal/mol}$ ,  $\Delta S^\ddagger = -2.0 \text{ eu}$ . The relatively low  $\Delta H^\ddagger$  of each process suggests that the rate limiting step involves bond breaking and forming in a fairly concerted fashion, while the low absolute value of  $\Delta S^\ddagger$  is likely due to pre-organization of the ground-state resulting from the strong  $\beta$ -agostic interaction.

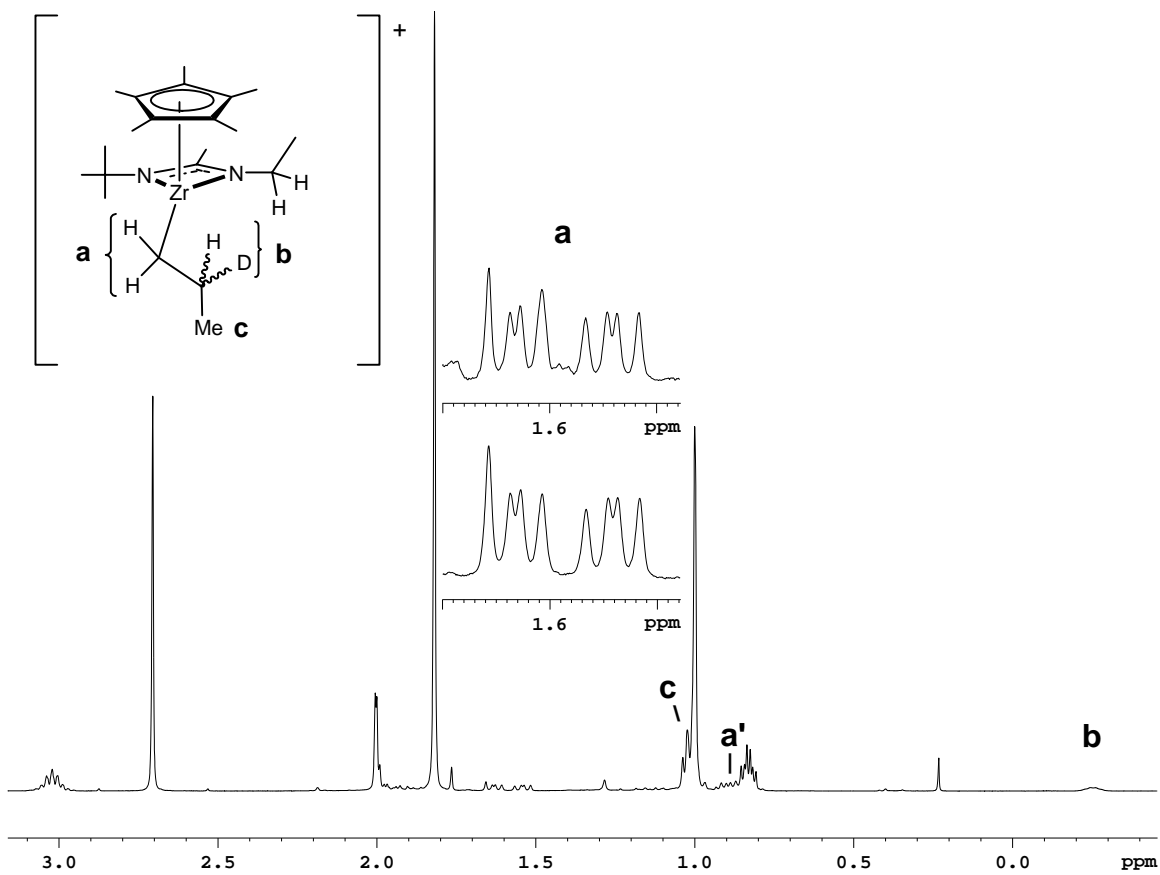


**Figure 34:**  $^1\text{H}$  NMR (500 MHz, 40 °C,  $\text{C}_6\text{D}_5\text{Cl}$ ) of **33-(2- $d_1$ )- $n$ Pr** as a 1:1 mixture of diastereomers. Insert: expansion of the  $\alpha$ -hydrogen resonance immediately upon warming to 40 °C (bottom) and after 5 h at 40 °C (top). Note that the coupling pattern does not change.

**Table 6:** Kinetic parameters of isomerization/decomposition of **33-R**.

R	T(°C)	k ( $\text{h}^{-1}$ )	$t_{1/2}$ (h)	$\Delta H^\ddagger$ (kcal/mol)	$\Delta S^\ddagger$ (eu)
$i\text{Pr}$	5	0.010	67.6	22.0	3.3
	10	0.021	33.4		
	15	0.042	16.4		
	20	0.082	8.4		
$(2-d_1)\text{-}n\text{Pr}$	20	0.012	59.8	21.6	-2.0
	30	0.029	23.9		
	35	0.073	9.5		
	40	0.105	6.6		
	45	0.246	2.8		
	50	0.343	2.0		

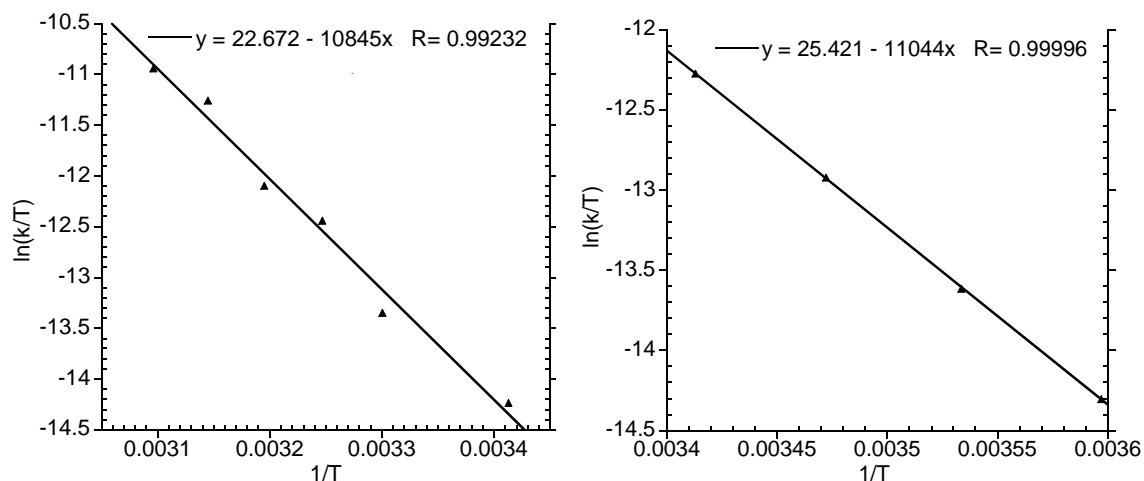


**Figure 35:** Eyring plots for the decomposition/isomerization of **33-nPr** (left) and **33-iPr** (right).

#### 2.4.2 Stability of CPHA Alkyl Cations

With respect to hafnium derivatives, activation of **49** with  $[\text{PhNHMe}_2][\text{B}(\text{C}_6\text{F}_5)_4]$  provided the cationic *tert*-butyl derivative **44**, as detailed above. This complex was found to be highly unstable, isomerizing to the unlabeled *iso*-butyl derivative **43** even at temperatures as low as  $-35\text{ }^\circ\text{C}$  ( $k_d = 0.060\text{ h}^{-1}$ ,  $t_{1/2} = 11.6\text{ h}$ ). At the standard polymerization temperature of  $-10\text{ }^\circ\text{C}$ , isomerization was extremely rapid, with  $t_{1/2} = 24\text{ min}$  ( $k = 1.72\text{ h}^{-1}$ ). The activation parameters ( $\Delta H^\ddagger = 16.4\text{ kcal/mol}$ ,  $\Delta S^\ddagger = -3.0\text{ eu}$ ) were fairly similar to those observed for **33-iPr** and **33-nPr**. The similarly low absolute value of  $\Delta S^\ddagger$  would suggest that while a static  $\beta$ -agostic interaction was not observed by NMR spectroscopy, the complex must initially form an intermediate which contains such an interaction before engaging in  $\beta$ -hydride elimination.

**Table 7:** Kinetic parameters of decomposition of **44**.

T(°C)	k (h <sup>-1</sup> )	t <sub>1/2</sub> (h)	ΔH <sup>‡</sup> (kcal/mol)	ΔS <sup>‡</sup> (eu)
-35	0.060	11.6		
-30	0.135	5.1		
-25	0.313	2.2	16.4	-3.3
-20	0.564	1.2		
-15	1.094	0.6		
-10	1.717	0.4		

The unlabeled *iso*-butyl derivative **43**, as obtained from the isomerization of **44**, was also found to be unstable, decomposing slowly even at -35 °C. The rate of decomposition of **43** was measured at 0 °C to be 0.055 h<sup>-1</sup> (t<sub>1/2</sub> = 12.6 h), compared to 0.034 h<sup>-1</sup> (t<sub>1/2</sub> = 20.4 h) for **33-<sup>i</sup>Bu** (vide supra). Following the decomposition of the doubly labeled derivative, **42**, revealed surprising results. By <sup>13</sup>C NMR, no detectable amount of isotopic label scrambling was observed in the cationic species itself, and decomposition products contained no doubly labeled methyl groups. The only resonances observable for the decomposition products were (1-<sup>13</sup>C)-isobutylene, resulting from the elimination of unscrambled **42** and (1-<sup>13</sup>C)-2-methylpropane, presumably with the deuterium label still residing in the 2-position.

## 2.5 Discussion

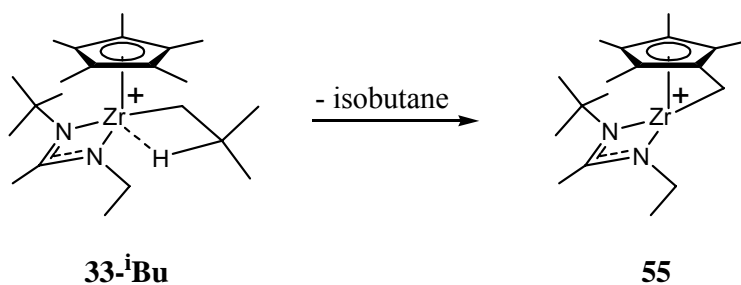
### 2.5.1 Decomposition of CPZA Alkyl Cations

The decomposition pathway of these species was found to be fairly complex, and, despite thorough experimentation as detailed above, retains some degree of mystery. When allowed to proceed to completion, the pendant alkyl groups of **33-<sup>i</sup>Bu** and **33-(2-**

**Et-Bu**) are not only transformed into alkene products, as expected from  $\beta$ -hydride elimination, but a significant amount of alkane and traces of other, as of yet unidentified products were also observed. In addition, while the possible detection of *n*-propane during the decomposition of **33-<sup>n</sup>Pr** or **33-<sup>i</sup>Pr** was obscured by other resonances in the alkane region of the <sup>1</sup>H NMR, resonances attributable to propylene, which would occur further downfield in the alkene region, were also not observed.

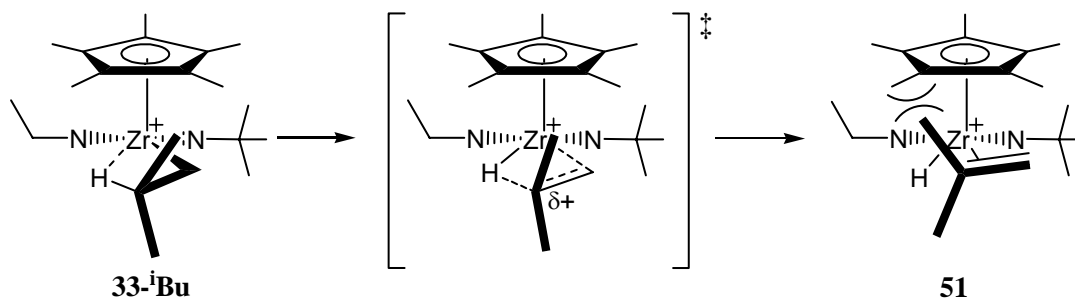
Given the strict first order decomposition of **33-<sup>i</sup>Bu** at different concentrations, we are accordingly led to believe, therefore, that formation of the saturated hydrocarbon co-product of decomposition of this species is due to a competitive first order intramolecular process. As shown in Scheme 34, the most likely decomposition path leading to isobutane from **33-<sup>i</sup>Bu** involves intramolecular H-abstraction from one of the methyl groups of the cyclopentadienyl ligand to produce the cationic ‘tuck-in’ metal species **50** which can reasonably be assumed to be highly reactive. Indeed, there is much precedence for this reaction in organometallic chemistry involving the Cp\* ligand.<sup>143-146</sup> Efforts are currently underway to unequivocally substantiate this decomposition pathway as it clearly has possible relevance to attempts to utilize the initiators **33-R** at temperatures well above that which has previously been shown to provide clear living character in the polymerizations of higher  $\alpha$ -olefins (e.g., -10° C in the case of 1-hexene). For the *n*-propyl and *iso*-propyl derivatives, at no temperature was propylene observed, and thus, it is possible that intramolecular H-abstraction from the cyclopentadienyl ligand is the dominant decomposition path for **33-<sup>n</sup>Pr**.

**Scheme 34:** Proposed mechanism of isobutane formation via the ‘tuck-in’ decomposition pathway.



When comparing derivatives of **33-R**, it is clear that this system is intensely sensitive to subtle steric and electronic effects. The electronic influence is evident in that the primary alkyls **33-<sup>i</sup>Bu** and **33-(2-Et-Bu)** are *less* stable than the secondary alkyl **33-<sup>i</sup>Pr**. It appears that increasing the substitution at the  $\beta$ -position has a significant effect on stability, which is to be expected if the transition state of  $\beta$ -hydride elimination places a partial positive charge onto the  $\beta$ -carbon (Scheme 35). This is consistent with the observation that the energy barrier of  $\beta$ -hydride elimination of polyethylene chains from metallocene catalysts is significantly higher than that of  $\beta$ -branched polymers.<sup>27</sup> Also, the coordinated isobutylene, hydride complex **51** that results from the  $\beta$ -hydride elimination of the *iso*-butyl derivative will be destabilized by the steric interactions between the isobutylene unit and the Cp\* ring. This effect would be intensified in the analogous coordinated 2-ethyl-1-butene, hydride complex resulting from the  $\beta$ -hydride elimination of the 2-ethyl-butyl group, a point which would suggest that the overall stability of a derivative of **33-R** can be limited by the stability of its olefin, hydride  $\beta$ -hydride elimination product.

**Scheme 35:** The transition state of  $\beta$ -hydride elimination of **33-<sup>i</sup>Bu**.



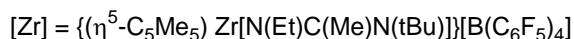
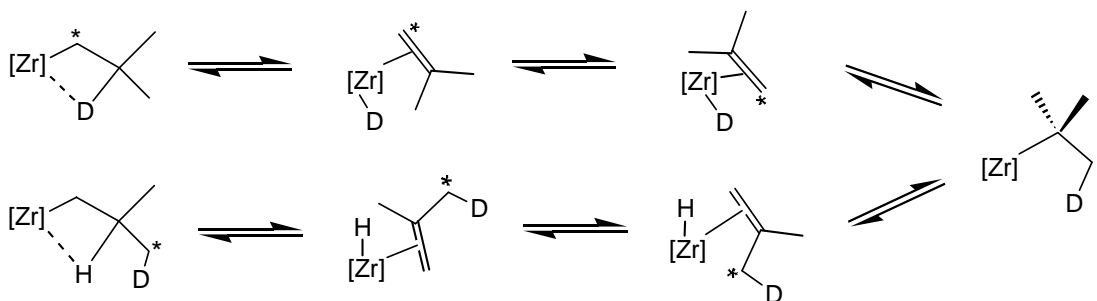
A partial positive charge at the  $\beta$ -position in the transition state of  $\beta$ -hydride elimination would also provide an explanation for the increased stability of **33-<sup>n</sup>Pr** and **33-<sup>i</sup>Pr**. Given that free propylene was not observed by  $^1\text{H}$  NMR, the decreased capacity of the secondary  $\beta$ -position to stabilize a partial cationic charge (relative to the tertiary  $\beta$ -position of the *iso*-butyl derivative) may render the  $\beta$ -hydride elimination noncompetitive with the intramolecular H-abstraction pathway shown in Scheme 34.

### 2.5.2 Isomerization of CPZA Alkyl Cations – Busico's Mechanism

Derivatives of **33-R** with  $\beta$ -substituted alkyl groups (poly(1-butene), 2-ethylbutyl, *iso*-butyl) undergo isomerization concurrent with decomposition in a process seemingly consistent with Busico's  $\beta$ -hydride elimination, alkene rotation, and reinsertion mechanism. Considering **33-<sup>i</sup>Bu**, assuming  $\beta$ -hydride elimination to be the rate-determining step for isomerization, both 1,2-reinsertion to regenerate unscrambled **33-(1-<sup>13</sup>C-2-*d*)-<sup>i</sup>Bu** and isomerization of the *iso*-butyl group through alkene rotation and 2,1-reinsertion to form a transient *tert*-butyl intermediate, according to Scheme 36, must both be very facile processes that effectively compete extremely well with irreversible chain-release from alkene, hydride intermediates. Indeed, scrambling of isotopic labels in **33-(1-<sup>13</sup>C-2-*d*)-<sup>i</sup>Bu** appears immediately by  $^{13}\text{C}$  NMR at  $0^\circ\text{C}$  at a point when minimal loss

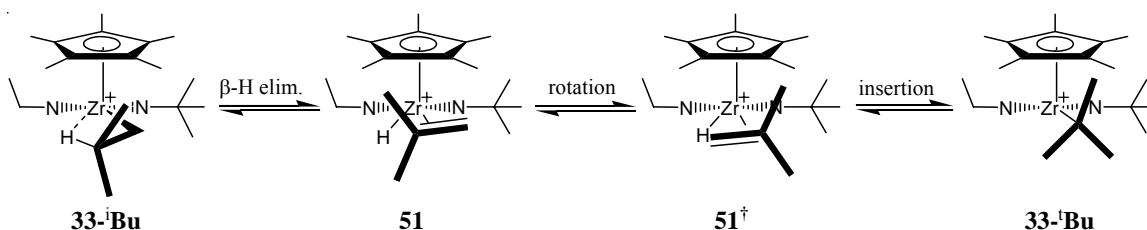
of compound through decomposition has occurred. Unfortunately, no NMR spectroscopic evidence for such a cationic *tert*-butyl intermediate has been obtained. More disappointingly, all attempts to identify a reagent that could be used to chemically trap the presumed alkene, hydride intermediates in order to eliminate the reversibility of the  $\beta$ -hydride elimination process and isotopic scrambling, and thereby, permit kinetic analyses to obtain clear cut thermodynamic parameters, including a kinetic isotope effect, have failed to produce a viable candidate as of yet.

**Scheme 36:** Isotopic label scrambling in **33**-(1-<sup>13</sup>C-2-*d*)-<sup>i</sup>Bu according to the Busico mechanism.



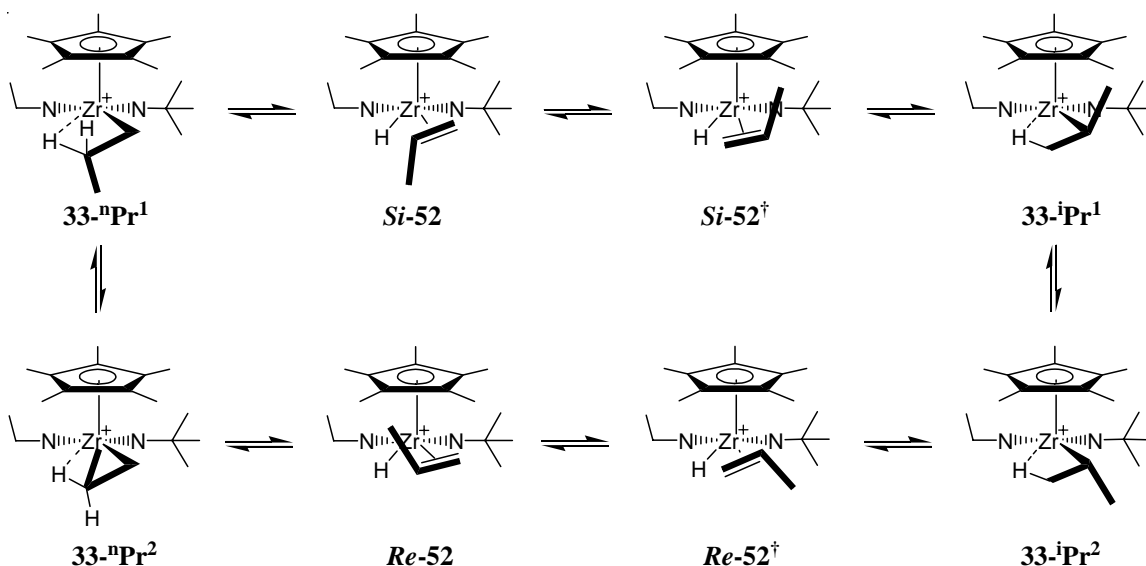
If the isomerization of **33**-<sup>i</sup>Bu is occurring through Busico's mechanism, complex **51** must be able to undergo reversible olefin rotation to form its rotational isomer, **51**<sup>†</sup>, which can then reinsert the coordinated isobutylene to transiently form **33h** before the process is reversed. This process may be facilitated by an inherent ground state destabilization in **51** and **51**<sup>†</sup> resulting from steric interactions between the coordinated isobutylene and the ligands (Scheme 37), serving to effectively lower the barrier of rotation. As such, **51** and **51**<sup>†</sup> can interchange freely, leading to the transient formation of the tertiary cation **33**-<sup>t</sup>Bu.

**Scheme 37:** Formation of a *tert*-butyl intermediate through coordinated alkene rotation.



The analogous transformations for **33-<sup>n</sup>Pr** and **33-<sup>i</sup>Pr**, as shown in Scheme 38, are complicated by the fact that each complex can form two different isomers with β-agostic interactions, due to the two diastereotopic β-hydrogens of **33-<sup>n</sup>Pr** and the two diastereotopic β-methyl groups of **33-<sup>i</sup>Pr** (see structures **33-<sup>n</sup>Pr<sup>1</sup>** vs. **33-<sup>n</sup>Pr<sup>2</sup>** and **33-<sup>i</sup>Pr<sup>1</sup>** vs. **33-<sup>i</sup>Pr<sup>2</sup>**). β-hydride elimination from these isomers result in two propylene/hydride complexes (**52**) that differ only in the coordination face of the prochiral propylene unit (see *Si-52* vs. *Re-52* and *Si-52<sup>†</sup>* vs. *Re-52<sup>†</sup>*). The asymmetry of the coordinated propylene may preclude free rotation of the olefin (*i.e.*, conversion of *Si-52<sup>†</sup>* → *Si-52* or *Re-52* → *Re-52<sup>†</sup>* is irreversible due to steric interactions between the propylene and the Cp\* ligand in the products), however, the isomerization of the cyclopentene insertion product **31** to **32** at low temperatures would suggest that alkene rotation to unfavorable conformations does not have a particularly high barrier. The fact that **33-<sup>i</sup>Pr** underwent full isomerization to **33-<sup>n</sup>Pr**, and yet **33-(2-*d*<sub>1</sub>)-<sup>n</sup>Pr** has not demonstrated any evidence of isomerization may be due to a large energy difference between barriers of 1,2-insertion and 2,1-insertion of **52**.

**Scheme 38:** Possible transformations of **33-<sup>n</sup>Pr** and **33-<sup>i</sup>Pr**.



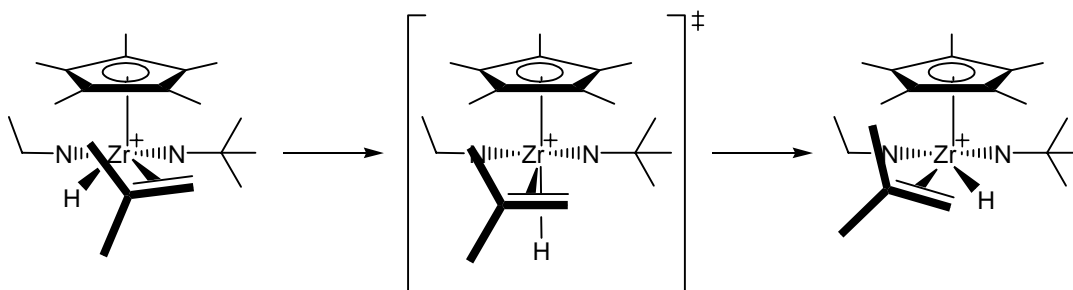
### 2.5.3 Isomerization of CPZA Alkyl Cations – Alternate Mechanism

As discussed in 2.3.3, the solution structure of each derivative of **33-R** was determined by difference-1D NOE <sup>1</sup>H NMR experiments, and each was found to have the Zr-H β-agostic interaction adjacent to the amidinate N-ethyl substituent. As such, upon β-hydride elimination, the olefin is coordinated adjacent to the amidinate N-*tert*-butyl substituent. However, it was previously demonstrated that the insertion of monomer occurs on the N-ethyl side,<sup>122</sup> presumably due to the reduced steric crowding of the N-ethyl group vs. the N-*tert*-butyl group. Furthermore, a previously reported solid-state structure of **16** with a molecule of diethyl ether (Et<sub>2</sub>O) coordinated to the N-*tert*-butyl side,<sup>137</sup> which most likely initially coordinated to the N-ethyl side, displays an ability of the cationic CPZA complexes to rearrange substituents to achieve the most energetically favorable conformation. Given this, it seems paradoxical that the isomerization steps

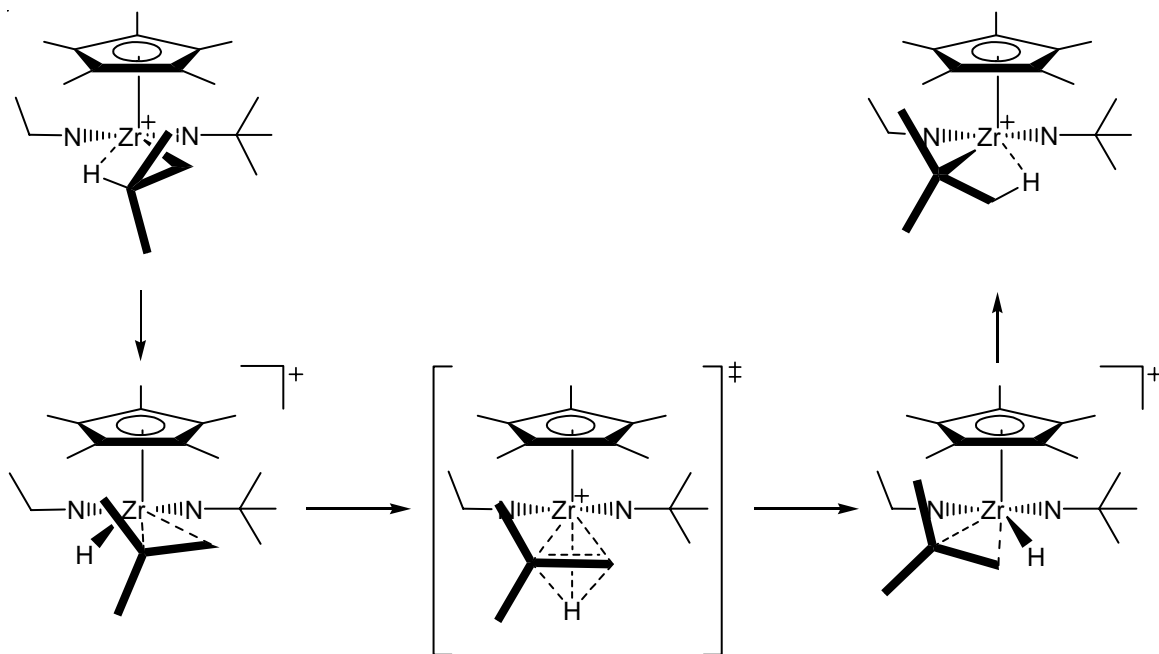
required for the Busico mechanism would proceed entirely while coordinated to the crowded N-*tert*-butyl side without rearrangement.

As depicted in Scheme 39, if **33-<sup>i</sup>Bu** necessarily β-hydride eliminates to yield the isobutylene, hydride complex, **51**, with the isobutylene unit coordinated to the N-*tert*-butyl side, an irreversible rearrangement may then occur in which the olefin ‘slips’ past the hydride and into the more open N-ethyl coordination site. The small hydride ligand could easily be accommodated in the open space between the amidinate and alkene ligands in the transition state of the rearrangement. In fact, one can envision a rapid rearrangement from **33-<sup>i</sup>Bu** to **33-<sup>t</sup>Bu** occurring *without* discrete formation of an alkene, hydride complex through intermediates with significant metallacyclopropane character, similar to a stepwise metal-assisted 1,2-hydride shift (Scheme 40). Indeed, the increased barrier of rotation of a metallacyclopropane relative to a coordinated alkene would explain why **51**, with the alkene coordinated to the more sterically open amidinate N-ethyl side, does not simply rotate to undergo 1,2-insertion preferentially over 2,1-insertion. In addition, reports from our group have shown that stable CPZA metallacyclopropane complexes can be synthesized.<sup>147</sup>

**Scheme 39:** Possible isomerization of an isobutylene, hydride complex.



**Scheme 40:** Formation of a *tert*-butyl intermediate through metal-assisted 1,2-hydride shift.

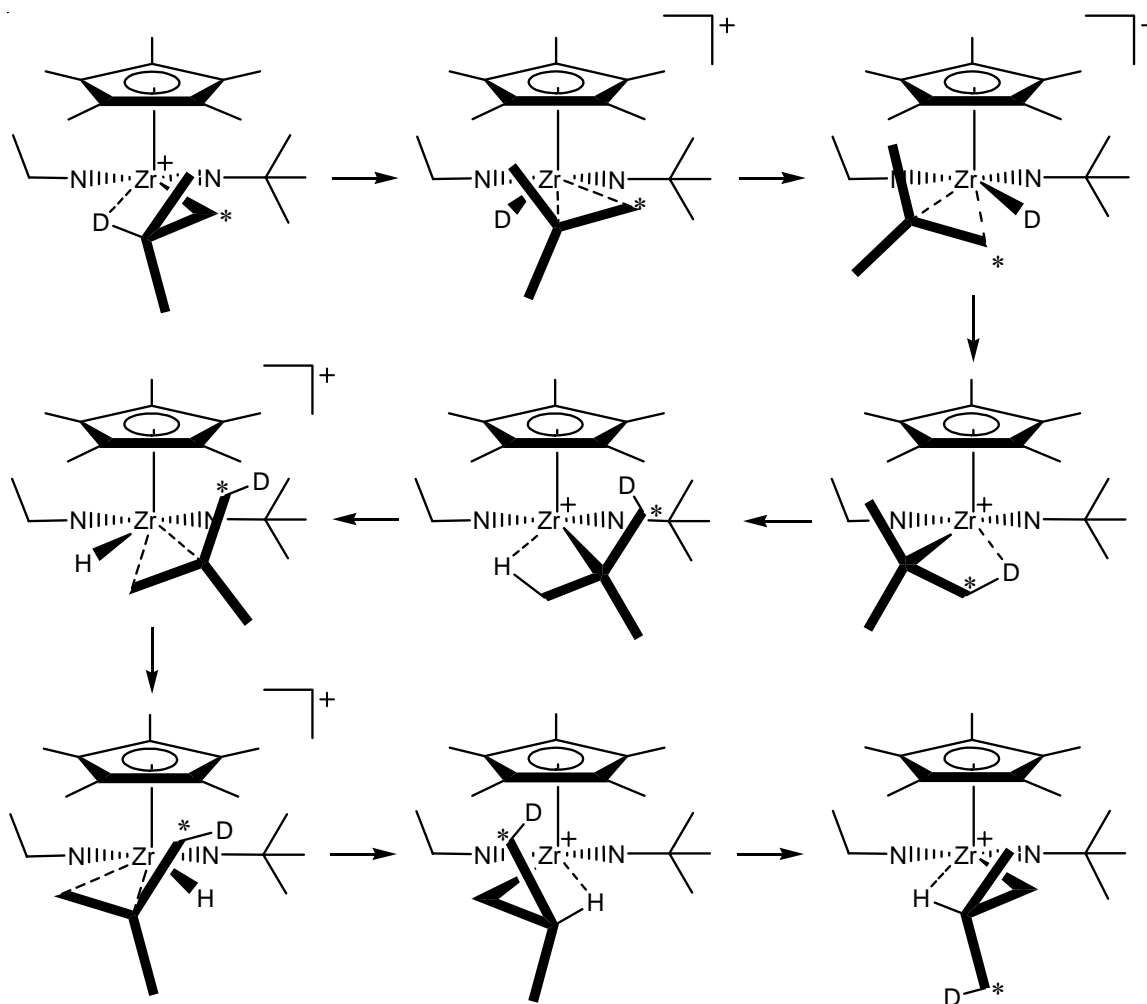


The initially formed *tert*-butyl cation in Scheme 40 is shown with the  $\beta$ -agostic interaction on the N-*tert*-butyl side. As mentioned above, all derivatives of **33** were found to have  $\beta$ -agostic interactions on the N-ethyl side; it would stand to reason that **33-<sup>t</sup>Bu** would undergo a simple rearrangement to form the agostic interaction on the N-ethyl side as well (Scheme 41). As such, another 1,2-hydride shift then reforms **33-<sup>i</sup>Bu**.

This most obvious advantage of this mechanism over Busico's is the elimination of the need for many reversible steps to compete with elimination. The initial rate-limiting  $\beta$ -hydride elimination, which may or may not be reversible, sets off a cascade of rearrangements which rapidly, and necessarily, lead back to the parent **33-<sup>i</sup>Bu**. If this mechanism is extended to the chain-end epimerization of propylene polymerization by metallocenes, the metallacyclopropane intermediates provide an explanation as to how this process can occur without displacement by free monomer. Although the *tert*-butyl

intermediate has not been observed, isomerization via 1,3-hydride shift or another mechanism not involving a *tert*-butyl intermediate is not consistent with the observation by  $^{13}\text{C}$  NMR of only doubly labeled methyl groups ( $^{13}\text{CH}_2\text{D}$ ), and no singly labeled methyl groups ( $^{13}\text{CH}_3$ ), in the *iso*-butyl group of scrambled **33**-(1- $^{13}\text{C}$ -2-*d*)-*i*Bu.

**Scheme 41:** Isotopic label scrambling in **33**-(1- $^{13}\text{C}$ -2-*d*)-*i*Bu according to the metal-assisted 1,2-hydride shift mechanism



#### 2.5.4 Hafnium Derivatives

The success in using hafnium derivatives to form the *tert*-butyl cation is quite significant. Currently, **44** is the only example reported of a group 4 metal tertiary alkyl cation, which is widely accepted as part of the chain-end epimerization mechanism despite the fact that no other direct observation has been made. Certainly, the rapid isomerization of the *tert*-butyl **44** to the *iso*-butyl **43** is in agreement with the transient nature of the unobservable intermediate implicated by the observed isotopic label scrambling. The relevance, however, is diminished by the fact that the isotopically labeled *iso*-butyl cation **42** *does not* scramble, and therefore shows no evidence of isomerization or formation of a *tert*-butyl intermediate during decomposition. Subsequently, the conclusions that can be drawn by comparison of the CPHA model complexes with the CPZA living polymers are limited.

Further demonstration of unique behavior of the CPHA derivatives presents itself in the lack of stability of the *iso*-butyl cation **43**, which decomposes at temperatures well below those at which **33-<sup>i</sup>Bu** is indefinitely stable. Considering the <sup>1</sup>H NMR, the  $\beta$ -hydrogen of **43** features relatively high chemical shift (1.55 ppm) and well-defined coupling pattern, which stands in stark contrast to the broad multiplets at lower chemical shifts (0.10 – -0.05 ppm) of agostically-bound  $\beta$ -hydrogens of cationic CPZA alkyls. This would appear to be in agreement with Bercaw's hypothesis that an energetically favorable  $\beta$ -agostic interaction can stabilize the ground state, thereby increasing the barrier to  $\beta$ -hydride elimination.<sup>28</sup> Cationic CPHA alkyls such as **43** may not be able to form a stabilizing  $\beta$ -agostic interaction, possibly due to a miss-match of orbital energies between the full C $\beta$ -H $\beta$  bonding orbital and the empty 5d orbital of the metal.

## 2.6 Conclusions

It is clear from the significant differences in stability of these cationic CPZA alkyl complexes that caution should be exercised when attempting to extrapolate properties of models to living polymers. Even so, these models have served to shed some light on the types of steric and electronic factors that affect stability, and the general trends revealed could aid in designing new initiators for living polymerization at higher temperatures. The isotopic labeling studies carried out with the *iso*-butyl derivative have also yielded valuable information on the mechanism of isomerization and decomposition, although there is still some question as to whether to reality of the situation is best represented by Busico's mechanism, the metal-assisted hydride-shift mechanism or another alternative. Hafnium derivatives were used to directly observe the first example of a group 4 metal tertiary-alkyl cation, which remains to date the only such observation reported. While the hafnium *iso*-butyl derivative did not demonstrate any evidence for isomerization during decomposition, the fact that it is significantly less stable than the zirconium analogue may be a demonstration of the stabilizing nature of a  $\beta$ -agostic interaction in the latter case.

## Chapter 3: Application of Living Degenerative Transfer

### Polymerizations

#### 3.1 Living Propylene Polymerization

In contrast to the libraries of catalysts available for non-living propylene polymerization, the *living* polymerization of propylene has only been demonstrated by a few systems, including the V(acac)<sub>3</sub>-AlEt<sub>2</sub>Cl (**25**) system developed by Doi<sup>103</sup> and bis(phenoxyimine) systems (**17** and **29**) developed by Coates<sup>81, 82, 85-87</sup> and Fujita<sup>80, 83, 84, 112, 113</sup> (vide supra). Living systems, by virtue of undergoing only negligible chain termination during propagation, provide access to polymers unachievable through non-living systems, such as well-defined block copolymers and end-functionalized polymers.

While the CPZA Ziegler-Natta initiators reported by our group have been productive for the isotactic and atactic living polymerization of  $\alpha$ -olefins, including sterically encumbered monomers<sup>148</sup> and  $\alpha,\omega$ -nonconjugated dienes,<sup>149</sup> none of these materials are, as of yet, technologically relevant. Indeed, the unique ability of **16** to polymerize  $\alpha$ -olefins in both an isotactic and atactic manner would clearly be advantageous if applied to propylene polymerizations, in the context of isotactic-atactic *sb*-PP materials as thermoplastic elastomers. However, many systems capable of the polymerization of high  $\alpha$ -olefins have not been found to be active for propylene and ethylene polymerization, and vice versa. As such, it was desirable to explore the activity of CPZA initiators for propylene polymerization.

### 3.1.1 Propylene Polymerization by CPZA Initiators

Due to potential complications involving the solubility of *iso*-PP in chlorobenzene at low temperatures, the degenerative transfer living polymerization of propylene was first attempted in the hopes that atactic polymer would be produced, as was found to be the case for other  $\alpha$ -olefins. Certainly, the high solubility of *a*-PP would allow the reaction to proceed in a controlled manner and lend itself more readily to analysis by room temperature GPC methods. Thus, upon activation of **12** with 0.5 equivalents of the cocatalyst **13** at -10 °C in chlorobenzene under a propylene atmosphere of 5 psi, the degenerative transfer polymerization was found to proceed smoothly, providing a soluble, amorphous PP material.<sup>150</sup> The <sup>13</sup>C NMR (Figure 36, top) confirmed that the microstructure was highly atactic, with a *mm:mr:rr* triad ratio of 27:52:21 (*cf.* 25:50:25 for perfectly atactic; see Table 8 for full pentad analysis), and the narrow PDI as determined by GPC analysis ( $M_n = 25,500$ , PDI = 1.11) suggested that the living character of the system had not been compromised. Further proof of the living character was obtained by kinetic analysis, accomplished by drawing aliquots over the course of a reaction and analyzing each by GPC. Since the propylene pressure, and hence the concentration in solution, is maintained constant, the molecular weight is expected to increase linearly with time in the absence of termination events. Indeed, this proved to be the case, as shown in Figure 37.

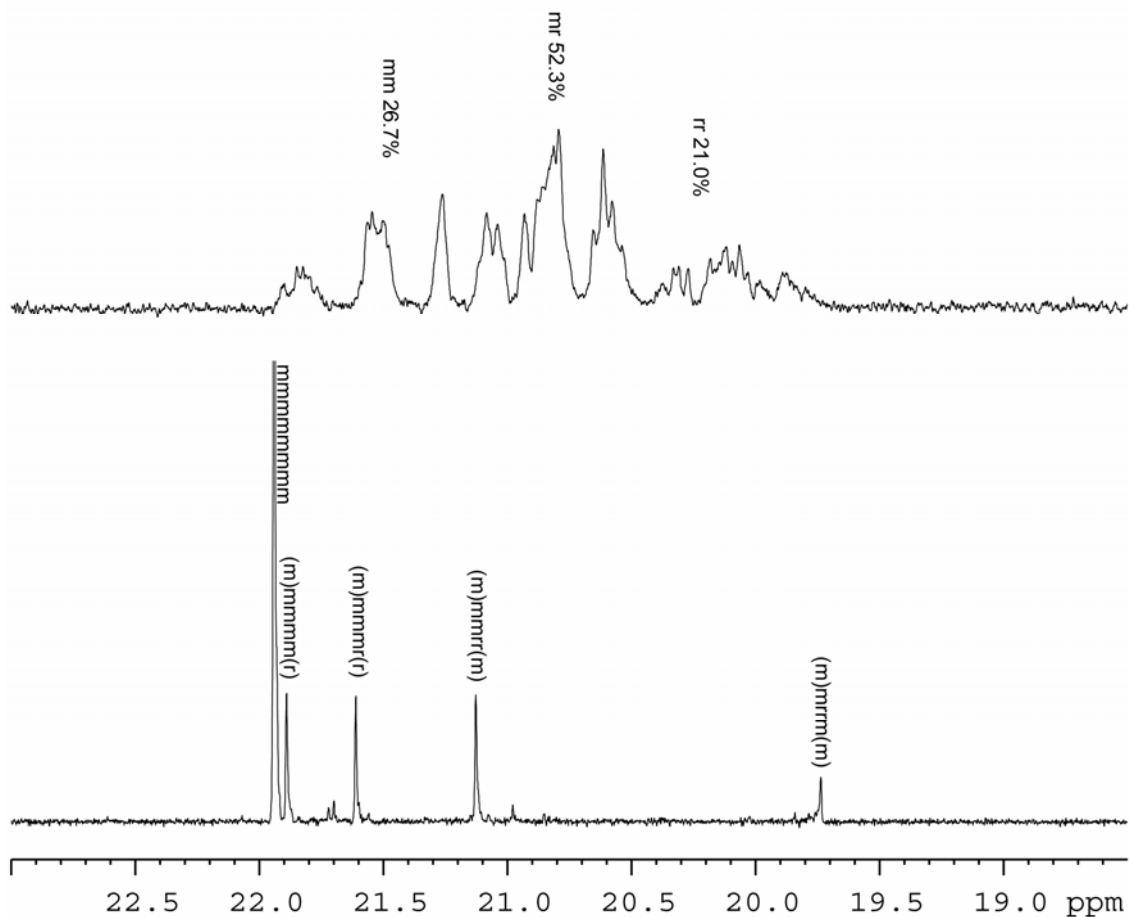


**Figure 36:**  $^{13}\text{C}\{^1\text{H}\}$  NMR (125 MHz, 1,1,2,2- $\text{C}_2\text{D}_2\text{Cl}_4$ , 70 °C) methyl region of atactic PP prepared under DT conditions (top) and isotactic PP prepared under non-DT conditions (bottom).

**Table 8:** Pentad distributions of PP produced at 100% activation and 50% activation.

Pentad	100% activated non-DT	50% activated DT
<i>mmmm</i>	0.713	0.052
<i>mmmr</i>	0.101	0.126
<i>rmmr</i>	0.009	0.070
<i>mmrr</i>	0.103	0.103
<i>mmrm+rmrr</i>	0.021	0.274
<i>rrrm</i>	0.003	0.159
<i>rrrr</i>	0.005	0.052
<i>rrrm</i>	0.003	0.103
<i>mrrm</i>	0.044	0.061

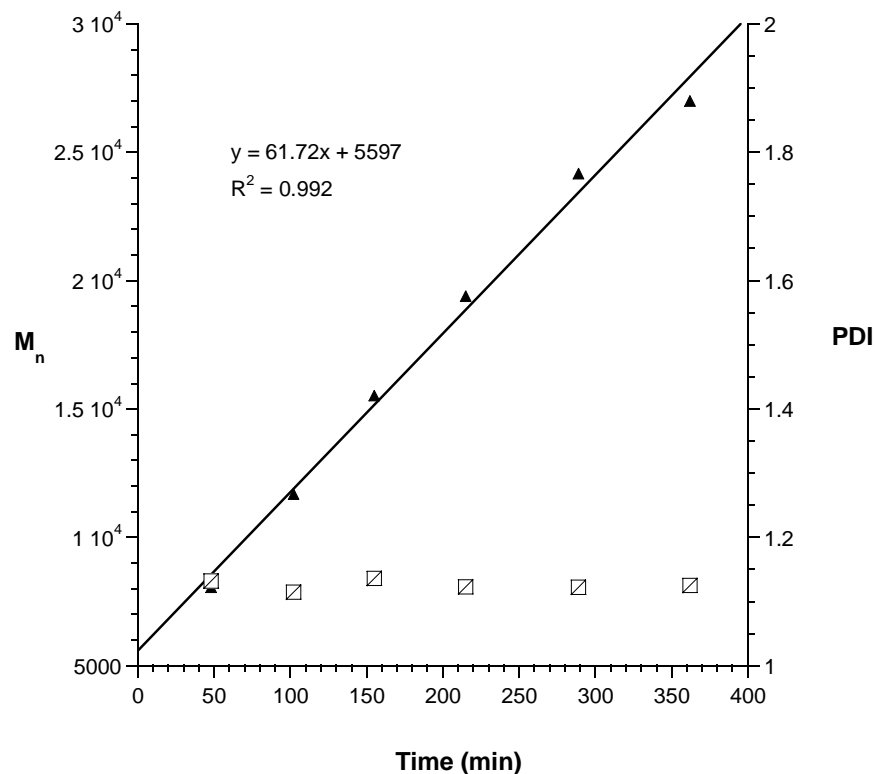


**Figure 37:** Kinetic profile of living DT propylene polymerization by **16**. The intercept does not reach zero due to the inherent error of calibration with polystyrene standards. ▲ =  $M_n$ , ◻ = PDI.

The isotactic polymerization of propylene was subsequently attempted by activation of **12** with a full equivalent of **13**, under otherwise identical conditions to those described above for the DT polymerization of propylene. A solid white powder was obtained, which, as expected, proved to be completely insoluble in THF, precluding molecular weight determination by room temperature GPC methods. However, high temperature  $^{13}\text{C}$  NMR confirmed that the PP was isotactic, with *mmmr*, *mmrr*, and *mrrm* stereoerrors indicative of enantiomorphic site control, as shown in Figure 36 (bottom). The isotacticity of the polymer was found to be  $[m m m m] = 0.71$  (Table 8), corresponding to a 94% face selectivity,<sup>9</sup> and DSC analysis revealed a melting temperature of 116 °C.

As this material was not found to be soluble in THF, kinetic analysis via GPC to confirm living behavior could not be performed with pure *iso*-PP. It was considered, however, that atactic-isotactic stereoblock diblock PP materials might be soluble enough for analysis. Hence, a sample of living *a*-PP (**16-a-PP**) was synthesized using **16** at half-activation, after which a second half-equivalent of **13** was added to convert the system from DT conditions to non-DT conditions, as had been previously demonstrated by the synthesis of the *a*-PH-*block-iso*-PO copolymer. The polymerization was then continued with aliquots sampled over time, which proved to be appropriately soluble for analysis by GPC. Once again, the molecular weight increased linearly with time, verifying the living nature of isotactic propylene polymerization by **16** (Figure 38).

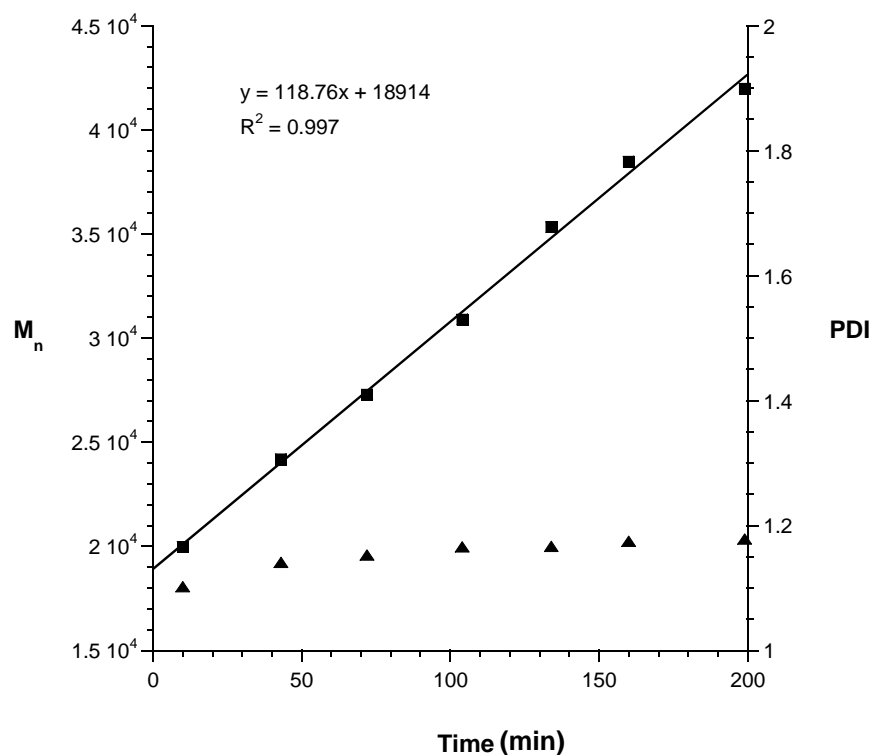


**Figure 38:** Kinetic profile of non-DT living propylene polymerization by **16**. The intercept does not reach zero because  $t = 0$  begins at full activation of the system. ■ =  $M_n$ , ▲ = PDI.

## 3.2 Stereoblock Polypropylene

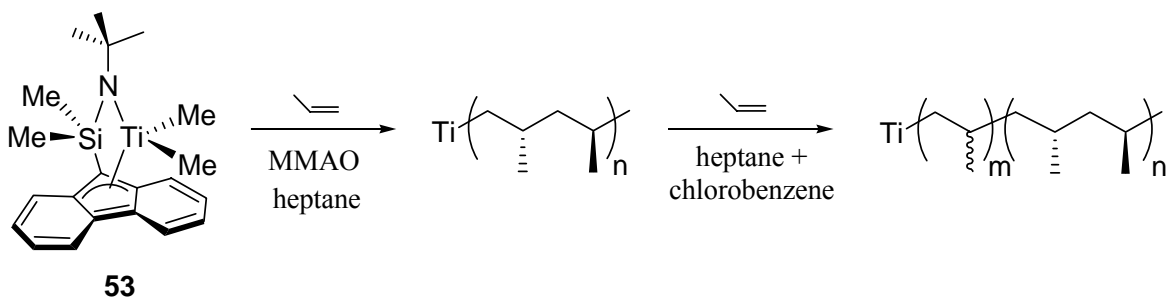
### 3.2.1 Stereoblock Polymers

The controlled synthesis of isotactic-atactic *sb*-PP, towards the development of novel elastomeric materials, has been the target of countless hours of research. Several systems have produced elastomeric PP materials which were proposed to have stereoblock architectures, including Chien's<sup>53</sup> C<sub>1</sub>-symmetric metallocenes (1.2.3) and the oscillating metallocenes<sup>73</sup> (1.4.1), but it was subsequently suggested through theoretical and experimental findings in each case by Collins<sup>54,55</sup> and Busico,<sup>77</sup> respectively, that the microstructures were not necessarily stereoblocks.

The first system capable of producing discrete PP stereoblock diblocks was reported in 2004 by Shiono and co-workers.<sup>151</sup> The titanium precatalyst (<sup>t</sup>BuNSiMe<sub>2</sub>Flu)TiMe<sub>2</sub> (**53**, Flu = fluorenyl) had previously been reported as being active for the syndioselective polymerization of propylene, when activated by MAO, [Ph<sub>3</sub>C][B(C<sub>6</sub>F<sub>5</sub>)<sub>4</sub>], or B(C<sub>6</sub>F<sub>5</sub>)<sub>3</sub> in toluene at 40 °C, via 1,2-insertion under chain-end control ([*rrrr*] = 0.30).<sup>152</sup> Subsequently, Shiono<sup>153</sup> discovered that lowering the temperature to -50 °C when activating with B(C<sub>6</sub>F<sub>5</sub>)<sub>3</sub> provided a living system for syndioselective propylene ([*rrrr*] = 0.24) and 1-hexene polymerization, as demonstrated by the linear increase of yield and MW with time. Upon further refinements, it was found that when the polymerization of propylene was conducted using modified MAO (MMAO) as the cocatalyst, in heptane at 0 °C, syndioselectivity was increased ([*rrrr*] = 0.60).<sup>154</sup> However, in chlorobenzene, under otherwise identical conditions, a largely *atactic* polymer (*mm:mr:rr* = 10:48:42) was produced. The difference in syndioselectivity between solvents was attributed to a close counterion association in heptane, which

prevented site isomerization and allowed the ligand set to impart site-control. Chlorobenzene, on the other hand, favored counterion disassociation, allowing site isomerization to dominate. In both cases, the living nature was verified by a linear increase of MW with time at constant propylene concentration. As such, it was possible to carry out a polymerization in heptane and then add a portion of chlorobenzene, thereby increasing solvent polarity sufficiently to convert propagation from syndiotactic to atactic, resulting in the first synthesis of uniform syndiotactic-atactic diblock PP ( $M_n = 94,700$ , PDI = 1.27), as shown in Scheme 42.<sup>151</sup> However, the polymer did not have a melting temperature according to differential scanning calorimetry (DSC), likely due to insufficient stereoregularity in the *syn*-PP segments to induce crystallization, and no other comments were made concerning the properties of the material. Recently, Shiono<sup>155</sup> used a modified version of the catalyst, which uses a 3,6-<sup>t</sup>Bu)<sub>2</sub>Flu ligand, to synthesize a crystallizable syndiotactic-atactic diblock PP with a melting point of 119 °C.

**Scheme 42:** Synthesis of *a-syn*-PP diblock polymers via **53**.



The synthesis of discrete isotactic-atactic *sb*-PP materials, as demonstrated by **16** as part of the living isotactic propylene polymerization kinetic study detailed above, had not been previously reported in the literature. Indeed, the versatility of **16** appeared to offer an avenue of investigation into whether a stereoblock structure would result in

elastomeric properties; a concept which was first suggested in 1959,<sup>49</sup> and yet has eluded concrete validation ever since.

### 3.2.2 Synthesis and Microstructural Analysis.

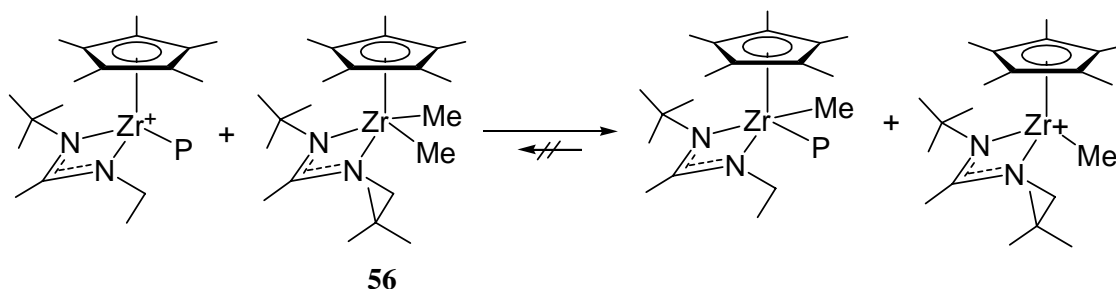
The synthesis of *iso-a*-PP stereoblock diblocks was easily accomplished by initially preparing a sample of **16-a-PP** under DT conditions before establishing isotactic propagation through the addition of a second portion of **13**, as demonstrated above. However, the synthesis of *multiblock* polymers would be required for an in-depth study of the relationship between stereoblock architecture and physical properties. This would then require a method of changing the system from non-DT to DT conditions by introducing transferable methyl groups, effectively *reducing* the level of activation. An appropriate methylating agent, and the resulting product upon methyl group donation, would need to be completely inactive for polymerization and unreactive towards **12**, **16** and the living polymers derived thereof. The task of finding such an agent is further complicated by the need to avoid coordinating solvents such as THF and Et<sub>2</sub>O, preventing the use of methyl lithium or methyl Grignard. Inspired by the facile transfer of methyl groups between **12** and **16**, it was conceived that another cyclopentadienyl zirconium amidinate derivative might serve as a suitable methylating reagent. However, in order to be useful, the cationic form must be *inactive* for polymerization. Fortunately, previous studies<sup>78, 79, 148, 156, 157</sup> examining many different cationic cyclopentadienyl zirconium and hafnium amidinate derivatives revealed several classes of inactive derivatives which might serve as methylating agents.

One class of potential methylating agents was *tert*-butyl amidinate derivatives, which, when ‘activated’ by **13**, had previously been shown to be inactive for 1-hexene polymerization.<sup>79</sup> Using low temperature <sup>1</sup>H NMR techniques, the *tert*-butyl amidinate derivative Cp\*ZrMe<sub>2</sub>[N(Et)C(<sup>t</sup>Bu)N(<sup>t</sup>Bu)] (**54**) was shown to transfer a methyl group to **16** in chlorobenzene-*d*<sub>5</sub> at -10 °C, resulting in the quantitative production of **12** and {Cp\*ZrMe[N(Et)C(<sup>t</sup>Bu)N(<sup>t</sup>Bu)]}[B(C<sub>6</sub>F<sub>5</sub>)<sub>4</sub>] (**55**).<sup>135</sup> The sharp, well-defined resonances of the spectrum suggested that **12** and **55** were static compounds, and not in equilibrium with **16** and **54**. Indeed, combining **16** with a half-equivalent of **54** provided *a*-PH identical to that obtained from activation of **12** with a half-equivalent of **13**. The utility of **54** as fully functional methylating agent was tested by Yonghui Zhang<sup>135</sup> through the planned synthesis of a stereoblock pentablock copolymer. Thus, beginning with the synthesis of living *a*-PH under DT conditions (50% activation), sequential additions of half-equivalents of **13** (to establish non-DT conditions) and **54** (to establish DT conditions) before additional portions of 1-octene and 1-hexene, respectively, resulted in the production of an *a*-PH-*iso*-PO-*a*-PH-*iso*-PO-*a*-PH stereoblock copolymer (*M*<sub>n</sub> = 28 500, PDI = 1.08). After the synthesis of each block, an aliquot was quenched and analyzed by GPC and inverse-gated <sup>13</sup>C NMR to verify that the MW and tacticity of each block was as expected.

Unfortunately, while **54** was a suitable methylating agent for high  $\alpha$ -olefin polymerization, the same was not found to be true for propylene. When a mixture of **12** and 0.5 equivalents of **54** was used to initiate propylene polymerization, *a*-PP was produced which was indistinguishable from *a*-PP produced from half-activated **12** under otherwise identical conditions. In fact, *a*-*iso*-*a*-PP stereoblock triblocks could be

synthesized using **54** as the methylating agent to establish DT conditions for the final atactic segment. However, it was found that the cationic **55**, when present in a *fully activated* system, whether alone or in the presence of **16**, *did* produce *a*-PP with low activity. As such, once **54** had been used to switch from fully activated to DT, the system could not be switched back to full activation without contamination by low MW *a*-PP. Because of this, a new methylating agent was required for the synthesis of isotactic-atactic multiblock *sb*-PP. Upon a screening of several *tert*-butyl amidinate and acetamidinate derivatives,<sup>135</sup> only Cp\*ZrMe<sub>2</sub>[N(*t*Bu)C(Me)N(CH<sub>2</sub><sup>*t*</sup>Bu)] (**56**) was found to meet all the requirements of an effective methylating reagent for propylene polymerization.

**Scheme 43:** Irreversible methyl group transfer from **56** to living polymers from **16**.

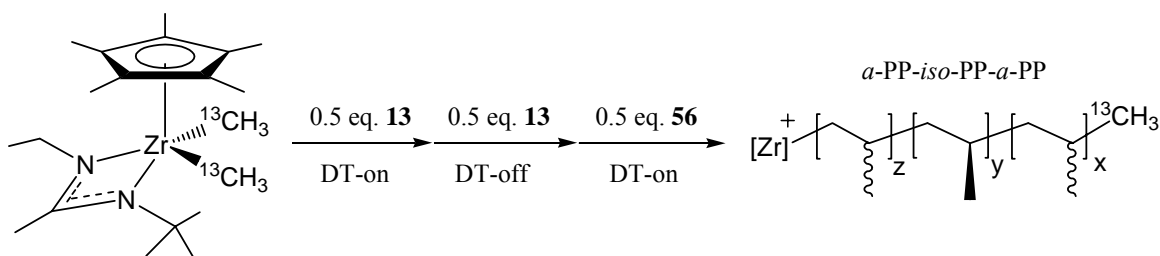


P = polymer chain, borate counterion not shown

Having at last developed a suitable methylating agent, the programmed synthesis of several unique discrete, multiblock, isotactic-atactic *sb*-PP architectures proved to be a straightforward task. In practice, polymerization time is used to define block length, with the MW of segments polymerized under DT conditions at 50% activation growing half as quickly as those polymerized when the system is fully activated. In order to obtain unequivocal proof that sharp block boundaries exist in the final isotactic-atactic *sb*-PP materials, a 1-(<sup>13</sup>C)-*a*-*iso*-*a*-PP triblock polymer was synthesized employing <sup>13</sup>C-labeled

**16** as the initiator and **56** as the methylating agent (Scheme 44). Aliquots were then taken after the synthesis of each new block, and difference  $^{13}\text{C}$  NMR spectra were produced by subtracting the initial *a*-PP block spectrum from the diblock spectrum, and the diblock spectrum from the final triblock spectrum, using the  $^{13}\text{C}$ -labeled methyl end group resonance as an internal reference. As shown in Figure 39, this allowed the direct observation of each individual stereoblock, and confirmed that each was either strictly isotactic or atactic as programmed. In this regard, it is important to stipulate that since we have not yet attempted to rigorously compensate for changes in mass transfer of propylene and viscosity effects that can occur as a function of polymerization time, or to a lesser extent in temperature and concentration, quantitative block lengths within a target isotactic-atactic *sb*-PP multiblock structure have been observed to vary slightly from run to run (e.g., observed 1.0:1.2:0.8 for a target 1:1:1 *a-iso-a*-PP triblock). Another problem encountered was the synthesis of *sb*-PP beginning with an isotactic segment, most likely due to solubility issues of even relatively low MW *iso*-PP. While attempts at *iso-a-iso*-PP and other architectures that necessarily begin with isotactic propagation provided low-crystallinity materials (*i.e.*, not simply *iso*-PP), the yields were often much lower than those with initial atactic segments. In addition, the *mmmm* content of quenched samples during synthesis of materials with initial isotactic segments was not in agreement with expected values.

**Scheme 44:** Synthesis of 1-( $^{13}\text{C}$ )-*a-iso-a*-PP.



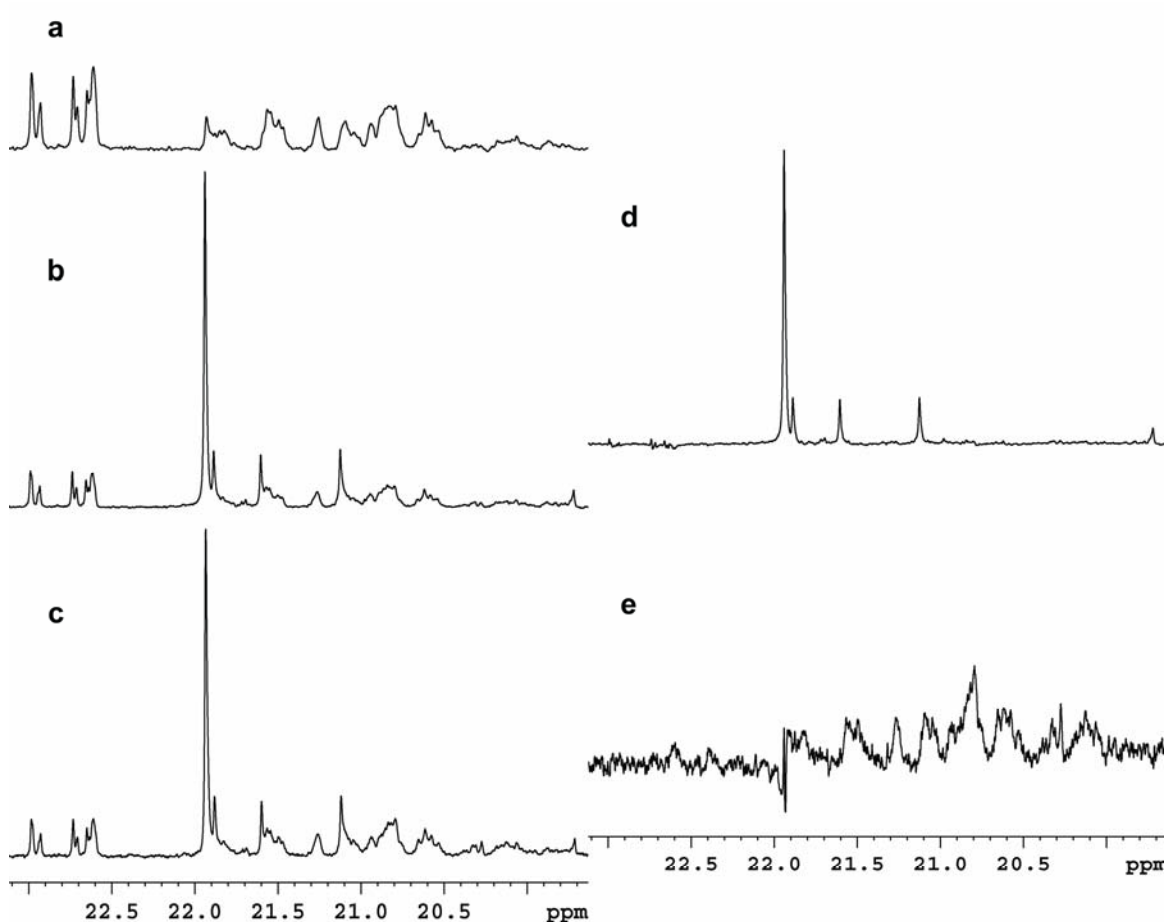


**Figure 39:**  $^{13}\text{C}\{^1\text{H}\}$  NMR (125 MHz,  $1,1,2,2\text{-C}_2\text{D}_2\text{Cl}_4$ , 70 °C) of the methyl region of aliquots taken during the synthesis of an *a-iso-a-PP* triblock prepared with a  $^{13}\text{C}$ -labeled methyl end group (note: the resonances for this end group appear between 22.5-23.0 ppm and are used as the internal reference to generate difference spectra). (a) atactic block aliquot, (b) atactic-isotactic diblock aliquot, (c) final atactic-isotactic-atactic triblock, (d) difference spectrum between a and b (the middle isotactic segment) and (e) difference spectrum between c and b (the final atactic segment).

### 3.2.3 Materials Properties

In order to probe whether the exact makeup of the stereoblock architecture could affect the physical properties of the material, three different isotactic-atactic stereoblock architectures, a 60-40 *a-iso-PP* diblock, a 30-40-30 *a-iso-a-PP* triblock, and a 30-20-30-

20 *a-iso-a-iso*-PP tetrablock, were synthesized with uniform MW and total relative isotactic/atactic ratio ( $M_n \sim 170,000$ , 40% isotactic,  $[m m m m] \sim 0.32$ ). It is worth stressing that the only significant difference between these three PP materials is in the stereoblock architecture, as shown in Figure 40.

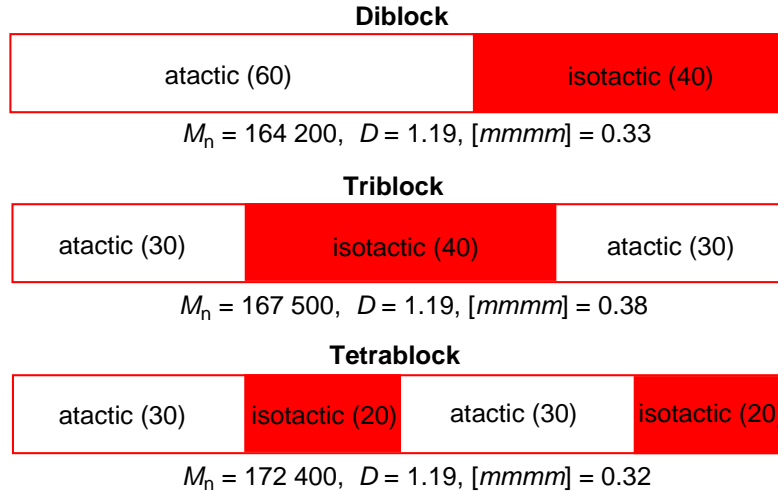


**Figure 40:** Schematic representation of the isotactic-atactic *sb*-PP architectures targeted for tensile testing.

**Table 9:** Pentad distributions of PP stereoblocks and quenched samples.

Pentad	diblock	triblock		tetrablock		
		2/3	full	1/2	3/4	full
<i>m m m m</i>	0.383	0.420	0.331	0.367	0.260	0.321
<i>m m m r</i>	0.177	0.151	0.148	0.172	0.164	0.153
<i>r m m r</i>	0.033	0.030	0.040	0.037	0.047	0.047
<i>m m r r</i>	0.093	0.100	0.092	0.091	0.096	0.098
<i>m m r m + r m r r</i>	0.181	0.157	0.182	0.184	0.220	0.186
<i>r m r m</i>	0.054	0.057	0.079	0.065	0.092	0.078
<i>r r r r</i>	0.009	0.011	0.027	0.013	0.021	0.025
<i>r r r m</i>	0.026	0.026	0.048	0.026	0.057	0.045
<i>m r r m</i>	0.043	0.048	0.052	0.043	0.046	0.049

Upon preliminary tensile-testing of standard dog bone-shaped samples (ASTM D638-5; thickness: 0.5 mm), the dependency of elastomeric properties on stereoblock architecture was clear. As shown in Figure 41, the triblock showed the highest strain to break at 1530%, although it occurred at low stress (7 MPa) and with fairly poor recovery (70%). The tetrablock proved to be the best performing elastomer, with the highest stress to break (19 MPa) at 1227% strain with 91% recovery. Interestingly, the diblock exhibited intermediate properties at break (11 MPa strain, 1325% stress, 84% recovery). Furthermore, from stress-strain hysteresis curves for 10 cycles, the *a-iso-a-iso*-PP tetrablock material proved to be an exceptional elastomer after initial strain-induced annealing (2 cycles), with virtually no further irreversible deformation taking place within subsequent stress-strain cycles involving an initial maximum strain of 300% (see inset of Figure 41).

### 3.3 Conclusions

The controlled synthesis of discrete isotactic-atactic *sb*-PP, as demonstrated using the modulated degenerative transfer living polymerization ability of **16**, stands as the only reported route to such materials in a well-defined and homogeneous manner. In addition, preliminary tensile testing has not only validated Natta's<sup>49</sup> hypothesis that such materials could be elastomeric, but also demonstrated a remarkable dependence of elastic properties on the exact stereoblock architecture. This opens a new concept in the targeted design of thermoplastic elastomers with specific properties, alleviating the need for exotic comonomers or low MW plasticizers, by which a countless variety of isotactic-atactic stereoblock materials are now accessible.

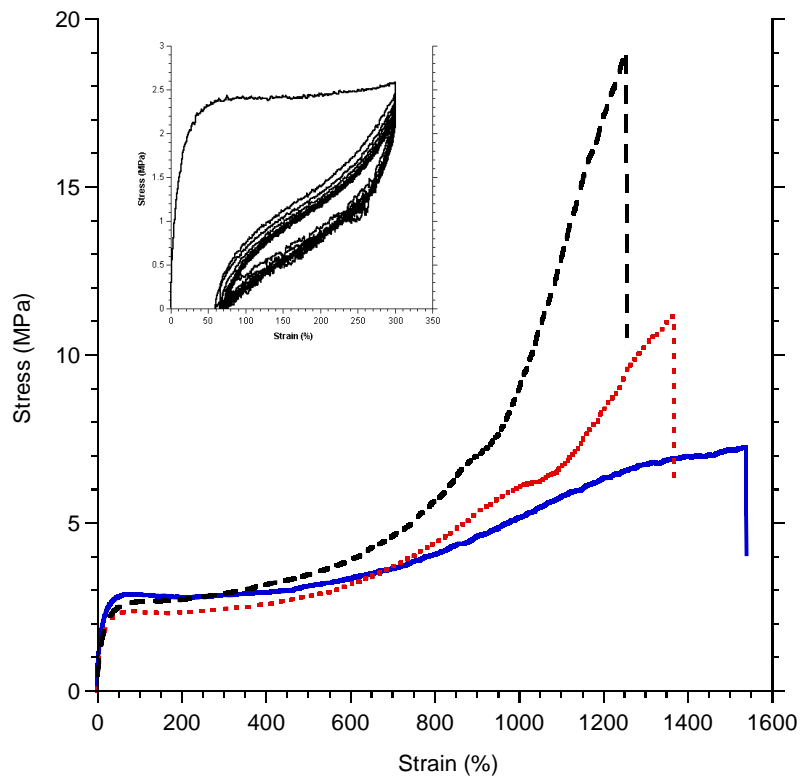


**Figure 41:** Stress-strain curves showing ultimate elongation to break for the 30-40-30 *a-iso-a-PP* triblock (solid line), the 60-40 *a-iso-PP* diblock (dotted line), and the 30-20-30-20 *a-iso-a-iso-PP* tetrablock (dashed line). Insert: strain hysteresis curves (10 cycles) for a fresh, as-prepared sample of the *a-iso-a-iso-PP* tetrablock.

## Chapter 4: Bimolecular Control of Polypropylene Microstructure

### 4.1 Control of Microstructure Through Substoichiometric Activation

As detailed in Chapter 3, the polymerization of propylene by **12** when activated by 0.5 equivalents provides *a*-PP with a pentad distribution indicative of nearly perfectly random chirality.<sup>150</sup> This is due to the degenerative transfer process (see section 1.6), in which metal centers rapidly transfer between neutral and dormant states, such that  $R_{tr} \gg R_p$  ( $R_{tr}$  = rate of transfer,  $R_p$  = rate of polymerization). Due to the conformational instability of the amidinate ligand in the dormant state, all metal centers are effectively racemized during polymerization, thereby resulting in the atactic microstructure observed for PP synthesized at 50% activation.

Accordingly, it was conceived that a new level of control over microstructure could be achieved by precisely controlling the level of activation, since the rate of bimolecular transfer of a methyl group from the neutral Zr-Me to the active  $Zr^+$  is defined by the relative concentrations ( $R_{tr} = k_{tr}[Zr-Me][Zr^+]$ ). Slowing the rate of methyl group transfer, relative to the rate of polymerization, through lowering the concentration of neutral species (accomplished by simply increasing the level of activation) should result in longer lifetimes of the active, configurationally static species, providing a more *iso*-rich polymer. In practice, this proved to be the case as evidenced by the series of <sup>13</sup>C NMR spectra shown in Figure 42, in which the isotactic microstructure obtained at 100% activation is gradually transformed to a fully atactic one by simply decreasing the level of activation.<sup>158</sup> The non-linear decrease in isotacticity is more apparent in Figure 43, which tracks the %*mm* as a function of % activation. The most significant changes take place at

the higher levels of activation, with  $[mm]$  dropping by 0.28 between 100% and 90% activation (0.82 and 0.54, respectively) compared to a difference in  $[mm]$  of only 0.21 between 90% and 70% activation (0.33).

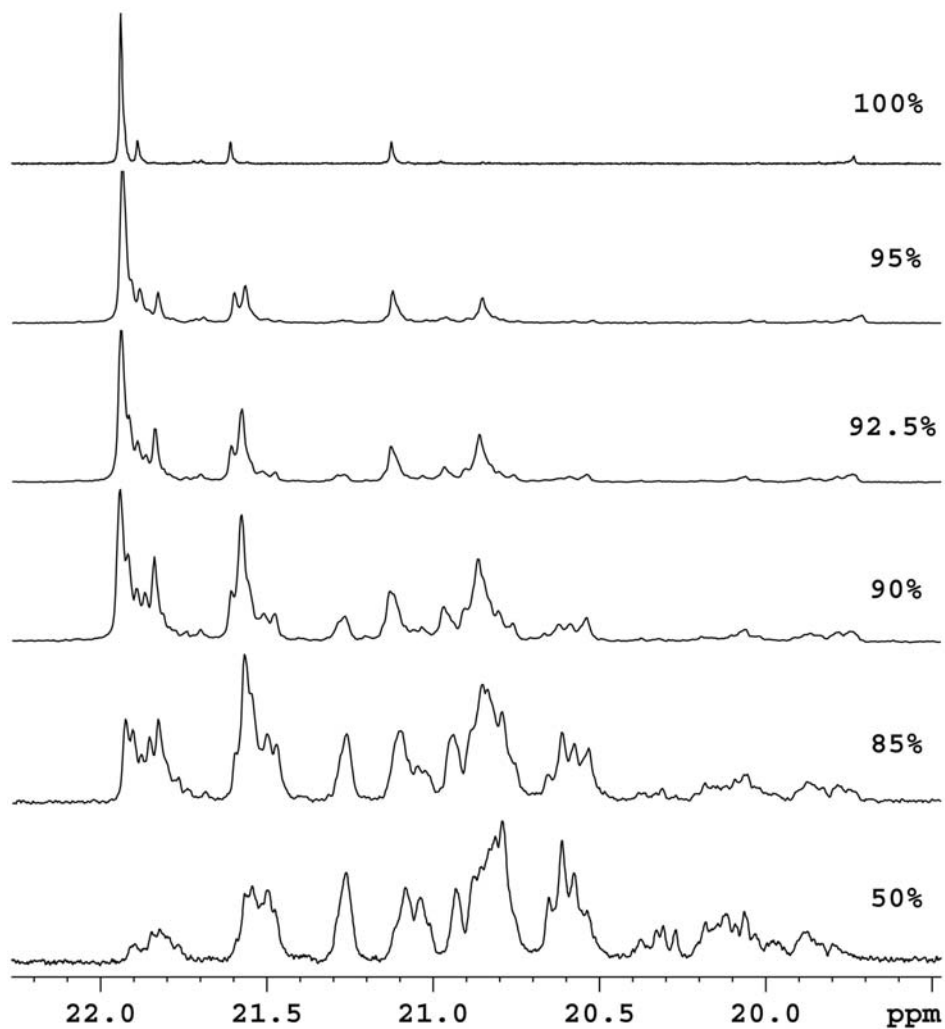


**Figure 42:**  $^{13}\text{C}\{^1\text{H}\}$  NMR (125 MHz,  $1,1,2,2\text{-C}_2\text{D}_2\text{Cl}_4$ , 70 °C) of polypropylene samples synthesized at varying levels of activation, as indicated on the right.

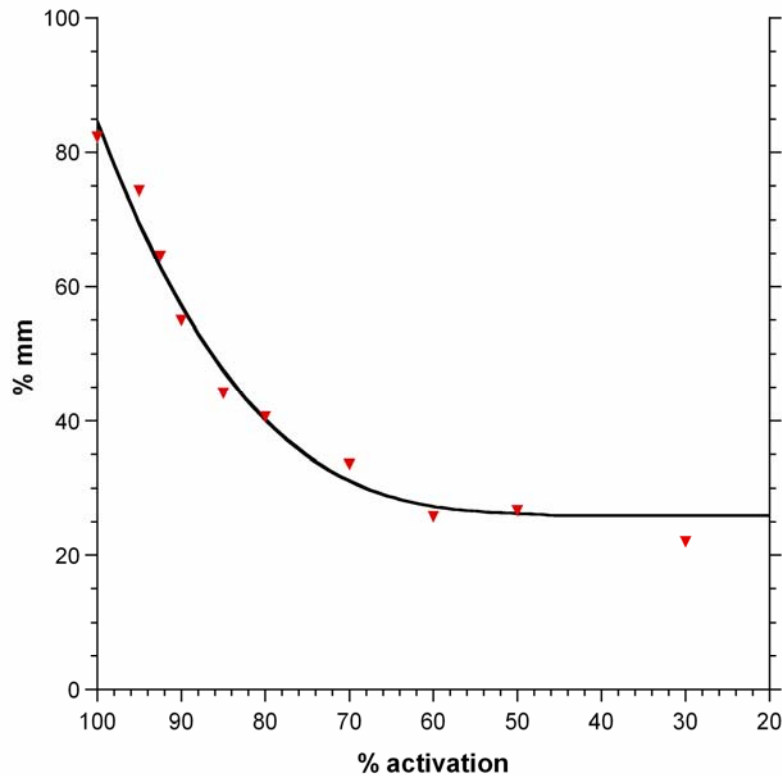


**Figure 43:** %*mm* of the spectra of Figure 42 and other polypropylene materials obtained as a function of % activation under the same polymerization conditions. The line is provided as a guide for the eye.

**Table 10:** Pentad distributions of PP synthesized at varying levels of activation.

activation (%)	<i>mmmm</i>	<i>mmmr</i>	<i>rmmr</i>	<i>mmrr</i>	<i>mmrm+rmmr</i>	<i>rmmr</i>	<i>rrrr</i>	<i>rrrm</i>	<i>mrrm</i>
100	0.713	0.101	0.009	0.103	0.021	0.003	0.005	0.003	0.044
95	0.602	0.142	0.005	0.095	0.087	0.007	0.002	0.012	0.047
92.5	0.422	0.202	0.022	0.092	0.179	0.031	0.004	0.018	0.035
90	0.302	0.210	0.037	0.092	0.221	0.059	0.008	0.031	0.040
85	0.190	0.201	0.050	0.098	0.254	0.094	0.016	0.050	0.047
80	0.162	0.194	0.055	0.099	0.267	0.110	0.016	0.055	0.043
70	0.105	0.166	0.061	0.102	0.269	0.135	0.032	0.079	0.051
60	0.067	0.144	0.069	0.106	0.274	0.146	0.044	0.098	0.051
50	0.052	0.126	0.070	0.103	0.274	0.159	0.052	0.103	0.061

It is of significant importance to note that the increasing frequency of isolated *mr* stereoerrors with decreasing levels of activation represents a fundamentally unique method of microstructural control. Typically, low-crystallinity PP is achieved through the introduction of *rr* stereoerrors, indicative of a single misinsertion within a segment of uniformly chiral methyl groups. This is accomplished either by modifying the ligand set to induce a lower level of monomer face selectivity, or adjusting the reaction conditions to favor competitive isomerization reactions. However, the partial activation of **16** results in lower degrees of isotacticity through the incorporation of increasing amounts (with decreasing activation) of isolated *r* stereoerrors, as shown in Figure 44, by virtue of slow racemization (relative to propagation) of the active species during polymerization. This results in the isotactic-isotactic stereoblock type microstructure<sup>159</sup> as demonstrated by the preliminary stereochemical analysis of the high activation level (100-90%) spectra at the heptad level and higher,<sup>39</sup> shown in Figure 45. As the level of activation decreases, these blocks decrease in length until they are indistinguishable, and an atactic microstructure is produced. Consequently, the overall microstructure of PP produced by this method at a higher level of activation is significantly different than that of a typical site-control catalyst, even at identical *mmmm* pentad content. While isolated *mr* stereoerrors are common in isotactic polymerization under chain-end control, there has yet to be reported a system that has demonstrated the ability to deliberately incorporate varying amounts of this type of stereoerror.

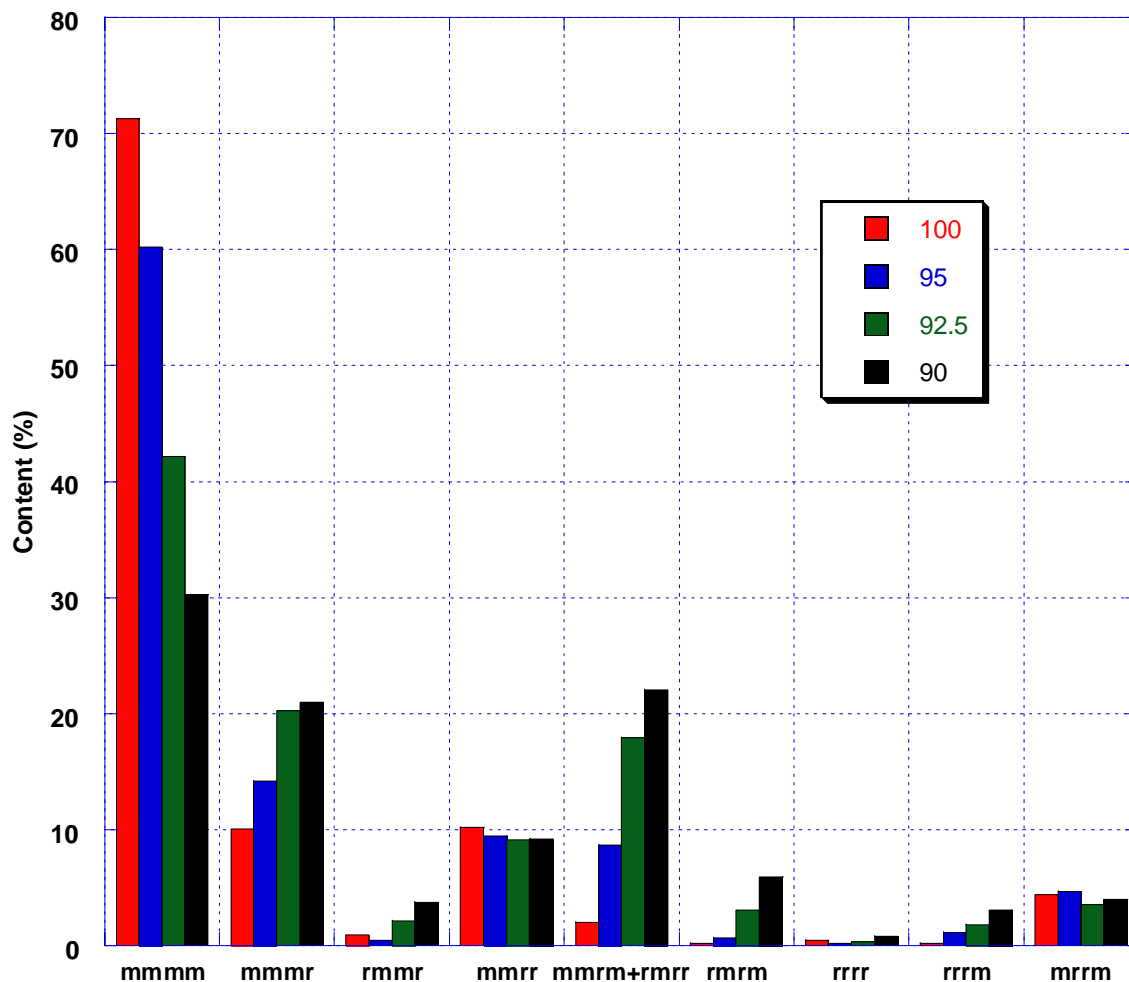


**Figure 44:** Comparison of the pentad distribution at 100%, 95%, 92.5%, and 90% activation. Note that as the *mmmm* pentad content decreases, isolated *r* stereoerrors increase rapidly, as shown in the *mmmr* and *mrrm* pentads.

Finally, preliminary investigations demonstrate that for any substoichiometric level of activation, the microstructure can be similarly affected by varying the absolute concentrations of the active and dormant species, accomplished by simply changing the solvent volume. As expected, isotacticity increases as the concentrations decrease.

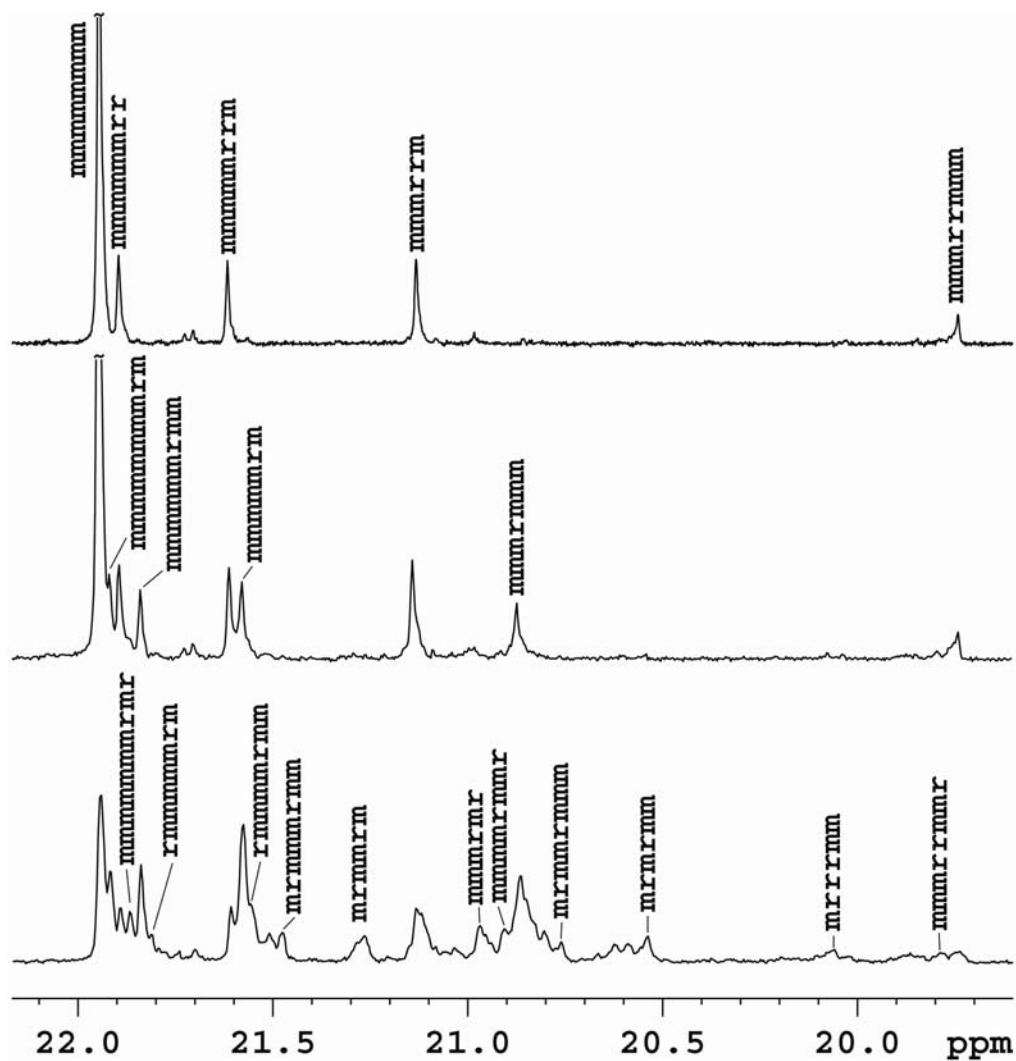


**Figure 45:**  $^{13}\text{C}\{^1\text{H}\}$  NMR (125 MHz, 1,1,2,2- $\text{C}_2\text{D}_2\text{Cl}_4$ , 70 °C) of polypropylene samples synthesized at 100% (top), 95% (middle) and 90% (bottom) activation, showing heptad and higher levels of stereoerror assignments.

#### 4.2 Stereogradient Polypropylene

The living nature of **16**, in combination with the degenerative transfer process, had already been shown to provide many unique PP microstructures. The *sb*-PP synthesis (Chapter 3) used sequential additions of discrete portions of cocatalyst, **13**, and a methylating agent, **56**, to modulate between 100 and 50% activation, providing fully isotactic and atactic microstructures, respectively. In addition, not only does the

bimolecular control of PP microstructure, as detailed above, provide another dimension of control for fine-tuning the properties of stereoblock PP materials (*i.e.*, *sb*-PP incorporating blocks synthesized at 90% activation, for example), but the gradual addition of **13** (or **56**) to a reaction should provide a fundamentally new microstructure in which the microstructure changes gradually from atactic at one end of the polymer to isotactic at the other: *stereogradient polypropylene*.

In practice, polymerization of propylene by  $^{13}\text{C}$ -labeled **16** at 60% activation was conducted for 30 minutes before a solution of **13** was added gradually via a programmable syringe pump over the next four hours, after which polymerization was continued for another 30 minutes before quenching with methanol (Scheme 45). During the reaction, aliquots were taken and quenched every 30 minutes for  $^{13}\text{C}$  NMR analysis. As shown in Figure 46 (left), these samples show a clear increase of overall isotacticity with time. Generating difference spectra (Figure 46, right), using the  $^{13}\text{C}$ -labeled methyl end-group resonances as an internal standard, allowed the examination of individual segments polymerized during the addition of **13**, as sampled every 10% increase in activation. Pentad analysis of the aliquot spectra (Table 11) and the difference spectra (Table 12) confirmed that the  $[mmmm]$  closely tracked the increase in activation, showing that propagation became increasingly isoselective until full isotactic propagation is reached at 100% activation (Figure 47). This experiment served to unequivocally authenticate the stereogradient microstructure.

**Scheme 45:** Synthesis of stereogradient-PP.

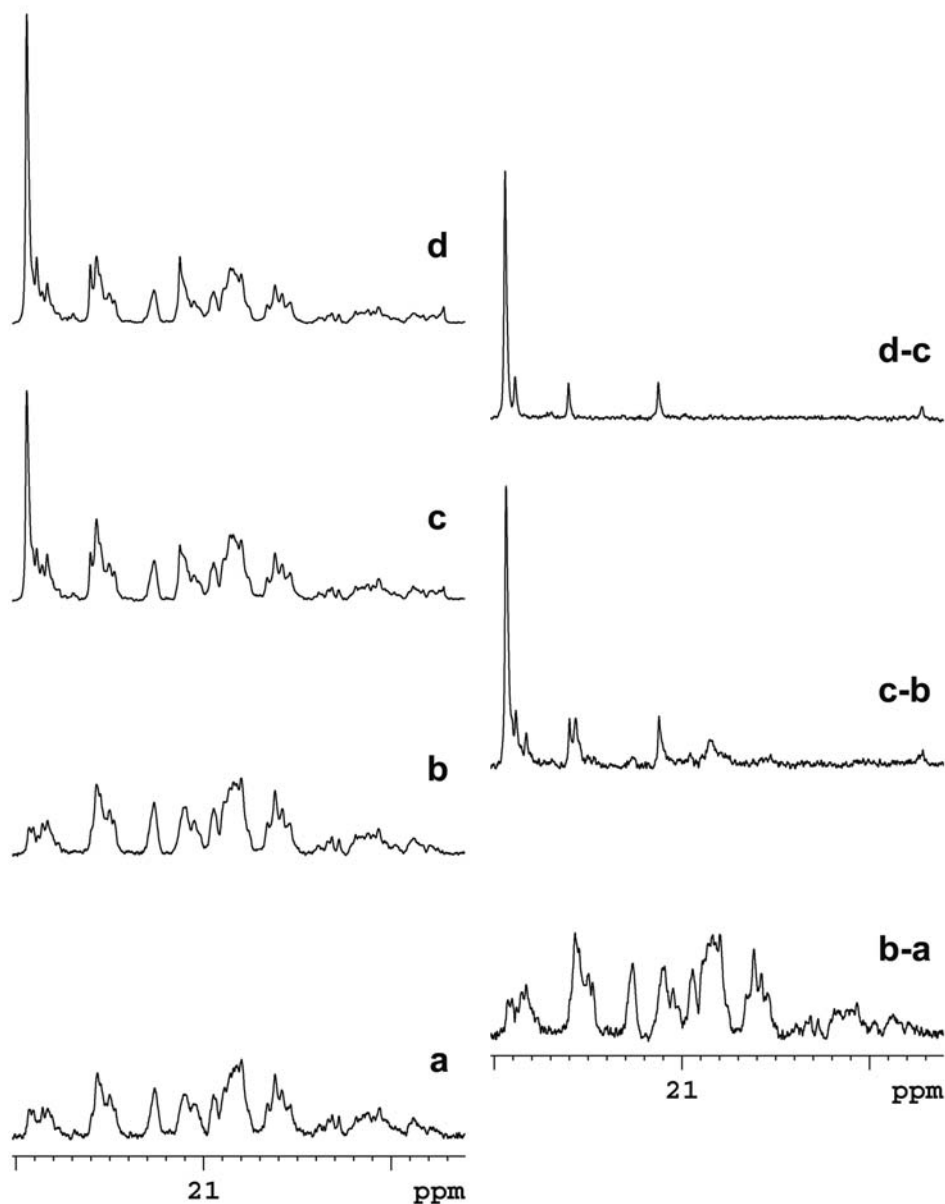
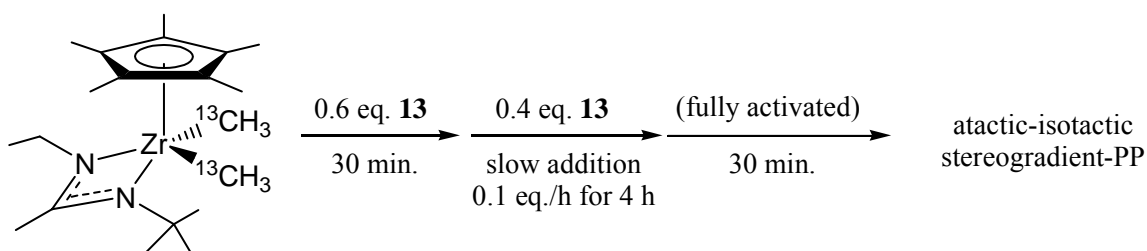


**Figure 46:**  $^{13}\text{C}\{^1\text{H}\}$  NMR (125 MHz, 1,1,2,2- $\text{C}_2\text{D}_4\text{Cl}_2$ , 70 °C) spectra of aliquots taken as a function of time (left) and their difference spectra (right) using the resonances (not shown) of the  $^{13}\text{C}$ -labeled methyl end group as an internal reference.

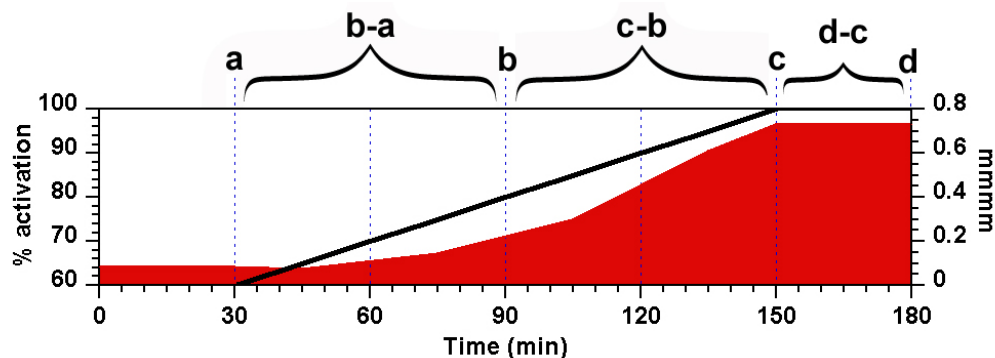


**Figure 47:** Ramp profile (black line) for addition of 0.4 equivalents of **13** to change the level of activation from 60% to 100% and *mmmm* content as a function of time (red shading) as determined by  $^{13}\text{C}$  NMR.

**Table 11:** Pentad distributions of samples taken during stereogradient-PP synthesis.

t (min)	activation*	<i>mmmm</i>	<i>mmmr</i>	<i>rmmr</i>	<i>mmrr</i>	<i>mmrm+rmrr</i>	<i>rmrm</i>	<i>rrrr</i>	<i>rrrm</i>	<i>mrrm</i>
30	60%	0.085	0.142	0.059	0.105	0.265	0.143	0.050	0.097	0.053
60	70%	0.076	0.144	0.061	0.105	0.269	0.146	0.044	0.097	0.057
90	80%	0.099	0.160	0.062	0.105	0.270	0.136	0.035	0.083	0.049
120	90%	0.132	0.168	0.055	0.099	0.266	0.124	0.032	0.074	0.049
150	100%	0.230	0.161	0.046	0.099	0.225	0.103	0.027	0.062	0.048
180	100%	0.296	0.152	0.041	0.099	0.196	0.088	0.024	0.055	0.050

\* at time of quench

**Table 12:** Pentad distributions of individual stereogradient-PP segments

t (min)	activation*	<i>mmmm</i>	<i>mmmr</i>	<i>rmmr</i>	<i>mmrr</i>	<i>mmrm+rmrr</i>	<i>rmrm</i>	<i>rrrr</i>	<i>rrrm</i>	<i>mrrm</i>
30	60%	0.085	0.142	0.059	0.105	0.265	0.143	0.050	0.097	0.053
30-60	60-70%	0.073	0.136	0.066	0.093	0.249	0.139	0.052	0.099	0.092
60-90	70-80%	0.146	0.196	0.064	0.106	0.273	0.118	0.013	0.052	0.033
90-120	80-90%	0.297	0.221	0.026	0.075	0.254	0.061	0.019	0.016	0.031
120-150	90-100%	0.612	0.121	0.010	0.089	0.057	0.019	0.017	0.015	0.060
150-180	100%	0.730	0.097	0.001	0.098	0.018	0.001	0.007	0.002	0.047

\* during time of segment with linear increase of activation level (20%/h)

### 4.3 Conclusions

In summary, by taking advantage of the bimolecular nature of degenerative transfer living Ziegler-Natta polymerization, and an intrinsic configurational instability of the dormant state, we have established a new dimension of control for the design and synthesis of elastomeric polypropylene. Ranging from fully isotactic to fully atactic, from discrete stereoblocks to gradual stereogradients, an unprecedented level of control has been achieved. The ability to synthesize an unlimited variety of polypropylene microstructures from a single catalytic system demonstrated; many of which could never be achieved through non-living systems. The investigation of these new materials, in the hopes of finding new technologically relevant materials, is currently under way.

## Appendix

### Experimentals

Manipulations were performed under an inert atmosphere of dinitrogen using standard Schlenk techniques or a Vacuum Atmospheres glovebox. Dry, oxygen-free solvents were employed throughout. Diethyl ether (Et<sub>2</sub>O) and pentane were distilled from sodium/benzophenone (with a few milliliters of triglyme being added to the pot in the case of pentane). Chlorobenzene was distilled from calcium hydride. Benzene-*d*<sub>6</sub> was vacuum transferred from sodium/potassium alloy (NaK) prior to being used for NMR spectroscopy. Chlorobenzene-*d*<sub>5</sub> was vacuum transferred from calcium hydride prior to being used for NMR spectroscopy. Research grade propylene (99.97%) was purchased from Matheson Trigas, and passed through Q5 and molecular sieves (4 Å). GPC analyses were performed using a Viscotek GPC system at 45 °C. THF was used as the eluant at a flow rate of 1.0 mL/min. *M*<sub>n</sub> and *M*<sub>w</sub>/*M*<sub>n</sub> values were obtained using the Viscotek OmniSEC software and seven polystyrene standards (Polymer Laboratories). [PhNMe<sub>2</sub>H][B(C<sub>6</sub>F<sub>5</sub>)<sub>4</sub>] (**13**) was purchased from Boulder Scientific. [Ph<sub>3</sub>C][B(C<sub>6</sub>F<sub>5</sub>)<sub>4</sub>] (**19**) and Cp\*ZrCl<sub>3</sub> (**35**) were purchased from Strem Chemical. (η<sup>5</sup>-C<sub>5</sub>Me<sub>5</sub>)ZrMe<sub>2</sub>[N(Et)C(Me)N(tBu)] (**12**), Cp\*ZrMe<sub>2</sub>[tBuN(H)NEt] (**14**), {Cp\*ZrMe[tBuN(H)NEt]}[B(C<sub>6</sub>F<sub>5</sub>)<sub>4</sub>] (**15**), {Cp\*ZrMe[tBuN(Me)NEt]}[B(C<sub>6</sub>F<sub>5</sub>)<sub>4</sub>] (**16**), Cp\*ZrMe<sub>2</sub>[iPrNC(Me)NiPr] (**23**), {Cp\*ZrMe[iPrNC(Me)NiPr]}[B(C<sub>6</sub>F<sub>5</sub>)<sub>4</sub>] (**24**), (η<sup>5</sup>-C<sub>5</sub>Me<sub>5</sub>)ZrCl<sub>2</sub>[N(Et)C(Me)N(tBu)] (**34**), {(η<sup>5</sup>-C<sub>5</sub>Me<sub>5</sub>)Zr(R)[N(Et)C(Me)N(tBu)]}[B(C<sub>6</sub>F<sub>5</sub>)<sub>4</sub>], R = Et, <sup>n</sup>Pr, <sup>i</sup>Pr, <sup>n</sup>Bu, <sup>i</sup>Bu (**33-R**), (η<sup>5</sup>-

$\text{C}_5\text{Me}_5\text{Zr}(\text{R})(\text{Cl})[\text{N}(\text{Et})\text{C}(\text{Me})\text{N}(\text{tBu})]$ , R = Et, <sup>n</sup>Pr, <sup>i</sup>Pr, <sup>n</sup>Bu, <sup>i</sup>Bu, <sup>t</sup>Bu (**36-R**), ( $\eta^5\text{-C}_5\text{Me}_5\text{Zr}(\text{R})(\text{Me})[\text{N}(\text{Et})\text{C}(\text{Me})\text{N}(\text{tBu})]$ , R = Et, <sup>n</sup>Pr, <sup>i</sup>Pr, <sup>n</sup>Bu, <sup>i</sup>Bu (**37-R**), ( $\eta^5\text{-C}_5\text{Me}_5\text{ZrCl}(\text{SiMe}_2\text{Ph})[\text{N}(\text{Et})\text{C}(\text{Me})\text{N}(\text{tBu})]$  (**38**), ( $\eta^5\text{-C}_5\text{Me}_5\text{HfCl}_2[\text{N}(\text{Et})\text{C}(\text{Me})\text{N}(\text{tBu})]$  (**45**),  $\text{Cp}^*\text{ZrMe}_2[\text{t-BuNC}(\text{t-Bu})\text{NEt}]$  (**54**),  $\{\text{Cp}^*\text{ZrMe}[\text{t-BuNC}(\text{t-Bu})\text{NEt}]\}[\text{B}(\text{C}_6\text{F}_5)_4]$  (**55**), and  $\text{Cp}^*\text{ZrMe}_2[\text{tBuNC}(\text{Me})\text{N}(\text{CH}_2\text{tBu})]$  (**56**) were prepared as previously reported. <sup>1</sup>H NMR spectra were recorded at 400 or 500 MHz and <sup>13</sup>C NMR spectra were recorded at 100 or 125 MHz using benzene-*d*<sub>6</sub>, chlorobenzene-*d*<sub>5</sub> or 1,1,2,2-tetrachloroethane-*d*<sub>2</sub> as the solvent. Elemental analyses were performed by Midwest Microlab.

**Preparation of ( $\eta^5\text{-C}_5\text{Me}_5\text{Zr}(\text{R})(\text{Cl})[\text{N}(\text{Et})\text{C}(\text{Me})\text{N}(\text{tBu})]$  (**36-R**):** The following is representative for **36-Me** and **33-(2-Et-Bu)** unless otherwise noted: To a  $-78\text{ }^\circ\text{C}$  solution of **34** (500 mg, 1.14 mmol) in 50 ml Et<sub>2</sub>O was added a solution of 1.14 mmol of MeMgCl, or 2-EtBuMgCl in Et<sub>2</sub>O. After slowly warming the mixture to RT, the reaction was quenched with 0.5 ml TMSCl, the volatiles were removed *in vacuo*, and the resulting yellow solid was taken up in pentane and filtered. The mother liquor was concentrated and recrystallized at  $-30\text{ }^\circ\text{C}$  to afford yellow crystals with an isolated yield of 80-90%.

**( $\eta^5\text{-C}_5\text{Me}_5\text{Zr}(\text{Me})(\text{Cl})[\text{N}(\text{Et})\text{C}(\text{Me})\text{N}(\text{tBu})]$  (**36-Me**):** <sup>1</sup>H NMR (400 MHz, C<sub>6</sub>D<sub>6</sub>, 293 K):  $\delta$  (ppm) 2.78 (m, 2H), 2.02 (s, 15H), 1.60 (s, 3H), 1.28 (s, 3H), 0.83 (t, <sup>3</sup>J=7.2 Hz, 3H), 0.45 (s, 3H).

**( $\eta^5\text{-C}_5\text{Me}_5\text{Zr}(\text{2-Et-Bu})(\text{Cl})[\text{N}(\text{Et})\text{C}(\text{Me})\text{N}(\text{tBu})]$  [**36-(2-Et-Bu)**):** <sup>1</sup>H NMR (400 MHz, C<sub>6</sub>D<sub>6</sub>, 293 K):  $\delta$  (ppm) 2.90 (dq, <sup>2</sup>J=14.2 Hz, <sup>3</sup>J=7.3 Hz, 1H), 2.71 (dq, <sup>2</sup>J=14.2 Hz, <sup>3</sup>J=7.3

Hz, 1H), 2.01 (s, 15H), 1.83 (m, 1H), 1.71 (s, 3H), 1.70 (m, 2H), 1.57 (m, 1H), 1.35 (m, 1H), 1.33 (s, 9H), 1.05 (t,  $^3J=7.3$  Hz, 3H), 1.03 (t,  $^3J=7.3$  Hz, 3H), 0.66, (dd,  $^2J=13.5$  Hz,  $^3J=7.1$  Hz), -0.08, (dd,  $^2J=13.5$  Hz,  $^3J=6.2$  Hz). Anal. Calcd. for  $C_{24}H_{45}ClN_2Zr$ : %C 59.02, %H 9.31, %N 5.74; Found %C 58.42, %H 9.25, %N 5.79.

**Preparation of  $(\eta^5-C_5Me_5)Zr(2-d)-^nPr(Cl)[N(Et)C(Me)N(tBu)]$  [36-(2-d)- $^nPr$ ]:** In a 50-ml Schlenk tube fitted with a gas tight Kontes Teflon valve, 0.30 g (0.56 mmol) of **38** was dissolved in 15 ml of pentane, after which time, the tube was sealed. After removal from the glove box, the tube was cooled to 77 K, evacuated and resealed. Upon warming to room temperature, the tube was pressurized to 15 psi with propylene, then pressurized to 35 psi with  $D_2$ , and resealed. The tube was shaken overnight, during which time the color changed from dark red to yellow, and the volatiles were removed *in vacuo*. Extraction in pentane and filtration through a thin pad of Celite afforded a yellow solution, which upon concentration and cooling to  $-35$  °C afforded yellow crystals (0.19 g, 79% yield).  $^1H$  NMR (400 MHz,  $C_6D_6$ , 293 K):  $\delta$  (ppm) 2.79 (dq,  $^2J=14.0$  Hz,  $^3J=7.0$  Hz, 1H), 2.62 (dq,  $^2J=14.4$  Hz,  $^3J=7.2$  Hz, 1H), 2.13 (m, 0.6H), 2.01 (s, 15H), 1.67 (s, 3H), 1.54 (m, 0.4H), 1.33 (s, 9H), 1.22 (t,  $^3J=7.0$  Hz, 3H), 0.80 (t,  $^3J=7.2$  Hz, 3H), 0.59 (dd,  $^2J=13.6$  Hz,  $^3J=10.8$  Hz, 1H), 0.27 (dd,  $^2J=13.6$  Hz,  $^3J=11.2$  Hz, 1H).

**Preparation of  $(\eta^5-C_5Me_5)Zr(2-d)-^iBu(Cl)[N(Et)C(Me)N(tBu)]$  [36-(2-d)- $^iBu$ ]:** In a 50-ml Schlenk tube fitted with a gas tight Kontes Teflon valve, 0.30 g (0.56 mmol) of **38** was dissolved in 15 ml of pentane and an excess of liquid isobutylene was added, after which time, the tube was sealed. After removal from the glove box, the tube was

pressurized to 35 psi with D<sub>2</sub>, resealed, and shaken overnight, during which time the color changed from dark red to yellow, and the volatiles were removed *in vacuo*. Extraction in pentane and filtration through a thin pad of Celite afforded a yellow solution, which upon concentration and cooling to -35 °C afforded yellow crystals (0.22 g, 85% yield). <sup>1</sup>H NMR (400 MHz, C<sub>6</sub>D<sub>6</sub>, 293 K): δ (ppm) 2.89 (dq, <sup>2</sup>J=14.3 Hz, <sup>3</sup>J=7.2 Hz 1H), 2.72 (dq, <sup>2</sup>J=14.3 Hz, <sup>3</sup>J=7.2 Hz, 1H), 2.00 (s, 15H), 1.70 (s, 3H), 1.33 (s, 9H), 1.32 (d, <sup>3</sup>J=6.4 Hz, 3H), 1.15 (d, <sup>3</sup>J=6.4 Hz, 3H), 0.82 (t, <sup>3</sup>J=7.2 Hz, 3H), 0.73 (dd, <sup>2</sup>J=13.6 Hz, <sup>3</sup>J=6.4 Hz), -0.03 (dd, <sup>2</sup>J=13.6 Hz, <sup>3</sup>J=6.4 Hz).

**Preparation of sodium methylsulfinyl methyllide stock solution:** Several portions of pentane were used to wash 10 g of sodium hydride dispersion (60%) in mineral oil. The powder was thoroughly dried *en vacuo* before 250 mL DMSO was added. The solution was heated to 60 °C and stirred for 4 hours before unreacted NaH was filtered away to give a pale blue-green solution. The solution was titrated using salicylaldehyde phenylhydrazone (0.315 M).

**Preparation of (<sup>13</sup>C-methyl)triphenylphosphonium iodide:** To a solution of 10.2 g (38.9 mmol) triphenylphosphine in 25 mL benzene at 0 °C was added dropwise 5.0 g (35.0 mmol) <sup>13</sup>C-iodomethane in 10 mL benzene, white precipitate forming immediately. The solution was stirred for 2 hours at RT before filtering, and the precipitate was washed with several portions of fresh benzene. The white powder was dried *en vacuo* (13.4 g, 94%). 99.1% <sup>13</sup>C by NMR.

**Preparation of 1-<sup>13</sup>C-isobutylene:** To 60 mL of NaMe<sub>2</sub>SO stock solution in DMSO (0.315 M, 18.9 mmol) was added 7.60 g (<sup>13</sup>C-methyl)triphenylphosphonium iodide, stirred for 1 hour. A suitable trap at -196° C was fitted to the setup and the solution was brought to 60 °C before 124 mg (2.13 mmol) of acetone in 6 mL DMSO was added dropwise via syringe with N<sub>2</sub> bubbling through the solution. The solution was stirred for 15 minutes after addition before the trap was sealed. The product was used without further purification.

**Preparation of (η<sup>5</sup>-C<sub>5</sub>Me<sub>5</sub>)Zr(1-<sup>13</sup>C)-<sup>i</sup>Bu(Cl)[N(Et)C(Me)N(tBu)] [36-(1-<sup>13</sup>C)-<sup>i</sup>Bu]:**

Into a 50-ml Schlenk tube fitted with a gas tight Kontes Teflon valve containing a solution of 0.30 g (0.56 mmol) of **38** in 15 ml of pentane was vacuum transferred 1 g of 1-<sup>13</sup>C-isobutylene. The tube was pressurized to 35 psi with H<sub>2</sub>, resealed, and shaken overnight, during which time the color changed from dark red to yellow. The volatiles were vacuum transferred away to recover unreacted 1-<sup>13</sup>C-isobutylene. Extraction in pentane and filtration through a thin pad of Celite afforded a yellow solution, which upon concentration and cooling to -35 °C afforded yellow crystals (0.20 g, 77% yield). <sup>1</sup>H NMR (400 MHz, C<sub>6</sub>D<sub>6</sub>, 293 K): δ (ppm) 2.89 (dq, <sup>2</sup>J=14.3 Hz, <sup>3</sup>J=7.2 Hz 1H), 2.72 (dq, <sup>2</sup>J=14.3 Hz, <sup>3</sup>J=7.2 Hz, 1H), 2.24 (d nonet, <sup>2</sup>J<sub>CH</sub>=1.6 Hz <sup>3</sup>J<sub>HH</sub>=6.4 Hz, 1H), 2.00 (s, 15H), 1.70 (s, 3H), 1.33 (s, 9H), 1.32 (dd, <sup>3</sup>J<sub>CH</sub>=4.4 Hz, <sup>3</sup>J<sub>HH</sub>=6.4 Hz, 3H), 1.15 (dd, <sup>3</sup>J<sub>CH</sub>=4.4 Hz, <sup>3</sup>J<sub>HH</sub>=6.4 Hz, 3H), 0.82 (t, <sup>3</sup>J=7.2 Hz, 3H), 0.73 (ddd, <sup>1</sup>J<sub>CH</sub>=115.7 Hz, <sup>2</sup>J<sub>HH</sub>=13.6 Hz, <sup>3</sup>J<sub>HH</sub>=6.4 Hz), -0.03 (ddd, <sup>1</sup>J<sub>CH</sub>=115.7 Hz, <sup>2</sup>J<sub>HH</sub>=13.6 Hz, <sup>3</sup>J<sub>HH</sub>=6.4 Hz).

**Preparation of (η<sup>5</sup>-C<sub>5</sub>Me<sub>5</sub>)Zr(1-<sup>13</sup>C-2-*d*)-<sup>i</sup>Bu(Cl)[N(Et)C(Me)N(tBu)] [36-(1-<sup>13</sup>C-2-*d*)-<sup>i</sup>Bu]:** Prepared in the same manner as **36-(1-<sup>13</sup>C)-<sup>i</sup>Bu** with D<sub>2</sub> in place of H<sub>2</sub> (0.18 g 70%

yield).  $^1\text{H}$  NMR (400 MHz,  $\text{C}_6\text{D}_6$ , 293 K):  $\delta$  (ppm) 2.89 (dq,  $^2\text{J}=14.3$  Hz,  $^3\text{J}=7.2$  Hz, 1H), 2.72 (dq,  $^2\text{J}=14.3$  Hz,  $^3\text{J}=7.2$  Hz, 1H), 2.00 (s, 15H), 1.70 (s, 3H), 1.33 (s, 9H), 1.32 (d,  $^3\text{J}_{\text{CH}}=4.4$  Hz, 3H), 1.15 (d,  $^3\text{J}_{\text{CH}}=4.4$  Hz, 3H), 0.82 (t,  $^3\text{J}=7.2$  Hz, 3H), 0.73 (dd,  $^1\text{J}_{\text{CH}}=115.7$  Hz,  $^2\text{J}_{\text{HH}}=13.6$  Hz), -0.03 (dd,  $^1\text{J}_{\text{CH}}=115.7$  Hz,  $^2\text{J}_{\text{HH}}=13.6$  Hz).

**Preparation of  $(\eta^5\text{-C}_5\text{Me}_5)\text{Zr}(\text{R})(\text{Me})[\text{N}(\text{Et})\text{C}(\text{Me})\text{N}(\text{tBu})]$  (**37-R**):** The following is representative for **37-R** [R = (2-*d*)- $^n\text{Pr}$ , (2-*d*)- $^i\text{Bu}$ , (1- $^{13}\text{C}$ )- $^i\text{Bu}$ , (1- $^{13}\text{C}$ -2-*d*)- $^i\text{Bu}$ , 2-Et-Bu] unless otherwise noted: To a -78 °C solution of **36-R** (1.0 mmol) in 25 mL of  $\text{Et}_2\text{O}$  was added a solution of MeLi (1.0 mmol) in  $\text{Et}_2\text{O}$ . After slowly warming the mixture to RT, the reaction was quenched with 0.5 ml TMS-Cl, the volatiles were removed *in vacuo* and the yellow solid was taken up in pentane and filtered. The mother liquor was concentrated and the product was recrystallized at -30 °C to afford yellow crystals with an isolated yield of 60-85%.

**$(\eta^5\text{-C}_5\text{Me}_5)\text{Zr}(\text{2-Et-Bu})(\text{Me})[\text{N}(\text{Et})\text{C}(\text{Me})\text{N}(\text{tBu})]$  [**37(2-Et-Bu)**]:**  $^1\text{H}$  NMR (400 MHz,  $\text{C}_6\text{D}_6$ , 293 K):  $\delta$  (ppm) 2.98 (dq,  $^2\text{J}=14.1$  Hz,  $^3\text{J}=7.1$  Hz, 1H), 2.73 (dq,  $^2\text{J}=14.1$  Hz,  $^3\text{J}=7.1$  Hz, 1H), 1.98 (s, 9H), 1.81 (s, 3H), 1.75 (m, 1H), 1.63 (m, 3H), 1.44 (m, 1H), 1.20 (s, 9H), 1.052 (t,  $^3\text{J}=7.3$  Hz, 3H), 1.048 (t,  $^3\text{J}=7.3$  Hz, 3H), 0.89 (t,  $^3\text{J}=7.1$  Hz, 3H), 0.32 (dd,  $^2\text{J}=14.0$  Hz,  $^3\text{J}=7.2$  Hz, 1H), 0.21 (s, 3H), -0.34 (dd,  $^2\text{J}=14.0$  Hz,  $^3\text{J}=6.8$  Hz, 1H). Anal. Calcd. for  $\text{C}_{25}\text{H}_{48}\text{N}_2\text{Zr}$ : %C 64.16, %H 10.35, %N 5.99; Found: %C 62.68, %H 10.03, %N 6.04.

$(\eta^5\text{-C}_5\text{Me}_5)\text{Zr}(\text{2-}d\text{-}^n\text{Pr}(\text{Me})[\text{N}(\text{Et})\text{C}(\text{Me})\text{N}(\text{tBu})]$  [37(2-*d*)-<sup>n</sup>Pr]: <sup>1</sup>H NMR (400 MHz, C<sub>6</sub>D<sub>6</sub>, 293 K): δ (ppm) 2.90 (dq, <sup>2</sup>J=14.0 Hz, <sup>3</sup>J=7.2 Hz, 1H), 2.70 (b, 1H), 1.99 (s, 15H), 1.98 (m, 1H), 1.74 (s, 3H), 1.23 (d, <sup>3</sup>J=7.0 Hz, 3H), 1.18 (s, 9H), 0.88 (t, <sup>3</sup>J=6.8 Hz, 3H), 0.88 (m, 1H), 0.27 (m, 1H), 0.14 (s, 3H).

$(\eta^5\text{-C}_5\text{Me}_5)\text{Zr}(\text{2-}d\text{-}^i\text{Bu}(\text{Me})[\text{N}(\text{Et})\text{C}(\text{Me})\text{N}(\text{tBu})]$  [37-(2-*d*)-<sup>i</sup>Bu]: <sup>1</sup>H NMR (400 MHz, C<sub>6</sub>D<sub>6</sub>, 293 K): δ (ppm) 2.97 (dq, <sup>2</sup>J=14.4 Hz, <sup>3</sup>J=7.2 Hz, 1H), 2.75 (dq, <sup>2</sup>J=14.4 Hz, <sup>3</sup>J=7.2 Hz, 1H), 1.98 (s, 15H), 1.80 (s, 3H), 1.27 (s, 3H), 1.23 (s, 3H), 1.19 (s, 9H), 0.85 (t, <sup>3</sup>J=7.2 Hz, 3H), 0.41 (d, <sup>2</sup>J=13.2 Hz, 1H), 0.23 (s, 3H), -0.26 (d, <sup>2</sup>J=13.2 Hz, 1H).

$(\eta^5\text{-C}_5\text{Me}_5)\text{Zr}(\text{1-}^{13}\text{C}\text{-}^i\text{Bu}(\text{Me})[\text{N}(\text{Et})\text{C}(\text{Me})\text{N}(\text{tBu})]$  [37-(1-<sup>13</sup>C)-<sup>i</sup>Bu]: <sup>1</sup>H NMR (400 MHz, C<sub>6</sub>D<sub>6</sub>, 293 K): δ (ppm) 2.97 (dq, <sup>2</sup>J=14.4 Hz, <sup>3</sup>J=7.2 Hz, 1H), 2.75 (dq, <sup>2</sup>J=14.4 Hz, <sup>3</sup>J=7.2 Hz, 1H), 2.20 (bm, 1H), 1.98 (s, 15H), 1.80 (s, 3H), 1.27 (m, 3H), 1.23 (m, 3H), 1.19 (s, 9H), 0.85 (t, <sup>3</sup>J=7.2 Hz, 3H), 0.41 (ddd, <sup>1</sup>J<sub>CH</sub>=114.0 Hz, <sup>2</sup>J=13.2 Hz, <sup>3</sup>J=6.4 Hz, 1H), 0.23 (s, 3H), -0.26 (ddd, <sup>1</sup>J<sub>CH</sub>=114.0 Hz, <sup>2</sup>J=13.2 Hz, <sup>3</sup>J=6.4 Hz, 1H).

$(\eta^5\text{-C}_5\text{Me}_5)\text{Zr}(\text{1-}^{13}\text{C}\text{-}2\text{-}d\text{-}^i\text{Bu}(\text{Me})[\text{N}(\text{Et})\text{C}(\text{Me})\text{N}(\text{tBu})]$  [37-(1-<sup>13</sup>C-2-*d*)-<sup>i</sup>Bu]: <sup>1</sup>H NMR (400 MHz, C<sub>6</sub>D<sub>6</sub>, 293 K): δ (ppm) 2.97 (dq, <sup>2</sup>J=14.4 Hz, <sup>3</sup>J=7.2 Hz, 1H), 2.75 (dq, <sup>2</sup>J=14.4 Hz, <sup>3</sup>J=7.2 Hz, 1H), 1.98 (s, 15H), 1.80 (s, 3H), 1.27 (m, 3H), 1.23 (m, 3H), 1.19 (s, 9H), 0.85 (t, <sup>3</sup>J=7.2 Hz, 3H), 0.41 (ddd, <sup>1</sup>J<sub>CH</sub>=114.0 Hz, <sup>2</sup>J=13.2 Hz, 1H), 0.23 (s, 3H), -0.26 (dd, <sup>1</sup>J<sub>CH</sub>=114.0 Hz, <sup>2</sup>J=13.2 Hz, 1H).

**Preparation of  $\{(\eta^5\text{-C}_5\text{Me}_5)\text{Zr}(\text{R})[\text{tBuNC}(\text{Me})\text{NEt}]\}[\text{B}(\text{C}_6\text{F}_5)_4]$  (**33-R**):** The following is representative for **33-R** [R = (2-*d*)-<sup>n</sup>Pr, (2-*d*)-<sup>i</sup>Bu, (1-<sup>13</sup>C)-<sup>i</sup>Bu, (1-<sup>13</sup>C-2-*d*)-<sup>i</sup>Bu, 2-Et-Bu] unless otherwise noted: To 11 mg (14 μmol) of [PhNHMe<sub>2</sub>][B(C<sub>6</sub>F<sub>5</sub>)<sub>4</sub>] was added a solution of 13 μmol of **37-R** in 1.0 ml of C<sub>6</sub>D<sub>5</sub>Cl at -10 °C to provide a clear, deep yellow solution.

**Preparation of  $(\eta^5\text{-C}_5\text{Me}_5)\text{Hf}(\text{SiMe}_2\text{Ph})(\text{Cl})[\text{N}(\text{Et})\text{C}(\text{Me})\text{N}(\text{tBu})]$  (**39**):** To a -78 °C solution of **45** (0.50 g, 0.95 mmol) in 100 ml Et<sub>2</sub>O was added 5.0 ml (0.95 mmol) of LiSiMe<sub>2</sub>Ph (0.19 M in Et<sub>2</sub>O). After slowly warming the mixture to RT, the volatiles were removed *in vacuo*, and the resulting brown oil was taken up in pentane and filtered. Removal of the volatiles *in vacuo* afforded a brown oil which could not be further purified (0.55 g, 93%). <sup>1</sup>H NMR (400 MHz, C<sub>6</sub>D<sub>6</sub>, 293 K): δ (ppm) 7.94 (dd, <sup>3</sup>J=7.6 Hz, <sup>4</sup>J=1.2 Hz, 2H), 7.27 (t, <sup>3</sup>J=7.6 Hz, 2H), 7.13 (tt, <sup>3</sup>J=7.6 Hz, <sup>4</sup>J=1.2 Hz, 1H), 2.90 (dq, <sup>2</sup>J=14.0 Hz, <sup>3</sup>J=7.2 Hz, 1H), 2.82 (dq, <sup>2</sup>J=14.0 Hz, <sup>3</sup>J=7.2 Hz, 1H), 2.09 (s, 15H), 1.17 (s, 9H), 1.16 (s, 3H), 0.76 (s, 3H), 0.71 (t, <sup>3</sup>J=7.2 Hz, 3H) 0.59 (s, 3H).

**Preparation of  $(\eta^5\text{-C}_5\text{Me}_5)\text{Hf}(1\text{-}^{13}\text{C}\text{-}2\text{-}d\text{-iBu})(\text{Cl})[\text{N}(\text{Et})\text{C}(\text{Me})\text{N}(\text{tBu})]$  (**40**):** Into a 50-ml Schlenk tube fitted with a gas tight Kontes Teflon valve containing a solution of 0.38 g (0.61 mmol) of **39** in 15 ml of pentane was vacuum transferred 1 g of 1-<sup>13</sup>C-isobutylene. The tube was pressurized to 35 psi with D<sub>2</sub>, resealed, and shaken overnight. The volatiles were vacuum transferred away to recover unreacted 1-<sup>13</sup>C-isobutylene. Extraction in pentane and filtration through a thin pad of Celite afforded a yellow solution, which upon concentration and cooling to -35 °C afforded yellow crystals (0.16 g, 48% yield). <sup>1</sup>H

NMR (400 MHz, C<sub>6</sub>D<sub>6</sub>, 293 K):  $\delta$  (ppm) 2.91 (dq, <sup>2</sup>J=14.0 Hz, <sup>3</sup>J=7.0 Hz, 1H), 2.80 (dq, <sup>2</sup>J=14.0 Hz, <sup>3</sup>J=7.0 Hz, 1H), 2.05 (s, 15H), 1.66 (s, 3H), 1.32 (d, <sup>3</sup>J<sub>CH</sub>=4.4 Hz, 3H), 1.31 (s, 9H), 1.14 (d, <sup>3</sup>J<sub>CH</sub>=4.4 Hz, 3H), 0.83 (t, <sup>3</sup>J=7.0 Hz, 3H), 0.54 (dd, <sup>1</sup>J<sub>CH</sub>=111.1 Hz, <sup>2</sup>J<sub>HH</sub>=13.9 Hz), -0.17 (dd, <sup>1</sup>J<sub>CH</sub>=111.1 Hz, <sup>2</sup>J<sub>HH</sub>=13.9 Hz).

**Preparation of ( $\eta^5$ -C<sub>5</sub>Me<sub>5</sub>)Hf(1-<sup>13</sup>C-2-*d*-iBu)(Me)[N(Et)C(Me)N(tBu)] (41):** To a -78 °C solution of **40** (0.11 g, 0.20 mmol) in 25 mL of Et<sub>2</sub>O was added 0.1 ml (0.2 mmol) of MeLi (2.0 M in Et<sub>2</sub>O). After slowly warming the mixture to RT, the reaction was quenched with 0.5 ml TMSCl, the volatiles were removed *in vacuo* and the yellow solid was taken up in pentane and filtered. The mother liquor was concentrated and the product was recrystallized at -30 °C to afford yellow crystals (0.75 g, 71% yield). <sup>1</sup>H NMR (400 MHz, C<sub>6</sub>D<sub>6</sub>, 293 K):  $\delta$  (ppm) 3.00 (dq, <sup>2</sup>J=14.0 Hz, <sup>3</sup>J=7.0 Hz, 1H), 2.82 (dq, <sup>2</sup>J=14.0 Hz, <sup>3</sup>J=7.0 Hz, 1H), 2.02 (s, 15H), 1.73 (s, 3H), 1.27 (d, <sup>3</sup>J<sub>CH</sub>=4.0 Hz, 3H), 1.21 (d, <sup>3</sup>J<sub>CH</sub>=4.4 Hz, 3H), 1.17 (s, 9H), 0.89 (t, <sup>3</sup>J=7.0 Hz, 3H), 0.22 (dd, <sup>1</sup>J<sub>CH</sub>=109.2 Hz, <sup>2</sup>J<sub>HH</sub>=13.8 Hz), -0.48 (dd, <sup>1</sup>J<sub>CH</sub>=109.2 Hz, <sup>2</sup>J<sub>HH</sub>=13.8 Hz).

**Preparation of ( $\eta^5$ -C<sub>5</sub>Me<sub>5</sub>)Hf(tBu)(Cl)[N(Et)C(Me)N(tBu)] (46):** To a -78 °C solution of **37** (0.75 g, 1.43 mmol) in 100 ml Et<sub>2</sub>O was added 0.89 ml (1.43 mmol) of tBuLi (1.61 M in tetrahydrofuran). After slowly warming the mixture to RT, the reaction was quenched with 0.5 ml TMSCl, the volatiles were removed *in vacuo*, and the resulting yellow solid was taken up in pentane and filtered. The mother liquor was concentrated and recrystallized at -30 °C to afford white crystals (0.70 g, 89% yield). <sup>1</sup>H NMR (400 MHz, C<sub>6</sub>D<sub>6</sub>, 293 K):  $\delta$  (ppm) 3.09 (dq, <sup>2</sup>J=14.4 Hz, <sup>3</sup>J=7.1 Hz, 1H), 2.81 (dq, <sup>2</sup>J=14.4 Hz,

$^3J=7.1$  Hz, 1H), 2.08 (s, 15H), 1.64 (s, 3H), 1.46 (s, 9H), 1.35 (s, 9H), 0.87 (t,  $^3J=7.1$  Hz, 3H).

**Preparation of  $(\eta^5\text{-C}_5\text{Me}_5)\text{Hf}(\text{Me})(\text{Cl})[\text{N}(\text{Et})\text{C}(\text{Me})\text{N}(\text{tBu})]$  (**48**):** To a  $-78$  °C solution of **37** (0.75 g, 1.43 mmol) in 100 ml  $\text{Et}_2\text{O}$  was added 0.53 ml (1.43 mmol) of  $\text{MeMgCl}$  (2.71 M in tetrahydrofuran). After slowly warming the mixture to RT, the reaction was quenched with 0.5 ml  $\text{TMSCl}$ , the volatiles were removed *in vacuo*, and the resulting yellow solid was taken up in pentane and filtered. The mother liquor was concentrated and recrystallized at  $-30$  °C to afford white crystals (0.58 g, 80% yield).  $^1\text{H}$  NMR (400 MHz,  $\text{C}_6\text{D}_6$ , 293 K):  $\delta$  (ppm) 2.82 (m, 2H), 2.07 (s, 15H), 1.57 (s, 3H), 1.28 (s, 9H), 0.82 (t,  $^3J=7.1$  Hz, 3H), 0.23 (s, 3H).

**Preparation of  $(\eta^5\text{-C}_5\text{Me}_5)\text{Hf}(\text{tBu})(\text{Me})[\text{N}(\text{Et})\text{C}(\text{Me})\text{N}(\text{tBu})]$  (**49**):** To a  $-55$  °C solution of **48** (0.30 g, 0.59 mmol) in 50 ml  $\text{Et}_2\text{O}$  was added 0.31 ml (0.59 mmol) of  $^t\text{BuLi}$  (1.90 M in pentane). The reaction was stirred overnight at  $-55$  °C before being quenched with 0.5 ml  $\text{TMSCl}$ , the volatiles were removed *in vacuo*, and the resulting yellow solid was taken up in pentane and filtered. The mother liquor was concentrated and recrystallized at  $-30$  °C to afford yellow crystals (0.25 g, 81% yield).  $^1\text{H}$  NMR (400 MHz,  $\text{C}_6\text{D}_6$ , 293 K):  $\delta$  (ppm) 3.06 (dq,  $^2J=14.5$  Hz,  $^3J=7.2$  Hz, 1H), 2.98 (dq,  $^2J=14.5$  Hz,  $^3J=7.2$  Hz, 1H), 2.02 (s, 15H), 1.71 (s, 3H), 1.37 (s, 9H), 1.20 (s, 9H), 0.87 (t,  $^3J=7.2$  Hz, 3H) 0.17 (s, 3H).

**Preparation of  $\{(\eta^5\text{-C}_5\text{Me}_5)\text{Hf}(\text{R})[\text{N}(\text{Et})\text{C}(\text{Me})\text{N}(\text{tBu})]\}\text{[B}(\text{C}_6\text{F}_5)_4]$  [R = (1-<sup>13</sup>C-2-*d*)-<sup>i</sup>Bu (42), <sup>t</sup>Bu (44)]:** Prepared in the same manner as **33-R**.

**Kinetic Study of Poly(1-butene):** To a solution of 83 mg (105 μmol) of **13** in 12 ml of chlorobenzene at -10° C was added a solution of 40 mg (100 μmol) of **12** in 8 ml of chlorobenzene also at -10° C, to produce a clear yellow solution. At this time 110 mg (2 mmol) of 1-butene, precooled to -10° C, was added all at once and the resulting mixture was allowed to stir for 2 hrs at -10° C, beginning at which time 2-mL samples were rapidly quenched by the addition of acidic methanol every 12 hrs. The volatiles were then removed *in vacuo*, and the crude material was purified through precipitation of a toluene solution into a large volume of acidic methanol. The final pure material was collected and dried overnight at 60° C/0.01 mmHg.

**Preparation of Living Poly(1-butene) (16-PB):** To a solution of 11 mg (14 μmol) **13** in 0.5 mL chlorobenzene-*d*<sub>5</sub> at -10° C was added a solution of 5 mg (13 μmol) **12** in 0.5 mL chlorobenzene-*d*<sub>5</sub> at -10° C, to produce a clear yellow solution. At this time 24 mg (0.42 mmol) 1-butene was added all at one and the resulting mixture was allowed to sit at -10° C for 2 hrs.

**Preparation of Living Poly(1-<sup>13</sup>C-1-decene) (16-PD):** The same procedure as that for **16-PB** was followed, except 33 mg (0.25 mmol) 1-<sup>13</sup>C-1-decene was used in place of 1-butene.

**Degenerative Transfer Polymerization of Propylene:** The following description of a 60% activated system is representative for any level of activation, unless otherwise noted. To a solution of 24.2 mg (0.030 mmol) **13** in 0.5 ml of chlorobenzene at -10 °C was added 20.0 mg (0.050 mmol) of **12** in 0.5 ml of chlorobenzene at -10 °C. This solution was then rapidly added to a 250 ml Schlenk flask charged with 20 ml of chlorobenzene at -10 °C, which was previously pressurized to 5 psi with propylene and stirred for 10 minutes. The flask was then repressurized and the pressure maintained for 2 hours while stirring before quenching with 1 ml of acidic methanol. The volatiles were then removed *in vacuo* and the crude polymeric material was purified through precipitation of a hot toluene solution into a large volume of acidic methanol. The final pure polypropylene was collected and dried overnight at 60 °C (0.01 mmHg). 735 mg.  $M_n = 25,200$ , PDI = 1.41.

50% activation: 20.1 mg (0.025 mmol) **13**, 2h 50 min, yield: 926 mg.  $M_n = 25,500$ , PDI = 1.11.

70% activation: 28.2 mg (0.035 mmol) **13**, yield: 0.692 g.  $M_n = 21,700$ , PDI = 1.18.

80% activation: 32.2 mg (0.040 mmol) **13**, yield: 0.681 g.  $M_n = 27,400$ , PDI = 1.20.

85% activation: 34.2 mg (0.0425 mmol) **13**, yield: 0.812 g.  $M_n = 25,000$ , PDI = 1.22.

90% activation: 36.3 mg (0.045 mmol) **13**, yield: 0.753 g.  $M_n = 24,400$ , PDI = 1.22.

92.5% activation: 40.0 mg (0.100 mmol) **12**, 74.5 mg (0.0925 mmol) **13**, 40 ml chlorobenzene, yield: 1.666 g.  $M_n = 22,400$ , PDI = 1.24.

95% activation: 38.3 mg (0.0475 mmol) **13**, yield: 0.756 g.  $M_n = 23,000$ , PDI = 1.22.

100% activation (non-DT): 10.0 mg (0.025 mmol) **12**, 20.1 mg (0.025 mmol) **13**, yield: 0.500 g.

**Kinetics of propylene polymerization under DT conditions:** The polymerization was carried out in the same manner as the general procedure, while 20.0 mg (0.05 mmol) of **12** and 20.0 mg (0.025 mmol) of **13** were used and the total solution volume was 35 ml. Aliquots were quenched with methanol after 48 min and 5 more points were collected within the next 5 h. Polypropylene samples were purified and GPC data was collected.

**Polymerization of propylene under non-DT conditions.**

General procedure conducted in an identical manner to DT conditions, but an equal molar ratio of  $(\eta^5\text{-C}_5\text{Me}_5)\text{ZrMe}_2[\text{N}(\text{Et})\text{C}(\text{Me})\text{N}(\text{tBu})]$  to  $[\text{PhNHMe}_2][\text{B}(\text{C}_6\text{F}_5)_4]$  was used.

**Kinetics of propylene polymerization under non-DT conditions:** In order to circumvent solubility issues, the kinetics of isotactic propagation were determined by first synthesizing an atactic polypropylene block under DT conditions using 20.5 mg (0.051 mmol) **12** and 21.2 mg (0.026 mmol) **13** in 60 ml chlorobenzene for 2 hours. The reaction was switched to non-DT conditions by fully activating the system with a second portion of 21.2 mg of **13**. Aliquots were quenched with acidic methanol at 10 min. from full activation and approximately every 30 min. thereafter for 3 h.

**Synthesis of  $^{13}\text{C}$ -labeled *a-iso-a*-polypropylene stereoblock triblock:** Under DT conditions, a polymerization was carried out using 20.0 mg (0.05 mmol)  $^{13}\text{C}$ -labeled **12** and 20.0 mg (0.025 mmol) **13** in 30 mL chlorobenzene for 2 h. At this point the reaction was switched to non-DT by the addition of a second portion of 20.0 mg (0.025 mmol) of

**13** for 1 h, after which the reaction was returned to DT by the addition of 11.0 mg (0.025 mmol) **56** for another 2 h before being quenched with ~1 mL of acidic methanol. The volatiles were removed *in vacuo* and the crude polymeric material was purified through precipitation of a hot toluene solution into a large volume of acidic methanol. The final pure polypropylene was collected and dried overnight at 60 °C (0.01 mmHg).  $M_n = 31\,100$ , PDI = 1.28.

**Synthesis of *a*-iso-polypropylene stereoblock diblock:** Under non-DT conditions, a polymerization was carried out using 25.0 mg (0.063 mmol) **12** and 25.2 mg (0.031 mmol) **13** in 100 ml chlorobenzene for 30 h. At this point the reaction was switched to non-DT by the addition of a second portion of 25.2 mg (0.031 mmol) of **13** in ~ 0.5 ml chlorobenzene for 10 h, after which the reaction was quenched with ~1 mL of acidic methanol, the volatiles were removed *in vacuo* and the crude polymeric material was purified through precipitation of a hot toluene solution into a large volume of acidic methanol. The final pure polypropylene was collected and dried overnight at 60 °C (0.01 mmHg). Yield: 5.70 g.  $M_n = 162,100$ , PDI = 1.20.

**Synthesis of *a*-iso-*a*-polypropylene stereoblock triblock:** Under non-DT conditions, a polymerization was carried out using 25.0 mg (0.063 mmol) **12** and 25.2 mg (0.031 mmol) **13** in 100 ml chlorobenzene for 15 h. At this point the reaction was switched to non-DT by the addition of a second portion of 25.2 mg (0.031 mmol) of **13** in ~ 0.5 ml chlorobenzene for 10 h, after which the reaction was returned to DT by the addition of 13.8 mg (0.031 mmol) **56** for another 15 h. The reaction was then quenched with ~1 mL

of acidic methanol, the volatiles were removed *in vacuo* and the crude polymeric material was purified through precipitation of a hot toluene solution into a large volume of acidic methanol. The final pure polypropylene was collected and dried overnight at 60 °C (0.01 mmHg). Yield: 6.92 g.  $M_n = 167,500$ , PDI = 1.19.

**Synthesis of *a-iso-a-iso*-polypropylene stereoblock tetrablock:** Under non-DT conditions, a polymerization was carried out using 25.0 mg (0.063 mmol) **12** and 25.2 mg (0.031 mmol) **13** in 100 ml chlorobenzene for 15 h. At this point the reaction was switched to non-DT by the addition of a second portion of 25.2 mg (0.031 mmol) of **13** in ~ 0.5 ml chlorobenzene for 5 h, after which the reaction was returned to DT by the addition of 13.8 mg (0.031 mmol) **56** for another 15 h. The reaction was then returned to non-DT by a final addition of 25.2 mg (0.031 mmol) **13** in ~ 0.5 ml chlorobenzene for 5 h before being quenched with ~1 mL of acidic methanol. The volatiles were removed *in vacuo* and the crude polymeric material was purified through precipitation of a hot toluene solution into a large volume of acidic methanol. The final pure polypropylene was collected and dried overnight at 60 °C (0.01 mmHg). Yield: 6.54 g.  $M_n = 172,500$ , PDI = 1.19.

**Tensile test for stereoblock polypropylene materials:** The materials were compression molded at 135 °C into 0.5 mm-thick sheets from which dog bones were cut using the ASTM D638-5 cutter. The testing was conducted on an Instron model 3345 tensile tester with pneumatic grips at an extension rate of 2 in/min. Recovery after break and recovery after 300% elongation were calculated as defined in the ASTM D412 method.

**Synthesis of  $^{13}\text{C}$ -labeled Stereogradient Polypropylene:** To a solution of 48.1 mg (0.060 mmol) **13** in 0.5 ml of chlorobenzene at  $-10\text{ }^{\circ}\text{C}$  was added 40.1 mg (0.100 mmol) of  $^{12}\text{-}^{13}\text{C}_3$  in 0.5 ml of chlorobenzene at  $-10\text{ }^{\circ}\text{C}$  (60% activation). This solution was then rapidly added to a 250 ml Schlenk flask charged with 40 ml of chlorobenzene at  $-10\text{ }^{\circ}\text{C}$ , which was previously pressurized to 5 psi with propylene and stirred for 10 minutes. The flask was then repressurized and the pressure maintained for 30 minutes while stirring. A 0.5-ml aliquot was quenched, and 4.0 ml of a 10.0 mM solution of **2** in 1:1 chlorobenzene:dichloromethane was added via syringe pump at a constant rate of 2 ml/h, during which time 0.5-ml aliquots were taken every 30 minutes. Upon complete addition, another 0.2 ml of solution of **2** was added to ensure complete activation, and the reaction maintained for another 30 minutes before quenching with 1 ml of acidic methanol. The volatiles were then removed *in vacuo* and the crude polymeric material was purified through precipitation of a hot toluene solution into a large volume of acidic methanol. The final pure polypropylene was collected and dried overnight at  $60\text{ }^{\circ}\text{C}$  (0.01 mmHg). Yield: 1.803 g. Aliquot at 30 min:  $M_n = 7,500$ , PDI = 1.19. At 60 min:  $M_n = 12,400$ , PDI = 1.19. At 90 min:  $M_n = 16,600$ , PDI = 1.20. At 120 min:  $M_n = 20,800$ , PDI = 1.19. At 150 min:  $M_n = 22,900$ , PDI = 1.23. Final quench at 180 min:  $M_n = 25,200$ , PDI = 1.22.

## References

1. Severn, J. R.; Chadwick, J. C.; Duchateau, R.; Friederichs, N., *Chem. Rev.* **2005**, *105*, 4073-4147.
2. Ziegler, K., *Angew. Chem.* **1952**, *64*, 323-329.
3. Ziegler, K.; Holzkamp, E.; Breil, H.; Martin, H., *Angew. Chem., Int. Ed.* **1955**, *67*, 541-547.
4. Natta, G.; Pino, P.; Corradini, P.; Danusso, F.; Mantica, E.; Mazzanti, G.; Moraglio, G., *J. Am. Chem. Soc.* **1955**, *77*, 1708-1710.
5. Natta, G., *Angew. Chem., Int. Ed.* **1956**, *68*, 393-403.
6. Brintzinger, H. H.; Fischer, D.; Mulhaupt, R.; Rieger, B.; Waymouth, R. M., *Angew. Chem., Int. Ed.* **1995**, *34*, 1143-1170.
7. Coates, G. W., *Chem. Rev.* **2000**, *100*, 1223-1252.
8. Gibson, V. C.; Spitzmesser, S. K., *Chem. Rev.* **2003**, *103*, 283-315.
9. Odian, G., *Principles of Polymerization*. Third ed.; Wiley-Interscience: New York, 1991.
10. Stevens, M. P., *Polymer Chemistry*. Third ed.; Oxford University Press: New York, 1999.
11. Natta, G.; Pino, P.; Mazzanti, G.; Giannini, U., *J. Am. Chem. Soc.* **1957**, *79*, 2975-2976.
12. Breslow, D. S.; Newburg, N. R., *J. Am. Chem. Soc.* **1957**, *79*, 5072-5073.
13. Breslow, D. S.; Newburg, N. R., *J. Am. Chem. Soc.* **1959**, *81*, 81-86.
14. Long, W. P.; Breslow, D. S., *J. Am. Chem. Soc.* **1960**, *82*, 1953-1957.
15. Eisch, J. J.; Piotrowski, A. M.; Brownstein, S. K.; Gabe, E. J.; Lee, F. L., *J. Am. Chem. Soc.* **1985**, *107*, 7219-7221.
16. Arlman, E. J., *J. Catal.* **1964**, *3*, 89-98.
17. Arlman, E. J.; Cossee, P., *J. Catal.* **1964**, *3*, 99-104.
18. Cossee, P., *J. Catal.* **1964**, *3*, 80-88.
19. Sinn, H.; Kaminsky, W., *Adv. Organomet. Chem.* **1980**, *18*, 99-149.
20. Sinn, H.; Kaminsky, W.; Vollmer, H. J.; Woldt, R., *Angew. Chem., Int. Ed.* **1980**, *19*, 390-392.
21. Jungling, S.; Mulhaupt, R., *J. Organomet. Chem.* **1995**, *497*, 27-32.
22. Resconi, L.; Cavallo, L.; Fait, A.; Piemontesi, F., *Chem. Rev.* **2000**, *100*, 1253-1345.
23. Ewen, J. A., *J. Am. Chem. Soc.* **1984**, *106*, 6355-6364.
24. Wild, F.; Zsolnai, L.; Huttner, G.; Brintzinger, H. H., *J. Organomet. Chem.* **1982**, *232*, 233-247.
25. Kaminsky, W.; Kulper, K.; Brintzinger, H. H.; Wild, F., *Angew. Chem., Int. Ed.* **1985**, *24*, 507-508.
26. Ewen, J. A.; Jones, R. L.; Razavi, A.; Ferrara, J. D., *J. Am. Chem. Soc.* **1988**, *110*, 6255-6256.
27. Resconi, L.; Camurati, I.; Sudmeijer, O., *Top. Catal.* **1999**, *7*, 145-163.
28. Burger, B. J.; Thompson, M. E.; Cotter, W. D.; Bercaw, J. E., *J. Am. Chem. Soc.* **1990**, *112*, 1566-1577.

29. Lohrenz, J. C. W.; Woo, T. K.; Fan, L. Y.; Ziegler, T., *J. Organomet. Chem.* **1995**, *497*, 91-104.
30. Cavallo, L.; Guerra, G., *Macromolecules* **1996**, *29*, 2729-2737.
31. Resconi, L.; Bossi, S.; Abis, L., *Macromolecules* **1990**, *23*, 4489-4491.
32. Bochmann, M.; Lancaster, S. J., *Organometallics* **1993**, *12*, 633-640.
33. Bochmann, M.; Lancaster, S. J., *J. Organomet. Chem.* **1992**, *434*, C1-C5.
34. Chien, J. C. W.; Tsai, W. M.; Rausch, M. D., *J. Am. Chem. Soc.* **1991**, *113*, 8570-8571.
35. Fan, G. Q.; Dong, J. Y., *J. Mol. Catal. A-Chem.* **2005**, *236*, 246-252.
36. Kang, K. K.; Shiono, T.; Ikeda, T., *Macromolecules* **1997**, *30*, 1231-1233.
37. Mogstad, A. L.; Waymouth, R. M., *Macromolecules* **1994**, *27*, 2313-2315.
38. Busico, V.; Cipullo, R.; Monaco, G.; Vacatello, M.; Bella, J.; Segre, A. L., *Macromolecules* **1998**, *31*, 8713-8719.
39. Busico, V.; Cipullo, R.; Monaco, G.; Vacatello, M.; Segre, A. L., *Macromolecules* **1997**, *30*, 6251-6263.
40. Busico, V.; Cipullo, R., *Prog. Polym. Sci.* **2001**, *26*, 443-533.
41. Ewen, J. A.; Elder, M. J.; Jones, R. L.; Haspeslagh, L.; Atwood, J. L.; Bott, S. G.; Robinson, K., *Makromol. Chem., Macromol. Symp.* **1991**, *48-9*, 253-295.
42. Miller, S. A.; Bercaw, J. E., *Organometallics* **2002**, *21*, 934-945.
43. Ewen, J. A.; Jones, R. L.; Elder, M. J.; Camurati, I.; Pritzkow, H., *Macromol. Chem. Phys.* **2004**, *205*, 302-307.
44. Giardello, M. A.; Eisen, M. S.; Stern, C. L.; Marks, T. J., *J. Am. Chem. Soc.* **1995**, *117*, 12114-12129.
45. Kaminsky, W.; Rabe, O.; Schauwienold, A. M.; Schupfner, G. U.; Hanss, J.; Kopf, J., *J. Organomet. Chem.* **1995**, *497*, 181-193.
46. Razavi, A.; Thewalt, U., *Coord. Chem. Rev.* **2006**, *250*, 155-169.
47. Miller, S. A.; Bercaw, J. E., *Organometallics* **2006**, *25*, 3576-3592.
48. Busico, V.; Cipullo, R.; Talarico, G.; Segre, A. L.; Chadwick, J. C., *Macromolecules* **1997**, *30*, 4786-4790.
49. Natta, G., *Journal of Polymer Science* **1959**, *34*, 531-549.
50. Muller, G.; Rieger, B., *Prog. Polym. Sci.* **2002**, *27*, 815-851.
51. Collette, J. W.; Tullock, C. W.; Macdonald, R. N.; Buck, W. H.; Su, A. C. L.; Harrell, J. R.; Mulhaupt, R.; Anderson, B. C., *Macromolecules* **1989**, *22*, 3851-3858.
52. Collette, J. W.; Ovenall, D. W.; Buck, W. H.; Ferguson, R. C., *Macromolecules* **1989**, *22*, 3858-3866.
53. Mallin, D. T.; Rausch, M. D.; Lin, Y. G.; Dong, S. Z.; Chien, J. C. W., *J. Am. Chem. Soc.* **1990**, *112*, 2030-2031.
54. Gauthier, W. J.; Corrigan, J. F.; Taylor, N. J.; Collins, S., *Macromolecules* **1995**, *28*, 3771-3778.
55. Gauthier, W. J.; Collins, S., *Macromolecules* **1995**, *28*, 3779-3786.
56. De Rosa, C.; Auriemma, F.; Di Capua, A.; Resconi, L.; Guidotti, S.; Camurati, I.; Nifant'ev, I. E.; Laishevtsev, I. P., *J. Am. Chem. Soc.* **2004**, *126*, 17040-17049.
57. Cobzaru, C.; Hild, S.; Boger, A.; Troll, C.; Rieger, B., *Coord. Chem. Rev.* **2006**, *250*, 189-211.

58. Dietrich, U.; Hackmann, M.; Rieger, B.; Klinga, M.; Leskela, M., *J. Am. Chem. Soc.* **1999**, *121*, 4348-4355.
59. Moscardi, G.; Resconi, L.; Cavallo, L., *Organometallics* **2001**, *20*, 1918-1931.
60. Resconi, L.; Fait, A.; Piemontesi, F.; Colonna, M.; Rychlicki, H.; Zeigler, R., *Macromolecules* **1995**, *28*, 6667-6676.
61. Busico, V.; Cipullo, R., *J. Organomet. Chem.* **1995**, *497*, 113-118.
62. Busico, V.; Cipullo, R., *J. Am. Chem. Soc.* **1994**, *116*, 9329-9330.
63. Chirik, P. J.; Day, M. W.; Labinger, J. A.; Bercaw, J. E., *J. Am. Chem. Soc.* **1999**, *121*, 10308-10317.
64. Johnson, L. K.; Killian, C. M.; Brookhart, M., *J. Am. Chem. Soc.* **1995**, *117*, 6414-6415.
65. Guan, Z. B.; Cotts, P. M.; McCord, E. F.; McLain, S. J., *Science* **1999**, *283*, 2059-2062.
66. Babu, G. N.; Newmark, R. A.; Chien, J. C. W., *Macromolecules* **1994**, *27*, 3383-3388.
67. Leclerc, M. K.; Brintzinger, H. H., *J. Am. Chem. Soc.* **1995**, *117*, 1651-1652.
68. Leclerc, M. K.; Brintzinger, H. H., *J. Am. Chem. Soc.* **1996**, *118*, 9024-9032.
69. Busico, V.; Caporaso, L.; Cipullo, R.; Landriani, L.; Angelini, G.; Margonelli, A.; Segre, A. L., *J. Am. Chem. Soc.* **1996**, *118*, 2105-2106.
70. Resconi, L., *J. Mol. Catal. A-Chem.* **1999**, *146*, 167-178.
71. Abrams, M. B.; Yoder, J. C.; Loeber, C.; Day, M. W.; Bercaw, J. E., *Organometallics* **1999**, *18*, 1389-1401.
72. Yoder, J. C.; Bercaw, J. E., *J. Am. Chem. Soc.* **2002**, *124*, 2548-2555.
73. Coates, G. W.; Waymouth, R. M., *Science* **1995**, *267*, 217-219.
74. Lin, S.; Waymouth, R. M., *Acc. Chem. Res.* **2002**, *35*, 765-773.
75. Busico, V.; Cipullo, R.; Kretschmer, W.; Talarico, G.; Vacatello, M.; Castelli, V. V., *Macromol. Symp.* **2002**, *189*, 127-141.
76. Busico, V.; Cipullo, R.; Kretschmer, W. P.; Talarico, G.; Vacatello, M.; Castelli, V. V., *Angew. Chem., Int. Ed.* **2002**, *41*, 505-508.
77. Busico, V.; Castelli, V. V. A.; Aprea, P.; Cipullo, R.; Segre, A.; Talarico, G.; Vacatello, M., *J. Am. Chem. Soc.* **2003**, *125*, 5451-5460.
78. Jayaratne, K. C.; Sita, L. R., *J. Am. Chem. Soc.* **2000**, *122*, 958-959.
79. Zhang, Y. H.; Reeder, E. K.; Keaton, R. J.; Sita, L. R., *Organometallics* **2004**, *23*, 3512-3520.
80. Matsui, S.; Tohi, Y.; Mitani, M.; Saito, J.; Makio, H.; Tanaka, H.; Nitabaru, M.; Nakano, T.; Fujita, T., *Chem. Lett.* **1999**, 1065-1066.
81. Tian, J.; Coates, G. W., *Angew. Chem., Int. Ed.* **2000**, *39*, 3626-3629.
82. Milano, G.; Cavallo, L.; Guerra, G., *J. Am. Chem. Soc.* **2002**, *124*, 13368-13369.
83. Mitani, M.; Saito, J.; Ishii, S. I.; Nakayama, Y.; Makio, H.; Matsukawa, N.; Matsui, S.; Mohri, J. I.; Furuyama, R.; Terao, H.; Bando, H.; Tanaka, H.; Fujita, T., *Chem. Rec.* **2004**, *4*, 137-158.
84. Makio, H.; Fujita, T., *Bull. Chem. Soc. Jpn.* **2005**, *78*, 52-66.
85. Hustad, P. D.; Coates, G. W., *J. Am. Chem. Soc.* **2002**, *124*, 11578-11579.
86. Mason, A. F.; Tian, J.; Hustad, P. D.; Lobkovsky, E. B.; Coates, G. W., *Isr. J. Chem.* **2002**, *42*, 301-306.
87. Mason, A. F.; Coates, G. W., *J. Am. Chem. Soc.* **2004**, *126*, 16326-16327.

88. Smolensky, E.; Kapon, M.; Woollins, J. D.; Eisen, M. S., *Organometallics* **2005**, *24*, 3255-3265.
89. Chien, J. C. W.; Iwamoto, Y.; Rausch, M. D.; Wedler, W.; Winter, H. H., *Macromolecules* **1997**, *30*, 3447-3458.
90. Chien, J. C. W.; Iwamoto, Y.; Rausch, M. D., *J. Polym. Sci. Pol. Chem.* **1999**, *37*, 2439-2445.
91. Lieber, S.; Brintzinger, H. H., *Macromolecules* **2000**, *33*, 9192-9199.
92. Britovsek, G. J. P.; Cohen, S. A.; Gibson, V. C.; Maddox, P. J.; van Meurs, M., *Angew. Chem., Int. Ed.* **2002**, *41*, 489-491.
93. Britovsek, G. J. P.; Cohen, S. A.; Gibson, V. C.; van Meurs, M., *J. Am. Chem. Soc.* **2004**, *126*, 10701-10712.
94. van Meurs, M.; Britovsek, G. J. P.; Gibson, V. C.; Cohen, S. A., *J. Am. Chem. Soc.* **2005**, *127*, 9913-9923.
95. Arriola, D. J.; Carnahan, E. M.; Hustad, P. D.; Kuhlman, R. L.; Wenzel, T. T., *Science* **2006**, *312*, 714-719.
96. Jayaratne, K. C.; Sita, L. R., *J. Am. Chem. Soc.* **2001**, *123*, 10754-10755.
97. Zhang, Y. H.; Keaton, R. J.; Sita, L. R., *J. Am. Chem. Soc.* **2003**, *125*, 9062-9069.
98. Zhang, Y. H.; Sita, L. R., *J. Am. Chem. Soc.* **2004**, *126*, 7776-7777.
99. Busico, V.; Talarico, G.; Cipullo, R., *Macromol. Symp.* **2005**, *226*, 1-16.
100. Szwarc, M.; Levy, M.; Milkovich, R., *J. Am. Chem. Soc.* **1956**, *78*, 2656-2657.
101. Szwarc, M., *Nature* **1956**, *178*, 1168-1169.
102. Quirk, R. P.; Lee, B., *Polym. Int.* **1992**, *27*, 359-367.
103. Doi, Y.; Ueki, S.; Keii, T., *Macromolecules* **1979**, *12*, 814-819.
104. Natta, G.; Zambelli, A.; Pasquon, I., *J. Am. Chem. Soc.* **1962**, *84*, 1488-&.
105. Coates, G. W.; Hustad, P. D.; Reinartz, S., *Angew. Chem., Int. Ed.* **2002**, *41*, 2236-2257.
106. Baumann, R.; Davis, W. M.; Schrock, R. R., *J. Am. Chem. Soc.* **1997**, *119*, 3830-3831.
107. Baumann, R.; Schrock, R. R., *J. Organomet. Chem.* **1998**, *557*, 69-75.
108. Schrock, R. R.; Baumann, R.; Reid, S. M.; Goodman, J. T.; Stumpf, R.; Davis, W. M., *Organometallics* **1999**, *18*, 3649-3670.
109. Mehrkhodavandi, P.; Bonitatebus, P. J.; Schrock, R. R., *J. Am. Chem. Soc.* **2000**, *122*, 7841-7842.
110. Mehrkhodavandi, P.; Schrock, R. R., *J. Am. Chem. Soc.* **2001**, *123*, 10746-10747.
111. Mehrkhodavandi, P.; Schrock, R. R.; Pryor, L. L., *Organometallics* **2003**, *22*, 4569-4583.
112. Mitani, M.; Mohri, J.; Yoshida, Y.; Saito, J.; Ishii, S.; Tsuru, K.; Matsui, S.; Furuyama, R.; Nakano, T.; Tanaka, H.; Kojoh, S.; Matsugi, T.; Kashiwa, N.; Fujita, T., *J. Am. Chem. Soc.* **2002**, *124*, 3327-3336.
113. Mitani, M.; Nakano, T.; Fujita, T., *Chem.-Eur. J.* **2003**, *9*, 2397-2403.
114. Kui, S. C. F.; Zhu, N. Y.; Chan, M. C. W., *Angew. Chem., Int. Ed.* **2003**, *42*, 1628-1632.
115. Talarico, G.; Busico, V.; Cavallo, L., *Organometallics* **2004**, *23*, 5989-5993.
116. Liu, Z. X.; Somsook, E.; Landis, C. R., *J. Am. Chem. Soc.* **2001**, *123*, 2915-2916.
117. Landis, C. R.; Rosaaen, K. A.; Sillars, D. R., *J. Am. Chem. Soc.* **2003**, *125*, 1710-1711.

118. Sillars, D. R.; Landis, C. R., *J. Am. Chem. Soc.* **2003**, *125*, 9894-9895.
119. Liu, Z. X.; Somsook, E.; White, C. B.; Rosaaen, K. A.; Landis, C. R., *J. Am. Chem. Soc.* **2001**, *123*, 11193-11207.
120. Landis, C. R.; Sillars, D. R.; Batterton, J. M., *J. Am. Chem. Soc.* **2004**, *126*, 8890-8891.
121. Landis, C. R.; Rosaaen, K. A.; Uddin, J., *J. Am. Chem. Soc.* **2002**, *124*, 12062-12063.
122. Keaton, R. J.; Sita, L. R., *J. Am. Chem. Soc.* **2002**, *124*, 9070-9071.
123. Proscenc, M. H.; Brintzinger, H. H., *Organometallics* **1997**, *16*, 3889-3894.
124. Lohrenz, J. C. W.; Buhl, M.; Weber, M.; Thiel, W., *J. Organomet. Chem.* **1999**, *592*, 11-21.
125. Keaton, R. J.; Koterwas, L. A.; Fettinger, J. C.; Sita, L. R., *J. Am. Chem. Soc.* **2002**, *124*, 5932-5933.
126. Harney, M. B.; Keaton, R. J.; Sita, L. R., *J. Am. Chem. Soc.* **2004**, *126*, 4536-4537.
127. Rieger, B.; Mu, X.; Mallin, D. T.; Rausch, M. D.; Chien, J. C. W., *Macromolecules* **1990**, *23*, 3559-3568.
128. Busico, V.; Cipullo, R.; Chadwick, J. C.; Modder, J. F.; Sudmeijer, O., *Macromolecules* **1994**, *27*, 7538-7543.
129. Busico, V.; Guardasole, M.; Margonelli, A.; Segre, A. L., *J. Am. Chem. Soc.* **2000**, *122*, 5226-5227.
130. Borrelli, M.; Busico, V.; Cipullo, R.; Ronca, S.; Budzelaar, P. H. M., *Macromolecules* **2002**, *35*, 2835-2844.
131. Song, F. Q.; Cannon, R. D.; Bochmann, M., *J. Am. Chem. Soc.* **2003**, *125*, 7641-7653.
132. Keaton, R. J. Amidinate Based Catalysts for the Stereospecific and Living Ziegler-Natta Polymerization of  $\alpha$ -Olefins. Doctoral Thesis, University of Maryland, College Park, MD, 2003.
133. Harney, M. B.; Keaton, R. J.; Fettinger, J. C.; Sita, L. R., *J. Am. Chem. Soc.* **2006**, *128*, 3420-3432.
134. Kissounko, D. A.; Sita, L. R., *J. Am. Chem. Soc.* **2004**, *126*, 5946-5947.
135. Zhang, Y. Degenerative Transfer Living Ziegler-Natta Polymerization of  $\alpha$ -Olefins. Doctoral Thesis, University of Maryland, College Park, MD, 2005.
136. Jordan, R. F.; Bradley, P. K.; Baenziger, N. C.; Lapointe, R. E., *J. Am. Chem. Soc.* **1990**, *112*, 1289-1291.
137. Keaton, R. J.; Jayaratne, K. C.; Fettinger, J. C.; Sita, L. R., *J. Am. Chem. Soc.* **2000**, *122*, 12909-12910.
138. Zhang, Y. H.; Keaton, R. J.; Sita, L. R., *J. Am. Chem. Soc.* **2003**, *125*, 8746-8747.
139. Kissounko, D. A.; Zhang, Y. H.; Harney, M. B.; Sita, L. R., *Adv. Synth. Catal.* **2005**, *347*, 426-432.
140. Buchwald, S. L.; Kreutzer, K. A.; Fisher, R. A., *J. Am. Chem. Soc.* **1990**, *112*, 4600-4601.
141. Erker, G.; Schlund, R.; Kruger, C., *Organometallics* **1989**, *8*, 2349-2355.
142. Atwood, J. L.; Hunter, W. E.; Hrcir, D. C.; Samuel, E.; Alt, H.; Rausch, M. D., *Inorg. Chem.* **1975**, *14*, 1757-1762.
143. Schock, L. E.; Brock, C. P.; Marks, T. J., *Organometallics* **1987**, *6*, 232-241.

144. Bulls, A. R.; Schaefer, W. P.; Serfas, M.; Bercaw, J. E., *Organometallics* **1987**, *6*, 1219-1226.
145. Carney, M. J.; Walsh, P. J.; Bergman, R. G., *J. Am. Chem. Soc.* **1990**, *112*, 6426-6428.
146. Horton, A. D., *Organometallics* **1992**, *11*, 3271-3275.
147. Kissounko, D.; Epshteyn, A.; Fettingner, J. C.; Sita, L. R., *Organometallics* **2006**, *25*, 531-535.
148. Keaton, R. J.; Jayaratne, K. C.; Henningsen, D. A.; Koterwas, L. A.; Sita, L. R., *J. Am. Chem. Soc.* **2001**, *123*, 6197-6198.
149. Jayaratne, K. C.; Keaton, R. J.; Henningsen, D. A.; Sita, L. R., *J. Am. Chem. Soc.* **2000**, *122*, 10490-10491.
150. Harney, M. B.; Zhang, Y. H.; Sita, L. R., *Angew. Chem., Int. Ed.* **2006**, *45*, 2400-2404.
151. Nishii, K.; Shiono, T.; Ikeda, T., *Macromol. Rapid Commun.* **2004**, *25*, 1029-1032.
152. Hagihara, H.; Shiono, T.; Ikeda, T., *Macromolecules* **1997**, *30*, 4783-4785.
153. Hagihara, H.; Shiono, T.; Ikeda, T., *Macromolecules* **1998**, *31*, 3184-3188.
154. Nishii, K.; Matsumae, T.; Dare, E. O.; Shiono, T.; Ikeda, T., *Macromol. Chem. Phys.* **2004**, *205*, 363-369.
155. Cai, Z.; Nakayama, Y.; Shiono, T., *Kinetics and Catalysis* **2006**, *47*, 274-277.
156. Zhang, Y. H.; Kissounko, D. A.; Fettingner, J. C.; Sita, L. R., *Organometallics* **2003**, *22*, 21-23.
157. Kissounko, D. A.; Fettingner, J. C.; Sita, L. R., *Inorg. Chim. Acta* **2003**, *345*, 121-129.
158. Harney, M. B.; Zhang, Y. H.; Sita, L. R., *Angew. Chem., Int. Ed.* **2006**, *45*, 6140-6144.
159. Busico, V.; Cipullo, R.; Talarico, G.; Castelli, V. V., *Isr. J. Chem.* **2002**, *42*, 295-299.